NATIONAL ADVISORY COMMITTEE FOR AERONAUTICS

TECHNICAL NOTE

No. 1766

WIND-TUNNEL INVESTIGATION OF EFFECTS OF TAIL LENGTH ON THE LONGITUDINAL AND LATERAL STABILITY CHARACTERISTICS OF A SINGLE-PROPELLER AIRPLANE MODEL

By Harold S. Johnson

Langley Aeronautical Laboratory
Langley Field, Va.

Washington

December 1948

NATIONAL ADVISORY COMMITTEE FOR AERONAUTICS

TECHNICAL NOTE NO. 1766

WIND-TUNNEL INVESTIGATION OF EFFECTS OF TAIL LENGTH ON THE LONGITUDINAL AND LATERAL STABILITY CHARACTERISTICS OF A SINGLE-PROPELLER AIRPLANE MODEL

By Harold S. Johnson

SUMMARY

An investigation has been made of a powered model of a single-propeller low-wing airplane with three values of tail length and three horizontal tails to determine the effects of tail length and tail volume on the longitudinal and lateral stability.

The destabilizing shift in neutral point caused by power increased with increasing tail length for either the condition of constant horizontal-tail volume or constant horizontal-tail area. For a given tail length, the destabilizing shift in neutral point caused by power increased with increasing tail area. The increase in directional stability caused by power became larger as the tail length was increased. The tendency toward rudder lock decreased as the tail length was increased in the positive yaw range but was practically unaffected by tail-length variations in the negative yaw range.

INTRODUCTION

The Langley Laboratory of the NACA has undertaken a study of the problems of obtaining adequate stability and control for high-performance, single-propeller airplanes. In order to obtain a solution of these problems, a general investigation has been made in the Langley 7- by 10-foot tunnel of a typical single-propeller airplane model. Previously included in the study have been an analysis of the effects of slipstream rotation on the lateral characteristics (reference 1), an unpublished analysis of the effects of engine skew on directional and lateral-control characteristics, and the results of an investigation to determine the effects of an unsymmetrical horizontal tail on longitudinal stability (reference 2). This paper presents the results of the investigation conducted to determine the effects of tail length and horizontal-tail volume upon longitudinal and lateral stability.

COEFFICIENTS AND SYMBOLS

The results of the tests are presented as standard NACA coefficients of forces and moments. Rolling-moment, yawing-moment, and pitching-moment coefficients are given about the center-of-gravity location shown in figure 1 (28.2 percent M.A.C.). The data are referred to the stability system of axes with the origin at the center of gravity. The Z-axis is in the plane of symmetry and perpendicular to the relative wind, the X-axis is in the plane of symmetry and perpendicular to the Z-axis, and the Y-axis is perpendicular to the plane of symmetry. The positive directions of the stability axes and of angular displacements of the airplane and control surfaces are shown in figure 2.

The coefficients and symbols are defined as follows:

C_L	lift coefficient (Lift/qS)
C_{L_t}	tail lift coefficient $\left(L_t/q_tS_t\right)$
C_X	longitudinal-force coefficient (X/qS)
C_Y	lateral-force coefficient (Y/qS)
C_l	rolling-moment coefficient (L/qSb)
C_n	yawing-moment coefficient (N/qSb)
C_m	pitching-moment coefficient (M/qSc̄)
T_c'	effective thrust coefficient based on wing area $\left(T_{eff}/qS\right)$
Q_c	torque coefficient $(Q/\rho V^2D^3)$
V/nD	propeller advance-diameter ratio
η	propulsive efficiency $\left(T_{eff}V/2\pi nQ\right)$

Lift = -Z

X	longitudinal force, pounds
Y	lateral force, pounds
Z	vertical force, pounds
L	rolling moment, pound-feet
M	pitching moment, pound-feet

N	yawing moment, pound-feet
L_t	lift of isolated horizontal tail, pounds
T_{eff}	propeller effective thrust, pounds
Q	propeller torque, pound-feet
q	free-stream dynamic pressure, pounds per square foot $(\rho V^2/2)$
q_t	effective dynamic pressure at tail, pounds per square foot
S	wing area (9.40 sq ft on model)
S_t	horizontal-tail area, square feet (see Table I)
c	airfoil section chord, feet
$\bar{c}$	wing mean aerodynamic chord (1.31 ft on model) $\left(\frac{2}{S}\int_0^{b/2} c^2\, db\right)$
c_t	horizontal-tail mean aerodynamic chord
c_v	vertical-tail mean aerodynamic chord
b	wing span (7.509 ft on model)
C_{m_e}	pitching-moment coefficient at effective tail-off aerodynamic-center location (zero-lift intercept of tangent to tail-off pitching-moment curve)
l_t	horizontal-tail length measured from quarter-chord point of wing mean aerodynamic chord to quarter-chord point of horizontal-tail mean aerodynamic chord
l_v	vertical-tail length measured from center of gravity to quarter-chord point of vertical-tail mean aerodynamic chord
v_t	horizontal-tail-volume coefficient $\left(S_t l_t/S\bar{c}\right)$
v_v	vertical-tail-volume coefficient $\left(S_v l_v/Sb\right)$
V	air velocity, feet per second
D	propeller diameter, (2.27 ft on model)
n	propeller speed, revolutions per second

ρ mass density of air, slugs per cubic foot

α angle of attack of thrust line, degrees

α_t angle of attack of horizontal-tail chord, degrees

ψ angle of yaw, degrees

ϵ average angle of downwash, degrees

σ angle of sidewash, degrees

i_t angle of stabilizer with respect to thrust line, degrees

δ control-surface deflection, degrees

n_o effective tail-off aerodynamic-center location, percent wing mean aerodynamic chord

n_p neutral-point location, percent wing mean aerodynamic chord (center-of-gravity location for neutral stability when $C_m = 0$)

n_t tail contribution to the neutral-point location

n_b trimming contribution to the neutral-point location

C_{L_α} slope of curve of wing lift coefficient against angle of attack $\left(dC_L/d\alpha\right)$

$C_{L_{\alpha_t}}$ slope of curve of tail lift coefficient againt tail angle of attack $\left(dC_{L_t}/d\alpha_t\right)$

$$R = 1 - \frac{C_{L_b}}{q_t/q}\left[\frac{d\left(q_t/q\right)}{dC_{L_b}}\right]$$

$\Delta n_{p_{power}}$ shift in n_p due to power, percent wing mean aerodynamic chord $\left(\left(n_p\right)_p - \left(n_p\right)_w\right)$

$\Delta n_{p_{flap}}$ shift in n_p due to flap deflection, percent wing mean aerodynamic chord $\left(\left(n_p\right)_{\text{flaps deflected}} - \left(n_p\right)_{\text{flaps neutral}}\right)$

Subscripts:

t	horizontal tail
v	vertical tail
e	elevator
r	rudder
b	trimmed conditions with center of gravity at neutral point
w	power off (windmilling propeller)
p	power on
ψ	partial derivative of a coefficient with respect to angle of yaw $\left(\text{for example: } C_{n_\psi} = \frac{\partial C_n}{\partial \psi}\right)$
o	tail off

MODEL AND APPARATUS

The model used for the investigation was constructed with three interchangeable fuselage blocks which permitted tests to be made at three values of tail length, referred to as short, normal, and long tail lengths. With the normal tail length, the model was representative of modern fighter design and corresponded to a $\frac{1}{5}$-scale reproduction of a 37.5-foot span, single-propeller airplane.

The tail length was changed by contracting and expanding the distances between fuselage stations from a point near the trailing edge of the wing to the tail; a variation in tail length of twice the mean aerodynamic chord was thus obtained. The cross-sectional shape of the fuselage stations remained the same for the three tail lengths. The three tail lengths tested were $1.85\bar{c}$, $2.57\bar{c}$, and $3.85\bar{c}$ for the short, normal, and long tail lengths, respectively, measured from $\frac{1}{4}\bar{c}$ to $\frac{1}{4}c_t$. Drawings and photographs of the model showing the three tail lengths are presented as figures 1 and 3, respectively. The general dimensional characteristics of the model are given in table I.

The model had an adjustable stabilizer, retractable landing gear, and a 30-percent-chord partial-span slotted flap with an internally-sealed 10-percent-chord plain trailing-edge flap. The flap extended across the span inboard of the ailerons in four segments. There was

no flap beneath the fuselage. A cross section of the slotted-flap and plain-flap arrangement is shown in figure 4.

The model was tested with three horizontal tails at each of the three tail lengths in order to cover a broad range of horizontal-tail volumes. The three horizontal tails were of similar proportions (same aspect ratio and plan form) but of different areas, the areas of the large and small horizontal tails being such that a tail volume of 0.588 could be maintained at the three tail lengths tested, which fact enabled an analysis to be made of the effects of tail length on stability at constant tail volume. The normal horizontal tail was equipped with an internally sealed elevator, but the small and large horizontal tails were not. A line drawing of the three tails with the principal dimensions is presented as figure 5. Stabilizer settings were measured with the aid of a vernier inclinometer with a precision of $\pm 0.1^\circ$. For the elevator-free tests, the elevator was free to deflect through a range of 30° up and 20° down.

Tests were made of the three isolated horizontal tails in order to determine the characteristics to be used for determining the angle of downwash and the dynamic-pressure ratio at the tail. The small and normal horizontal tails were mounted as full-span models in the Langley 4- by 6-foot vertical tunnel, whereas the large horizontal tail was mounted as a semispan model. (See fig. 6.)

A drawing of the vertical tail is presented as figure 7. For the rudder-free tests, the rudder was free to deflect through a range of $\pm 30^\circ$.

Power for the model was obtained from a 56-horsepower electric motor mounted in the fuselage nose. The speed of the motor was determined from an electric tachometer which is accurate to within ± 0.2 percent.

The 2.27-foot diameter, three-blade right-hand metal propeller was set at a blade angle of 15° at the 0.75 radius for all tests.

The model configurations referred to in the text and on the figures are as follows:

Cruising configuration
- Flaps retracted
- Landing gear retracted
- Cowl flaps closed

Landing configuration
- Slotted flaps deflected 37°
- Plain flaps deflected 30° with respect to the slotted flaps
- Landing gear extended
- Cowl flaps open 15°

For the tests designated tail off, the vertical and horizontal tails were removed and replaced by a fairing as shown in figure 7.

TESTS AND RESULTS

Test Conditions

The tests of the complete model were made in the Langley 7- by 10-foot tunnel. The tests of the isolated small and normal horizontal tails and the semispan large horizontal tail were made in the Langley 4- by 6-foot vertical tunnel. The dynamic pressures and tunnel airspeeds of the tests, the test Reynolds numbers, and the effective Reynolds numbers (for maximum-lift coefficients) are listed in table II. The test Reynolds numbers were based on the wing mean aerodynamic chord for the complete model (1.31 ft) and on the average chord of the isolated tails (0.53, 0.64, and 0.76 ft for the small, normal, and large horizontal tails, respectively). The effective Reynolds numbers include the effect of the tunnel-turbulence factor, 1.6 for the Langley 7- by 10-foot tunnel and 1.93 for the Langley 4- by 6-foot vertical tunnel.

All of the tests in the Langley 7- by 10-foot tunnel were made at a dynamic pressure of 16.37 pounds per square foot except the power-on tests with the landing configuration which were made at a dynamic pressure of 9.21 pounds per square foot. This difference was necessitated by power limitations of the model motor.

Corrections

Complete model.- All data have been corrected for tares caused by the model support strut. Jet-boundary corrections have been applied to the angles of attack, the longitudinal-force coefficients, and the tail-on pitching-moment coefficients. The corrections were computed as follows by use of reference 3:

$$\Delta\alpha = 1.065C_L(\text{deg})$$

$$\Delta C_X = -0.0157C_L^2$$

$$\Delta C_m = -7.74C_L\left(\frac{\delta_T}{\sqrt{q_t/q}} - 0.116\right)\frac{\partial C_m}{\partial i_t}$$

where δ_T is the jet-boundary correction factor and equals 0.184, 0.206, and 0.222 for the short, normal, and long tail lengths, respectively. All jet-boundary corrections were added to the test data.

Tail surfaces.- The data for the full-span isolated tails were corrected for tares caused by the model support strut. The following

jet-boundary corrections were added to the angles of attack for the various isolated tails:

Small $\Delta\alpha_t = 0.88C_{L_t}$

Normal $\Delta\alpha_t = 1.59C_{L_t}$

Large semispan $\Delta\alpha_t = 0.57C_{L_t}$

Test Procedure

The model was tested with the propeller windmilling and in a high power condition for both the cruising and landing configurations. During the tests the thrust and torque coefficients varied with lift coefficient as shown in figure 8, and the coefficients used correspond to the values of horsepower shown in figure 9 for various model scales and airplane wing loadings.

For the power-on tests, the model propeller was calibrated with the model in the cruising configuration, tail-off, by measuring the longitudinal force for a range of propeller speeds at an angle of attack of 0°. The thrust coefficients were determined from the equation

$$T_c' = C_{X_{(\text{propeller operating})}} - C_{X_{(\text{propeller removed})}}$$

The torque coefficients were computed by use of a calibration of motor torque as a function of minimum current. The results of the model propeller calibration for the normal fuselage are presented in figure 10.

The thrust coefficients were reproduced during the power-on tests by the use of figures 8 and 10 to correspond to propeller speed and lift coefficient of the model. The thrust coefficient for the windmilling tests was about -0.02.

For the yaw tests, the propeller speed was held constant throughout the yaw range. The value of T_c' corresponding to the lift coefficient at zero yaw was used. Lateral-stability derivatives were obtained from pitch tests at angles of yaw of 5° and -5° by assuming a straight-line variation between these points.

Presentation of Results

Neutral points were determined from data obtained at different stabilizer settings (figs. 11 to 19) by the method outlined in reference 4. Effective

dynamic-pressure ratios and downwash angles at the tail were determined from the stabilizer tests and the isolated horizontal-tail tests (fig. 20) by the methods derived in reference 5.

DISCUSSION

LONGITUDINAL STABILITY CHARACTERISTICS

Tail-off Characteristics

The tail-off aerodynamic-center locations (fig. 21) were relatively unaffected by tail length, the stability increasing slightly with tail length, with the variation generally falling within the accuracy of the data. Power operation and flap deflection caused an appreciable increase in stability. The increase in stability caused by power results from the favorable thrust moments obtained when the thrust line is located above the center of gravity. The increase in stability caused by the deflection of the flaps results from the rearward shift of the center of pressure with flap deflection because the flap moves rearward considerably when it is deflected.

The discontinuity of the curves for the curising configuration with windmilling propeller reflects the breaks in the pitching-moment and lift curves, which are characteristic of this wing section at low Reynolds numbers where the flow is irregular in the region of transition from the low-drag to the moderate-drag range of the wing. This discontinuity disappears as the Reynolds numbers approach full-scale values.

Effect of Tail Length with Constant Tail Volume

Neutral points.- With windmilling propeller, cruising configuration, tail length generally had little effect on stability (fig. 22). The stability of the model decreased as the tail length was increased for the higher lift coefficients. With power on, the neutral-point location was relatively unaffected by tail length at low lift coefficients, but as the lift coefficient was increased, the neutral point moved forward as tail length increased. The model with the long tail length was unstable about the design center-of-gravity location above lift coefficients of 0.9.

With windmilling propeller, landing configuration, the stability of the model increased as the tail length was increased and decreased as the lift coefficient was increased, the model with the short tail length becoming unstable above $C_L = 1.5$. With power on, landing configuration, the neutral point generally moved forward as the lift

coefficient was increased. Although there was no consistant variation of n_p with tail length, the stability decreased as the tail length was increased below lift coefficients of about 1.5. There was little change in n_p with tail length at high lift coefficients.

Effect of power.- As shown by figure 23, the shift in neutral point due to power becomes less unfavorable as the tail length decreases. In fact, with flaps deflected, the application of power actually increases the stability of the model with the short tail length. In the examination of the probable causes of the increase in unfavorable shift in neutral point as tail length is increased, consideration of the neutral-point equation developed in reference 5 is helpful. This equation can be rewritten to express the shift in neutral point due to power as follows:

$$\Delta n_{p_{power}} = \left(n_o\right)_p - \left(n_o\right)_w + \left(n_t\right)_p - \left(n_t\right)_w + \left(n_b\right)_p - \left(n_b\right)_w$$

$$= \left(n_o\right)_p - \left(n_o\right)_w + \frac{C_{L_{\alpha_t}} v_t}{R}\left\{\frac{1}{\left(C_{L_{\alpha_b}}\right)_p}\left(\frac{q_t}{q}\right)_p\left[1-\left(\frac{d\epsilon}{d\alpha}\right)_p\right]\right.$$

$$\left. - \frac{1}{\left(C_{L_{\alpha_b}}\right)_w}\left(\frac{q_t}{q}\right)_w\left[1-\left(\frac{d\epsilon}{d\alpha}\right)_w\right]R\right\} + \frac{C_{m_e}}{C_{L_b}}\frac{1-R}{R} \qquad (1)$$

Equation (1) merely states that the shift in neutral point due to power is equal to the sum of the change in tail-off aerodynamic center caused by power, the change in the tail contribution due to power, and the change in neutral point due to trimming. The last term is not expressed as an increment because without power it is effectively zero.

When the thrust line is located above the center of gravity, the shift in n_o due to power is usually stabilizing. With flaps undeflected, the effect of the trimming term is small. The shift in neutral point due to power and its variation with tail length (for the flap-neutral case) must then result mainly from the changes in the tail-effectiveness term. The fact that the term is preceded by a positive sign indicates that it should have a stabilizing effect provided that the subtraction within the braces gives a positive result. Since the test data indicate that the total effect of power is destabilizing, the result of the subtraction of the terms within the braces must be negative. If the tail is in the slipstream, the dynamic-pressure ratio at the tail is always larger with power on than with power off. The power-on lift-curve slope is also larger than the power-off lift-curve slope. As a rough approximation, the value of $\frac{q_t/q}{C_{L_\alpha}}$ with power may be assumed to be about equal to the value without power. In order to produce the adverse effects of power shown by the tests, therefore, $d\epsilon/d\alpha$ with

power must be considerably larger than the value without power and this difference must increase with tail length.

In order to show the relative magnitude and variation with tail length of each of the terms of the equation, figure 24 was prepared for the flap-neutral condition with $C_L = 1.0$. The total shift in neutral point varies from 5 percent forward for the short tail length to about 12 percent forward for the long tail length. The tail-off aerodynamic center was shifted about 5 or 6 percent rearward and this movement did not vary greatly with tail length. The shift due to trimming was small, destabilizing, and practically invariant with tail length. As expected, the chief effect was the shift due to the change in tail effectiveness which varied from about 7 percent forward for the short tail length to 20 percent forward for the long tail length.

From the data of figure 25, figure 26 was prepared to show the variation of the component parts of the tail-effectiveness term at $C_L = 1.0$ for the model in the cruising configuration. The rate of change of downwash angle with angle of attack $d\epsilon/d\alpha$ generally increased slightly with tail length for the power-off case. With power on, however, $d\epsilon/d\alpha$ increases from 0.55 for the short tail length to 0.85 for the long tail length. The explanation for this large increase with tail length is not known. A possible explanation is that, as the tail length increases, a greater part of the tail is immersed in the slipstream because the tail span decreases with increase in tail length in order to maintain constant tail volume. Inspection of figure 27, for which the tail span was constant, indicates, however, a similar variation of $d\epsilon/d\alpha$ with tail length, although the magnitude of the variation is not quite so large. Theoretical studies have indicated that $d\epsilon/d\alpha$ in the slipstream should not vary greatly with tail length for tail lengths greater than one propeller diameter. Air-flow surveys behind a powered model (fig. 25 of reference 5), however, have shown the same trend for the variation of $d\epsilon/d\alpha$ with tail length as has been found in the present investigation. The analysis of reference 6 indicates that this increase in power-on $d\epsilon/d\alpha$ with tail length is a magnification of the increase in power-off downwash with tail length.

With flaps deflected, the variation with tail length of the neutral-point shift caused by power is in the same direction as with the flaps neutral (fig. 23). The shift at a given tail length, however, is less destabilizing with flaps deflected than with flaps neutral. In fact, for the short tail length, the shift is stabilizing with flaps deflected.

The data of figure 21 indicate that the change in tail-off aerodynamic center caused by power when the flaps are down is large and favorable (about 18 or 20 percent rearward) and does not vary much with tail length. On the basis of the previous discussion, this fact implies that the decrease in tail effectiveness must be much larger in the flap-deflected case than in the flap-neutral case. The values of $d\epsilon/d\alpha$ with

flaps down (fig. 25), however, are about the same as with flaps neutral. Furthermore, these values do not show a consistent variation with tail length. The changes in the tail-effectiveness term of equation (1) are not sufficient to overcome the large change in tail-off aerodynamic center nor to produce the regular variation with tail length of the neutral-point shift due to power. The trim term must, therefore, have an appreciable effect. It is known that the trim term will produce a large destabilizing neutral-point shift with flaps deflected (reference 5). In the present case, computations (not given) have indicated that this effect can be of the same order of magnitude as the tail-off aerodynamic-center movement. These computations have also shown that, with flaps deflected, attributing the variation of neutral-point shift with tail length to the variation of any one term of the equation is not possible. Thus, in one instance, the tail-off aerodynamic-center movement is about equal and opposite to the shift caused by the trim term, and the resultant neutral-point shift is determined by the change in tail effectiveness. In another instance, the change in tail effectiveness is about zero and the resultant neutral-point shift is determined by the difference between the n_o shift and the shift caused by the trim term.

Effect of flap deflection.- The neutral-point shift caused by deflection of the flaps is shown in figure 28. With windmilling propeller, flap deflection resulted in a destabilizing neutral-point shift for the model with the short and normal tail lengths and a stabilizing shift with the long tail length at lift coefficients below about 0.84. The neutral point moved forward as the lift coefficient was increased for the three tail lengths. With power, the neutral-point shift due to flap deflection was small and relatively unaffected by C_L except for the model with the long tail length at high values of lift coefficient at which the shift became increasingly favorable. Stability was increased for the model with the short and long tail lengths but decreased for the model with the normal tail length.

Effect of Tail Length with Constant Tail Area

Neutral points.- For the cruising configuration with power off, the neutral points moved rearward linearly as the tail length was increased (fig. 29). There was very little variation of neutral-point location with lift coefficient for the range tested. With power operation, cruising configuration, this linear relation of n_p with l_t existed only at low values of C_L where the thrust coefficients were small. The neutral-point location moved forward as C_L increased. The neutral-point shift increased as the tail length was increased.

With flaps deflected and propeller windmilling, the stability increased as the tail length increased. The neutral point moved forward with increasing lift coefficient except for the model with the long tail length above a C_L of about 1.4 where a rearward shift with C_L was noted. The model was unstable about the design center-of-gravity location ($0.282\bar{c}$) with the short tail length for most of the lift-coefficient range. For

the landing configuration, power on, the stability was reduced as C_L was increased for the three tail lengths tested. The model was unstable about the design center-of-gravity with the short tail length and exhibited marginal stability with the normal tail length at high values of lift coefficient.

Effect of power.- The displacement of the neutral points caused by the application of power for the case when tail length varied while the tail area remained constant is shown in figure 30. The effects of tail length, with flaps retracted, are similar to those obtained when the tail volume was held constant; that is, the shift in neutral point became more destabilizing as the tail length increased. In this case, the destabilizing effect of tail length also results from the increase in the power-on value of $d\epsilon/d\alpha$ with increase in tail length (fig. 27(b)). The variation of $d\epsilon/d\alpha$ is not quite so great with tail area constant as with tail volume constant because, for the latter condition, the tail span decreased with tail length so that, relatively, the part of the tail immersed in the slipstream increased as the tail length increased.

Inspection of equation (1) indicates that the contribution of the tail-effectiveness term varies directly with tail volume. Since, with a constant-area tail, the tail volume increases with tail length, the destabilizing shift in neutral point would be expected to increase with tail length even if the value of $d\epsilon/d\alpha$ did not vary. This effect may be illustrated by a comparison of the neutral-point shift, at a given tail length, for the condition of constant tail volume (fig. 23) and constant tail area (fig. 30). For the short tail length, the tail volume is greater for the constant-volume condition than for the constant-area condition and, consequently, the neutral-point shift is greater for the constant-volume condition (at $C_L = 1.0$, cruising configuration, $\Delta n_{p_{power}} = -5$ percent M.A.C. for constant volume and -3 percent M.A.C. for constant area). For the long tail length, the tail volume is smaller for the constant-volume condition than for the constant-area condition and the neutral-point shift is smaller for the former condition than for the latter (at $C_L = 1.0$, cruising configuration, $\Delta n_{p_{power}} = -12$ percent M.A.C. for constant volume and -19 percent M.A.C. for constant area).

With flaps deflected, the effect of tail length on the neutral-point shift is qualitatively similar to that obtained with flaps neutral. As in the case with constant tail volume, however, computation indicates that the contribution of the trim term is of considerable magnitude and that the relative influence of each component on the total shift varies in an unpredictable manner with tail length.

Effect of flap deflection.- With windmilling propeller, deflecting the flaps generally caused a forward shift in neutral-point location which increased with lift coefficient and tail length (fig. 31). As expected, ϵ and $d\epsilon/d\alpha$ increased because of flap deflection.

As shown in figures 27(a) and 27(c), the greatest increase in downwash occurred for the model with the short tail length (6.9° with flaps retracted and 9.8° with flaps deflected at $C_L = 0.8$), and the downwash decreased with tail length (5.2° with flaps retracted and 5.3° with flaps deflected for the model with the long tail length at $C_L = 0.8$). The dynamic-pressure ratio decreased because of flap deflection, the change becoming smaller as the tail length was increased. The increment of $\frac{d(q_t/q)}{dC_L}$ was positive and increased with tail length and lift coefficient (figs. 27(a) and 27(c)). Although the adverse effects of propeller slipstream decreased with tail length, the moment arm of the horizontal tail apparently accounts for the increasingly unfavorable shift in n_p with tail length, which increase more than offsets the rearward shift in n_o due to flap deflection (figs. 21(a) and 22).

With power on, flap deflection caused a small destabilizing shift in n_p which decreased as the tail length and lift coefficient were increased; the shift due to flap deflection became stabilizing for the model with the long tail length above lift coefficients of about 0.85 (fig 31(b)). The large forward shift in n_p with increasing C_L for the model with the long tail length in the cruising configuration (fig 22(a)) results in this stabilizing flap-deflection effect. Although the dynamic-pressure ratio increased because of flap deflection, the increment increasing with l_t, the destabilizing decrease in $\frac{d(q_t/q)}{dC_L}$, which was greatest for the model with the short tail length, is believed to have caused the forward shift in n_p (figs. 27(b) and 27(d)). Downwash increased because of flap deflection for the model with the short tail length but remained unchanged for the model with the normal tail length and decreased for the model with the long tail length. This decrease in ϵ for the model with the long tail length justifies the neutral-point results. The variation of downwash with angle of attack was relatively unaffected by flap deflection.

Elevator-free stability.- Stick-free neutral points determined from the elevator-free stabilizer tests (figs. 12, 15, and 18) are presented in figure 32. In the cruising configuration, both with windmilling propeller and with power on, freeing the elevator reduced the stability of the model for the three tail lengths tested, the loss in stability increasing with tail length (about 2.0 percent M.A.C. for the short tail length and 5.0 percent M.A.C. to 7.5 percent M.A.C. for the long tail length). The effects of power with free elevator were similar to those for the model with elevator fixed.

The stick-free neutral points for the landing configuration are not presented because it was found that the tail was operating at a large angle of attack where the slope of the tail lift curve is nonlinear due to a stalled or partially stalled condition and hence the data is not generally applicable. It is believed that tail stall will not occur at full-scale Reynolds numbers because the unstalled angle-of-attack range would be extended.

Effect of Tail Area with Constant Tail Length

Neutral points.- The effect on the neutral-point locations of varying the horizontal-tail area at a given tail length is shown in figures 33 to 35. The change in neutral-point location due to power and flap deflection is presented in figures 36 and 37. The changes in ϵ, $d\epsilon/d\alpha$, q_t/q, and $\frac{d(q_t/q)}{dC_L}$ with tail area are given in figures 38, 39, and 40.

With windmilling propeller and cruising configuration, the neutral point varied linearly with tail area and tail volume at low-lift coefficients (figs. 33 to 35). There was a small variation of n_p with C_L; the neutral point generally moved forward for the model with the small tail and moved rearward for the model with the large tail for the three tail lengths tested. The reason for this variation is believed to be the interference effects, proportionally greatest for the small tail and decreasing with tail area. With power on, cruising configuration, n_p varied nearly linearly with tail area, and tail area had but little effect on the change in n_p with C_L.

For the model in the landing configuration, the neutral-point location moved rearward an amount proportional to the increase in tail area. With the propeller windmilling, the variation of n_p with C_L was relatively unaffected by tail area. With power on, as the tail area was increased, the forward shift in n_p with C_L increased.

Effect of power.- With flaps neutral, and for each of the three tail lengths tested, the neutral-point shift caused by power became more destabilizing as the tail area increased (fig. 36). For these configurations the tail volume, of course, increases with tail area. The increase in the destabilizing neutral-point shift with increase in tail volume has already been noted. That tail volume is the chief factor in the variation of neutral-point shift with tail area is indicated by the variation of the stability parameters (figs. 38, 39, and 40). Thus, $d\epsilon/d\alpha$ and $\frac{d(q_t/q)}{dC_L}$ tend to decrease as tail area increases. Such variations should produce stabilizing neutral-point shifts with increasing tail area, but these variations are relatively small and their effects are masked by the effect of the tail-volume factor.

With flaps deflected, the effect of tail area on the neutral-point shift caused by power reveals no definite trend (fig. 36). For the normal and long tail length, the effect of tail area is relatively small and does not have a consistent trend throughout the lift range. As has been previously noted, the trim term has appreciable influence with flaps down and the effect on the trim term of the variations in q_t/q and $\frac{d(q_t/q)}{dC_L}$ with tail area may be sufficient to balance

the effect of the tail-volume factor. With the short tail length, the effect of tail area is reversed; that is, the neutral-point shift is most stabilizing for the large tail and becomes less stabilizing as the tail area decreases. The trim term is again the determining factor. The large tail gives the greatest value of $d\epsilon/d\alpha$, power on, which fact should result in the greatest destabilizing shift of the neutral point. The value of $\frac{d(q_t/q)}{dC_L}$ for the large tail is very low; consequently, the unfavorable shift caused by the trim term is very much lower for this tail than for the other tails.

In connection with the variation of $d\epsilon/d\alpha$, power on, with tail area for the short tail length, the reason for the much larger values for the large tail than for the small tail is not clear. Normally, the small tail, which has a larger percentage of area in the slipstream, would be expected to give the larger values of $d\epsilon/d\alpha$. Such was the case for the other tail lengths with flaps deflected and also for all tail lengths with flaps neutral.

Effect of flap deflection.- For the three tail lengths tested, increasing the tail area with windmilling propeller resulted in a forward neutral-point shift caused by flap deflection, the shift increasing as the tail length was increased and increasing with tail area as the lift coefficient was increased (fig. 37). With power on, the effect of tail area on the change in neutral-point location due to deflecting the flaps showed no consistent variation with tail length. For the model with the short tail length, the change in n_p due to flap deflection became less destabilizing with increasing tail area and was slightly stabilizing for the model with the large tail. With the normal tail length, tail area had no noticeable effect on $\Delta n_{p_{flap}}$ with power on. For the model with the long tail length the variation of $\Delta n_{p_{flap}}$ with increasing tail area was destabilizing with power on.

LATERAL STABILITY CHARACTERISTICS

Effect of Tail Length on Lateral-Stability Parameters

Tail off.- The effect of tail length on the parameters C_{n_ψ}, C_{l_ψ}, and C_{Y_ψ} of the model with the tail surfaces removed (tail off) is shown in figure 41. Except for the flap-deflected power-on configuration, the parameters were relatively unaffected by the variation in tail length. The application of power for both cruising and landing configurations caused an increase in C_{n_ψ} (destabilizing), an increase in C_{Y_ψ}, and a decrease in the effective dihedral C_{l_ψ}. These are the usual results of the application of power and are caused by the increase in propeller

side force and the velocity over the fuselage and wing. The effects of power do not vary with tail length.

Tail on.- With the tail on, the effect of tail length is reflected chiefly in the directional stability parameter C_{n_ψ}, the values of C_{l_ψ} and C_{Y_ψ} showing almost no change (fig. 42). For the windmilling condition with the flaps either neutral or deflected the value of C_{n_ψ} becomes increasingly stable (more negative) with increasing tail length at low lift coefficients, as is to be expected, but at high lift coefficients shows very little variation with tail length. Inasmuch as the tail-off data do not indicate such changes with lift coefficient, the changes must result from the variation of the tail contribution with lift coefficient and tail length. The contribution of the tail, as indicated by the difference between tail-on and tail-off values of C_{n_ψ}, has been obtained for each tail length and two lift coefficients for the case with flaps neutral and propeller windmilling. Values of the tail contribution were also calculated from the relation

$$\Delta C_{n_{\psi_V}} = -C_{L_{\alpha_V}} v_V \frac{q_V}{q}\left(1 - \frac{\partial\sigma}{\partial\psi}\right) \tag{2}$$

In equation (2) the vertical-tail lift-curve slope $C_{L_{\alpha_V}}$ was taken as 0.035, the value obtained from tests of the isolated tail (fig. 12, reference 1). The value of q_V/q was assumed to be 0.9. In reference 7 $\partial\sigma/\partial\psi$ was measured as -0.6 for a low-wing model. In the present paper this value was reduced to -0.3 to take into account the effects of the horizontal tail and the windmilling propeller, each of which tends to decrease the favorable sidewash. Both experimental and calculated results are given in the following table, and are indicated, respectively, by use of subscripts ex and c:

Tail length	v_V	C_{n_ψ}	$C_{n_{\psi_o}}$	$\left(\Delta C_{n_{\psi_V}}\right)_{ex}$	$\left(\Delta C_{n_{\psi_V}}\right)_c$	$\left(\Delta C_{n_{\psi_V}}\right)_c - \left(\Delta C_{n_{\psi_V}}\right)_{ex}$
$C_L = 0$						
Short	0.0412	-0.00115	0.00055	-0.00170	-0.00169	0.00001
Normal	.0580	-.00175	.00033	-.00208	-.00240	-.00032
Long	.0877	-.00299	.00040	-.00339	-.00359	-.00020
$C_L = 1.0$						
Short	0.0412	-0.00103	0.00032	-0.00135	-0.00169	-0.00034
Normal	.0580	-.00145	.00018	-.00163	-.00240	-.00077
Long	.0877	-.00151	.00061	-.00212	-.00359	-.00147

Inspection of the table shows that at $C_L = 0$ the tail contributions obtained experimentally are in fair agreement with the computed values. This agreement is coincidental in view of the assumptions, but it indicates that the tail contributions are as large as can be expected. For $C_L = 1.0$, the experimental tail contributions are considerably lower than the computed values. This loss in tail effectiveness may result either from a reduction in dynamic pressure or an increasingly unfavorable sidewash as the lift coefficient increases. The interference data of reference 8 indicate that any sidewash present will probably remain constant throughout the lift range. The loss in tail effectiveness is therefore more likely caused by the fact that part of the vertical tail is in the wake of the canopy. The part of the tail in the wake would increase with increase in angle of attack and with increase in tail length and could, therefore, account for the observed effects.

The application of power (fig. 42) caused a stabilizing increase in C_{n_ψ} which became larger with increase in lift coefficient and with tail length. The increase of C_{n_ψ} with lift coefficient results from the increase in slipstream velocity over the tail. The increase of C_{n_ψ} with tail length is a logical consequence of the increment of tail load caused by power which, when multiplied by increasing moment arms, results in increasing values of C_{n_ψ}.

Deflection of the flaps was found to increase the directional stability C_{n_ψ} slightly for both the power-off and power-on cases, the change in C_{n_ψ} due to flap deflection increasing as the tail length was increased. Flap deflection usually results in a favorable increment of sidewash which tends to increase the lift on the tail (reference 7). This lift increment in conjunction with the increasing tail-moment arms may explain the greater stabilizing flap effect with the longer tail lengths.

Effect of Tail Length at Large Yaw Angles

Tail off.- The slopes of the yawing-moment curves near $\psi = 0$ of the model with tail off are unstable (figs. 43 to 46). The values of C_{n_ψ} are in general agreement with the values of C_{n_ψ} obtained in the parameter tests (fig. 41) and indicate very little variation with tail length. For any given power or flap deflection, the unfavorable yawing moments at large angles of positive yaw tend to decrease with tail length. At the negative yaw angles, the yawing moment is largest for the normal tail length. These variations of tail-off yawing moment are significant in connection with the occurrence of rudder lock since this effect depends on whether the tail with rudder free can provide sufficient yawing moment to overcome the adverse wing-fuselage moments.

The application of power increased the unstable slopes of the yawing-moment curves. This increase showed no large or consistent variation

with tail length. A further effect of power was the introduction of asymmetry in the yawing-moment curves at zero angle of yaw. This asymmetry was largest on the model with the normal tail length.

Tail on, rudder fixed.- With tail on, rudder fixed, the data of figures 43 to 46 show the effect of increasing tail length on the directional stability. The values of C_{n_ψ} near zero yaw for the windmilling propeller condition are in fair agreement with the values of C_{n_ψ} obtained in the parameter tests (fig. 42). There is no agreement, however, between the two sets of values with power on. Such results are to be expected, since the yawing-moment curves for the power-on condition are not linear between $\psi = \pm 5^\circ$ as was assumed in the parameter tests.

With windmilling propeller (figs. 43 and 45), the yawing-moment curves indicate a tail stall at about $\psi = \pm 14^\circ$. The severity of this stall condition seems to decrease as the tail length increases. In fact, with flaps deflected, the yawing moments for the long tail length are fairly linear through a yaw range of $\pm 25^\circ$. Tests of the isolated vertical tail (reference 1) indicate that it stalls at an angle of attack of about 20° and that the lift remains fairly constant beyond the stall. The decrease in tail-off yawing moments at large yaw angles with increase in tail length combined with the indicated tail lift characteristics are thus responsible for the smoothing out of the tail-on curves.

The fact that the tail stalls on the model at 14°, whereas the isolated vertical tail stalls at 20°, indicates a favorable sidewash of 6° at this angle of yaw. These figures result in a value of $\frac{\partial \sigma}{\partial \psi} = -0.4$ if the sidewash is assumed to be linear in this yaw range.

Since the tests with power on were made at different angles of attack than were the tests with power off, only a qualitative examination of the effects of power can be made. With power on, a large asymmetrical yawing moment is present at zero yaw (figs. 44 and 46). Part of this asymmetric moment results from the slipstream effects on the wing-fuselage combination. (See tail-off curves.) Most of the moment, however, is caused by the effect of the slipstream rotation on the tail; that is, because of the rotation of the slipstream the tail has an appreciable angle of attack and, consequently, gives lift. This lift, of course, produces an increasingly larger yawing moment as the tail length increases.

The power-on yawing-moment curves (figs. 44 and 46) exhibit sharp breaks at very small angles of positive yaw and at moderate angles of negative yaw. Although these breaks may result, in part, from the changes in sidewash associated with power, the major effect is believed to be caused by the lateral displacement of the slipstream. The wing tends to

split the slipstream, and the lateral component of the rotation (for right-hand rotation) moves the upper portion of the slipstream to the right and the lower portion to the left. The vertical tail is affected chiefly by the upper portion, and since this portion has shifted to the right, only a small movement of the tail to the left (positive yaw) is required to cause the tail to move out of the slipstream. At moderate angles of negative yaw, the tail will move beyond the slipstream in the right-hand direction. When the tail leaves the slipstream, the dynamic pressure at the tail decreases and tail lift, and, therefore, yawing moment, are consequently reduced. Because the lateral movement of the slipstream presumably increases as the distance back from the propeller increases, the value of positive yaw at which the tail leaves the slipstream should decrease with increase in tail length, and the value of negative yaw should increase. The test data indicate, however, that although the values of positive yaw decrease, the values of negative yaw either do not change or tend to decrease with increase in tail length; that is, the range of yaw angles for which the tail is in the slipstream decreases with increase in tail length. This condition probably results from the fact that the lateral movement of the tail for a given change in yaw angle increases as the tail length increases so that the tail may be expected to move out of the slipstream more quickly in either direction for the longer tail lengths.

Tail on, rudder free.- At small angles of yaw the changes in directional stability C_{n_ψ} caused by freeing the rudder are small for all conditions (figs. 43 to 46) except for the case with the short tail length, flaps deflected and power on (fig. 46(a)). For this case, the yawing-moment curve showed an unaccountable decrease in stability when the rudder was freed. In general, if the rudder floats with the wind, the stability may be expected to decrease and this decrease should become larger with increase in tail length. If the rudder floats against the wind, the stability should be increased and this increase should become greater as the tail length is increased. The present rudder evidently has very little tendency to float since the stability changes are small.

The yawing moments of a model with the rudder free are a function of the hinge-moment characteristics of the rudder. At small angles of yaw, the hinge moments and, therefore, the yawing moments will depend on the type and amount of aerodynamic balance used on the rudder, and for that reason the application of the present results are more or less limited to configurations similar to the ones tested in the present investigation. At very large angles of yaw, the hinge-moment characteristics of most balances are such that the rudder floats with the wind and, at these large yaw angles, will usually be against the stop. The yawing moments at large angles of yaw will, therefore, be considerably less dependent on the balance arrangement. The effect of tail length on the tendency toward rudder lock as indicated by the present data should thus be generally applicable to other configurations.

With power off, no rudder lock was present with flaps deflected for all tail lengths (fig. 45). With flaps neutral and the short tail length, rudder lock existed at large angles of both positive and negative yaw (fig. 43(a)). As the tail length increased, however, the angles of yaw at which the rudder lock occurred increased. This increase was more rapid for the positive yaw angles than the negative yaw angles. With the long tail length, the rudder lock was eliminated entirely. The decrease in the tendency toward rudder lock as the tail length increases results from two effects. First, the adverse yawing moments of the wing-fuselage combination tend to decrease (in the positive yaw range) as the tail length increases so that a smaller tail contribution is required to avoid rudder lock when the tail length is greater. Second, whatever resultant force the stalled tail with the rudder free possesses at the large yaw angles is reflected in increasingly larger tail yawing moments as the tail length increases because of the increasing tail-moment arm.

With power on and with flaps either neutral or deflected, the model with the short tail length exhibits marked rudder lock at both positive and negative yaw angles (figs. 44(a) and 46(a)). The positive angle at which rudder lock occurs increases rapidly as the tail length is increased, so that with the long tail length there is no rudder lock present in the positive yaw range. In the negative yaw range there is no marked effect of tail length on the angle at which rudder lock occurs, although with flaps deflected there was a tendency for this yaw angle to increase as the tail length increased (fig. 46). The fact that increasing tail length is ineffective in reducing the rudder-lock tendency probably results because the tail moves out of the slipstream somewhat sooner as the tail length increases so that the increase in tail yawing moment caused by the increase in tail-moment arm is more or less balanced by a decrease caused by the reduction in dynamic pressure.

With power on, the rudder-free yawing-moment curves are considerably out of trim at $\psi = 0$. It might appear that if the moment were trimmed at $\psi = 0$ by means of tab deflection, the rudder-lock condition would improve. The data of reference 1 indicate, however, that because the tab becomes ineffective beyond tail stall, very little improvement of the rudder-lock condition is obtained.

CONCLUSIONS

The investigation of a model of a single-propeller, low-wing, fighter airplane with various tail lengths indicated the following conclusions:

1. The destabilizing shift in neutral point caused by power increased with increasing tail length for either the condition of constant horizontal-tail volume or constant horizontal-tail area.

2. For a given tail length, the destabilizing shift in neutral point caused by power increased with increasing tail area.

3. The increase in directional stability caused by power became larger as the tail length was increased.

4. At positive angles of yaw the tendency toward rudder lock decreased as the tail length increased. In the negative yaw range, variation of tail length had practically no effect on rudder lock.

Langley Aeronautical Laboratory
National Advisory Committee for Aeronautics
Langley Field, Va., September 15, 1948

REFERENCES

1. Purser, Paul E., and Spear, Margaret F.: Tests to Determine Effects of Slipstream Rotation on the Lateral Stability Characteristics of a Single-Engine Low-Wing Airplane Model. NACA TN No. 1146, 1946.

2. Purser, Paul E., and Spear, Margaret F.: Wind-Tunnel Investigation of Effects of Unsymmetrical Horizontal-Tail Arrangements on Power-On Static Longitudinal Stability of a Single-Engine Airplane Model. NACA TN No. 1474, 1947.

3. Gillis, Clarence L., Polhamus, Edward C., and Gray, Joseph L., Jr.: Charts for Determining Jet-Boundary Corrections for Complete Models in 7- by 10-Foot Closed Rectangular Wind Tunnels. NACA ARR No. L5G31, 1945.

4. Schuldenfrei, Marvin: Some Notes on the Determination of the Stick-Fixed Neutral Point from Wind-Tunnel Data. NACA RB No. 3I20, 1943.

5. Wallace, Arthur R., Rossi, Peter F., and Wells, Evalyn G.: Wind-Tunnel Investigation of the Effect of Power and Flaps on the Static Longitudinal Stability Characteristics of a Single-Engine Low-Wing Airplane Model. NACA TN No. 1239, 1947.

6. Weil, Joseph, and Sleeman, William C., Jr.: Prediction of the Effects of Propeller Operation on the Static Longitudinal Stability of Single-Engine Tractor Monoplanes with Flaps Retracted. NACA TN No. 1722, 1948.

7. Recant, Isidore G., and Wallace, Arthur R.: Wind-Tunnel Investigation of the Effect of Veterical Position of the Wing on the Side Flow in the Region of the Vertical Tail. NACA TN No. 804, 1941.

8. Recant, I. G., and Wallace, Arthur R.: Wind-Tunnel Investigation of Effect of Yaw on Lateral-Stability Characteristics. IV - Symmetrically Tapered Wing with a Circular Fuselage Having a Wedge-Shaped Rear and a Vertical Tail. NACA ARR, March 1942.

TABLE I

PHYSICAL CHARACTERISTICS OF THE SINGLE-PROPELLER AIRPLANE MODEL

Wing and Tail-Surface Data

	Wing	Small horizontal tail	Normal horizontal tail	Large horizontal tail	Vertical tail
Area, sq ft	9.40	1.44	2.15	2.99	1.25
Span, ft	7.51	2.72	3.33	3.93	1.34
Mean aerodynamic chord, ft	1.31	0.55	0.68	0.80	1.03
Root chord, ft	1.68	0.69	0.84	1.00	1.35
Theoretical tip chord, ft	0.84	0.39	0.47	0.56	0.59
Aspect ratio	6.00	5.17	5.17	5.17	1.30
Taper ratio	2.00	1.79	1.79	1.79	----
Dihedral of chord plane, deg					
Inboard panel	-0.73	0	0	0	----
Outboard panel	7.75	0	0	0	----
Sweepback at quarter-chord lines, deg	0	----	----	----	----
Root section	NACA 66(215)-216	NACA 65(216)-015.4 (modified)[a]	NACA 65(216)-015.4 (modified)[a]	NACA 65(216)-015.4 (modified)[a]	NACA 64,2-015 (modified)[a]
Tip section	NACA 66(215)-216	NACA 65(216)-012 (modified)[a]	NACA 65(216)-012 (modified)[a]	NACA 65(216)-012 (modified)[a]	NACA 64(215)-012 (modified)[a]
Incidence from root to tip, deg	0	----	----	----	----

Tail Length and Tail-Volume Data

	Small horizontal tail	Normal horizontal tail	Large horizontal tail	Vertical tail
Tail lengths, l_t and l_v, ft				
Short tail length	2.42	2.42	2.42	2.33
Normal tail length	3.37	3.37	3.37	3.27
Long tail length	5.04	5.04	5.04	4.95
Tail volume ratios, $S_t l_t/Sc$ and $S_v l_v/Sb$				
Short tail length	0.282	0.423	0.588	0.041
Normal tail length	0.393	0.588	0.817	0.058
Long tail length	0.588	0.880	1.223	0.088

Control-Surface Data

	Elevators[b]	Rudder
Area, behind hinge line, sq ft	0.592	0.371
Balance area, sq ft	0.158	0.102
Root-mean-square chord, ft	0.198	0.320
Control deflection, deg	30 up 20 down	30 right 30 left

[a]Straight-line contour behind hinge line
[b]Normal horizontal tail

TABLE II

TEST CONDITIONS

Model	Dynamic pressure (lb/sq ft)	Air-speed (mph)	Test Reynolds number	Turbu-lence factor	Effective Reynolds number
Complete, windmilling propeller and flaps up, power on	16.37	80	1.00×10^6	1.6	1.600×10^6
Complete, flaps down, power on	9.21	60	.750	1.6	1.200
Isolated small hori-zontal tail	15.00	76	.382	1.93	.740
Isolated normal horizontal tail	13.00	71	.415	1.93	.800
Isolated large hori-zontal tail (semispan)	15.00	76	.548	1.93	1.060

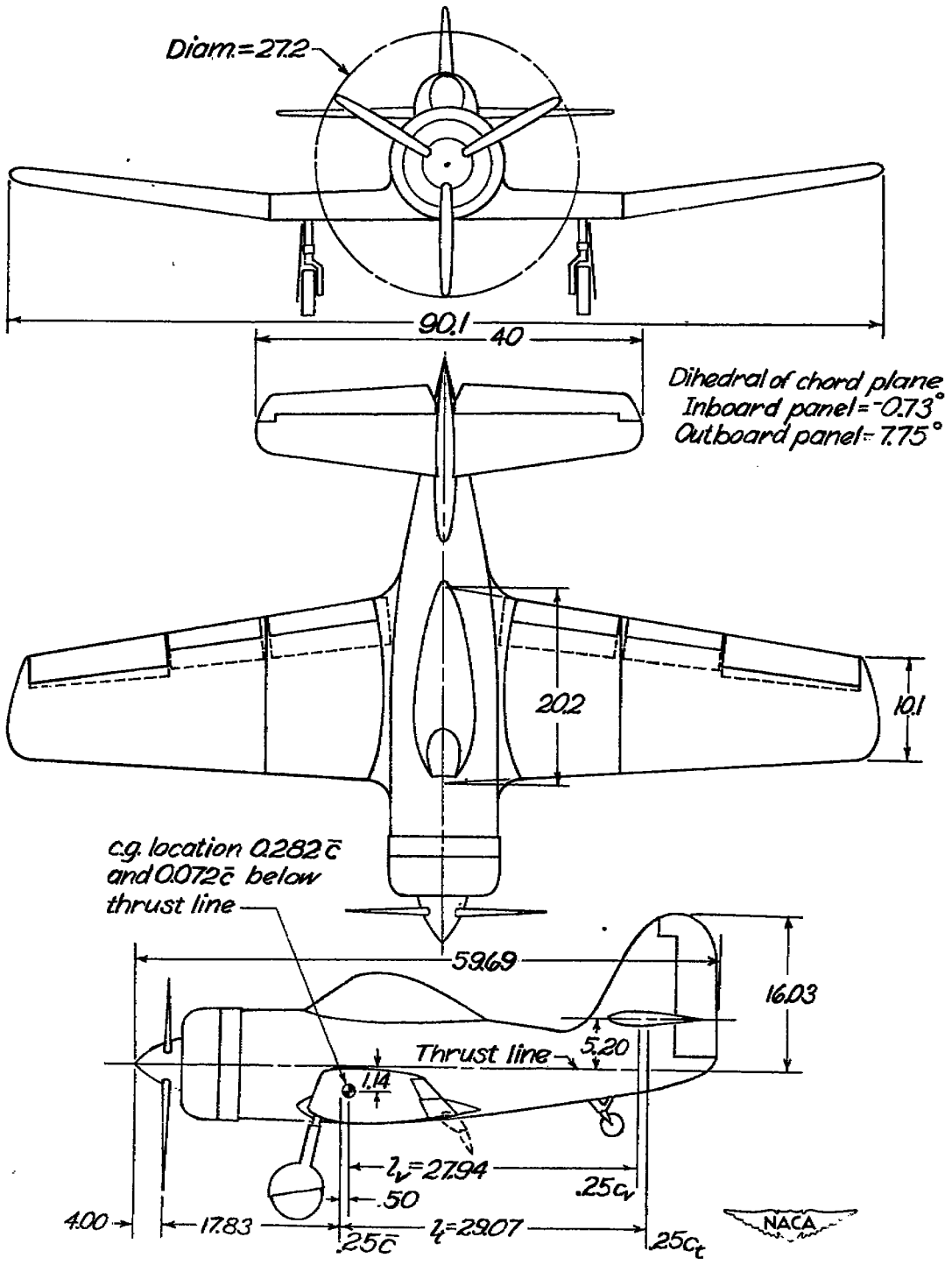

(a) Short tail length.

Figure 1.- Drawings of the single-propeller airplane model showing the three tail lengths tested. Normal horizontal tail. (All dimensions are in inches.)

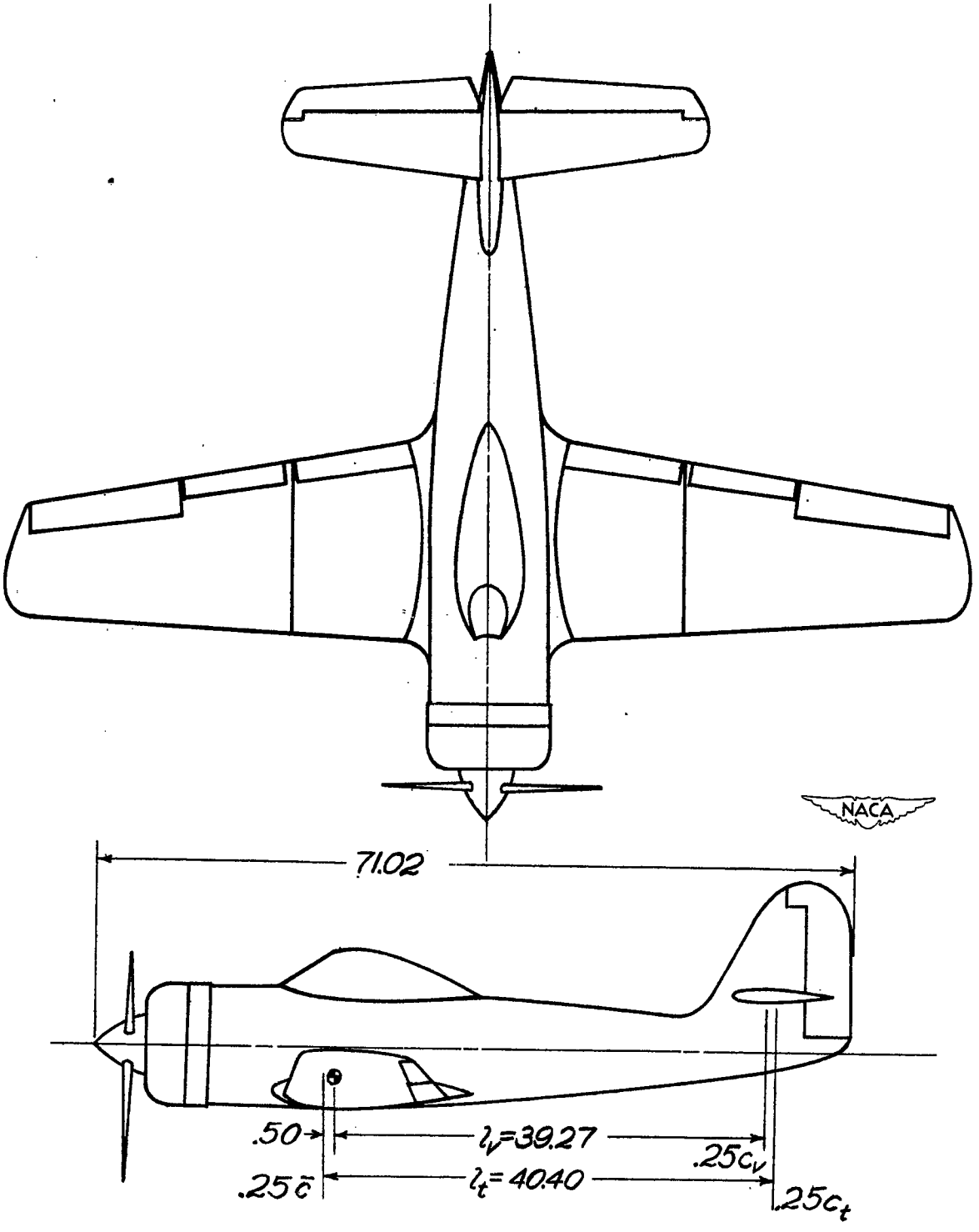

(b) Normal tail length.

Figure 1.- Continued.

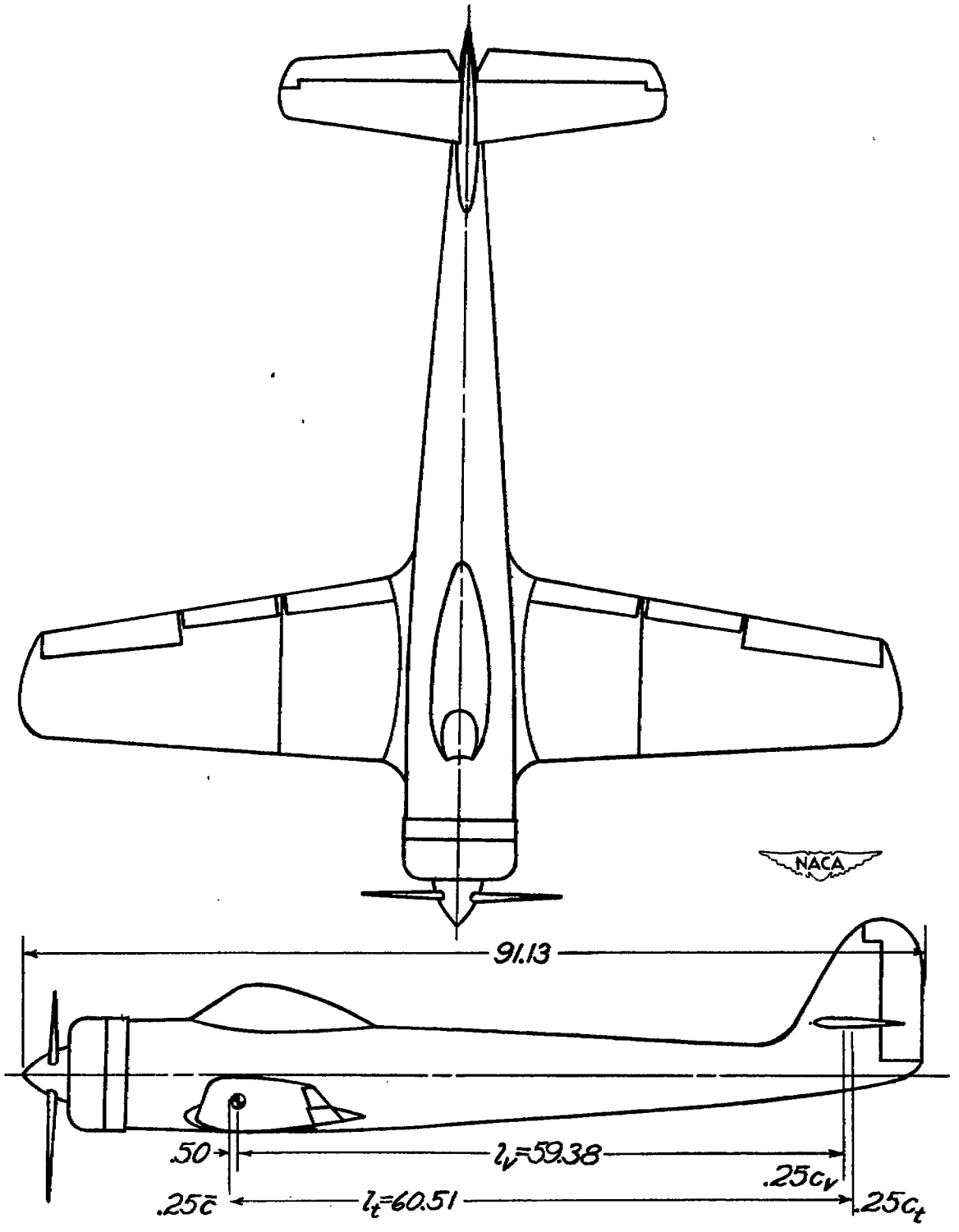

(c) Long tail length.

Figure 1.- Concluded.

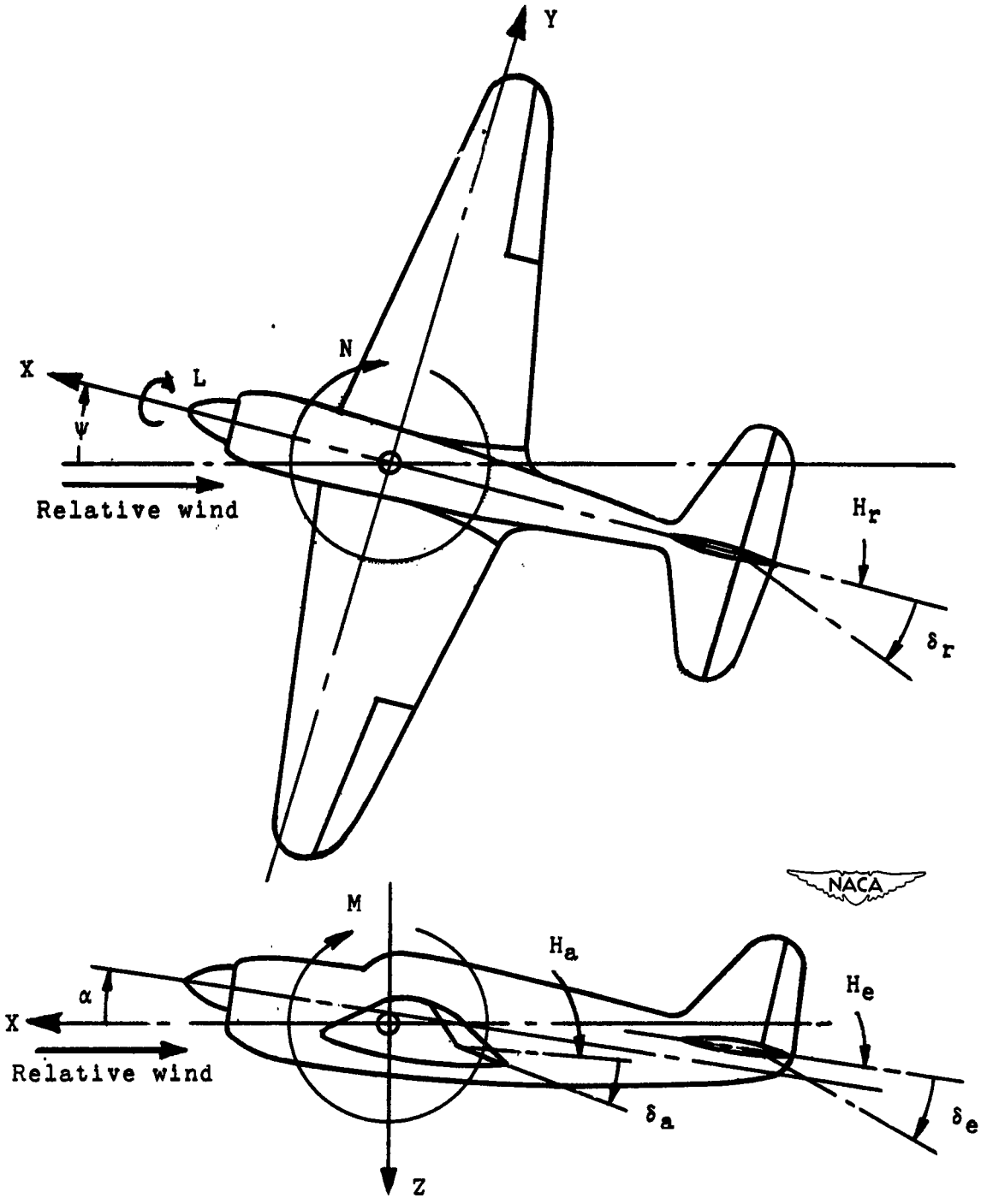

Figure 2.- System of axes and control-surface hinge moments and deflections. Positive values of forces, moments, and angles are indicated by arrows. Positive values of tab hinge moments and deflections are in the same directions as the positive values for the control surfaces to which the tabs are attached.

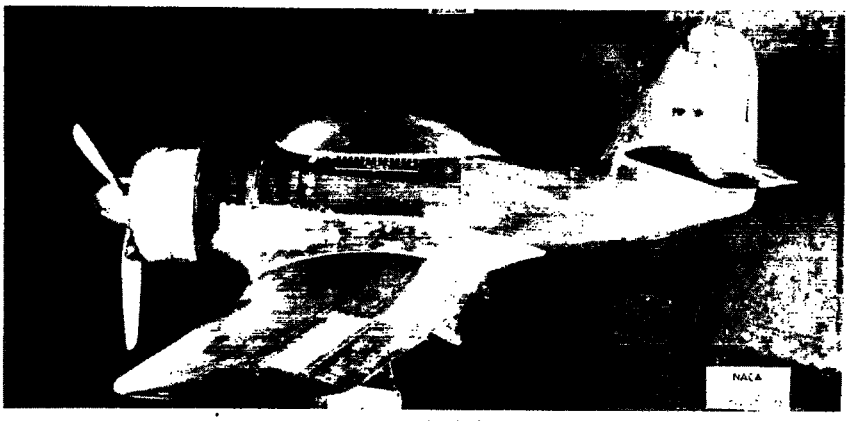

(a) Short tail length. $\frac{l_t}{c} = 1.85$.

(b) Normal tail length. $\frac{l_t}{c} = 2.57$.

(c) Long tail length. $\frac{l_t}{c} = 3.85$.

Figure 3.- Photographs of the single-propeller airplane model showing the three tail lengths tested.

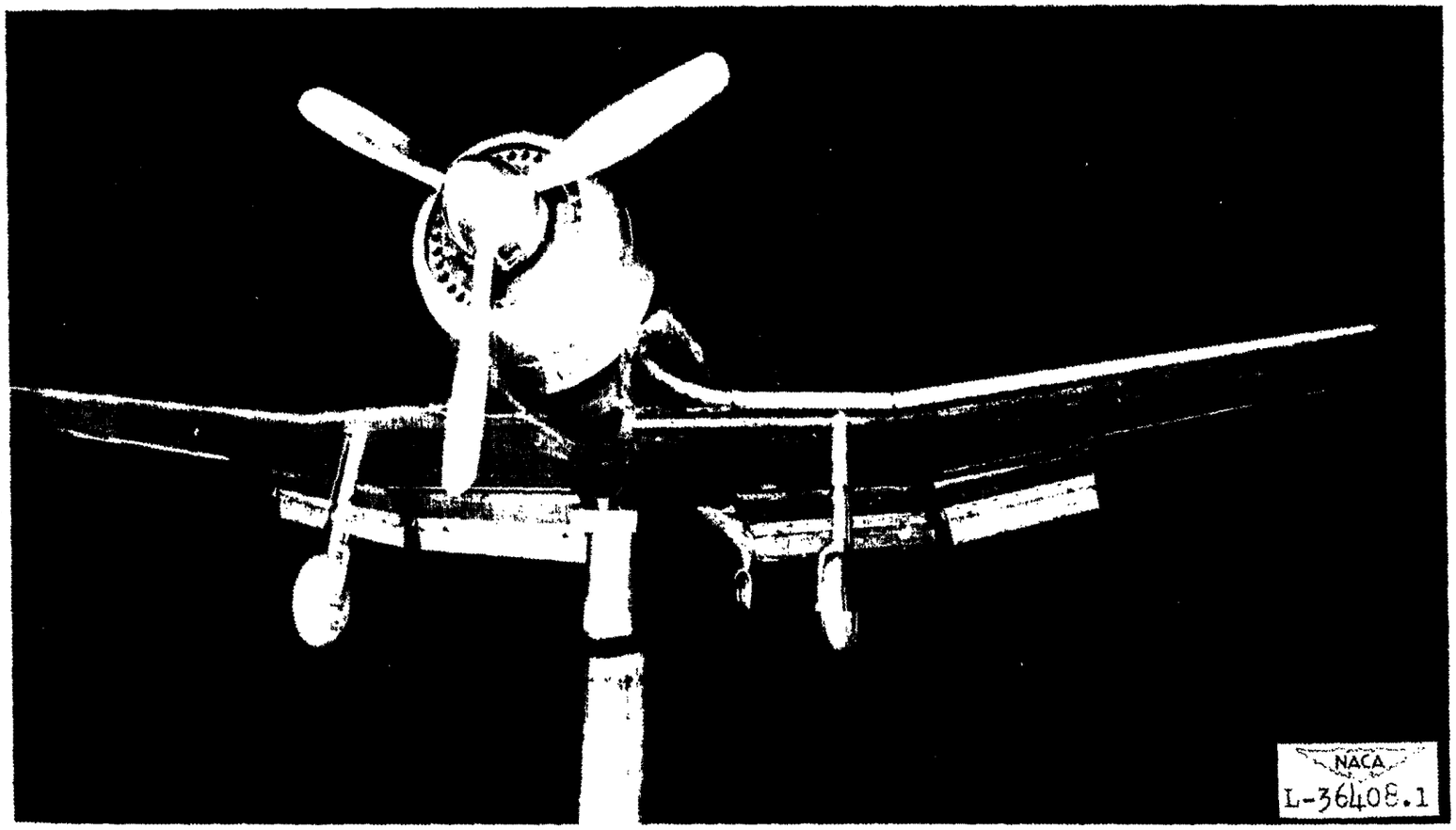

(d) Normal tail length, landing configuration.

Figure 3.- Concluded.

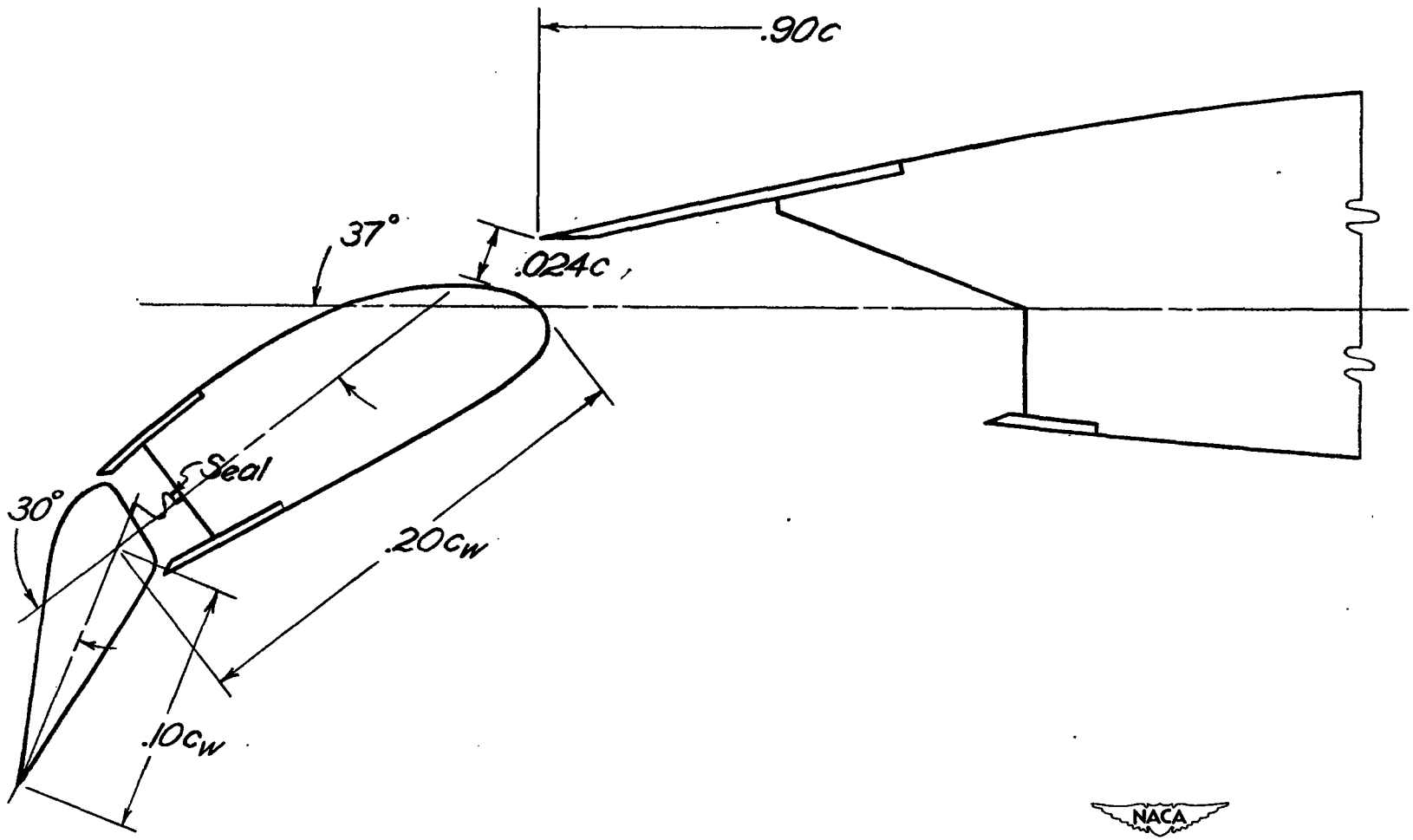

Figure 4.- Typical section of the slotted and plain flap arrangement used for tests of the single-propeller airplane model in the landing configuration.

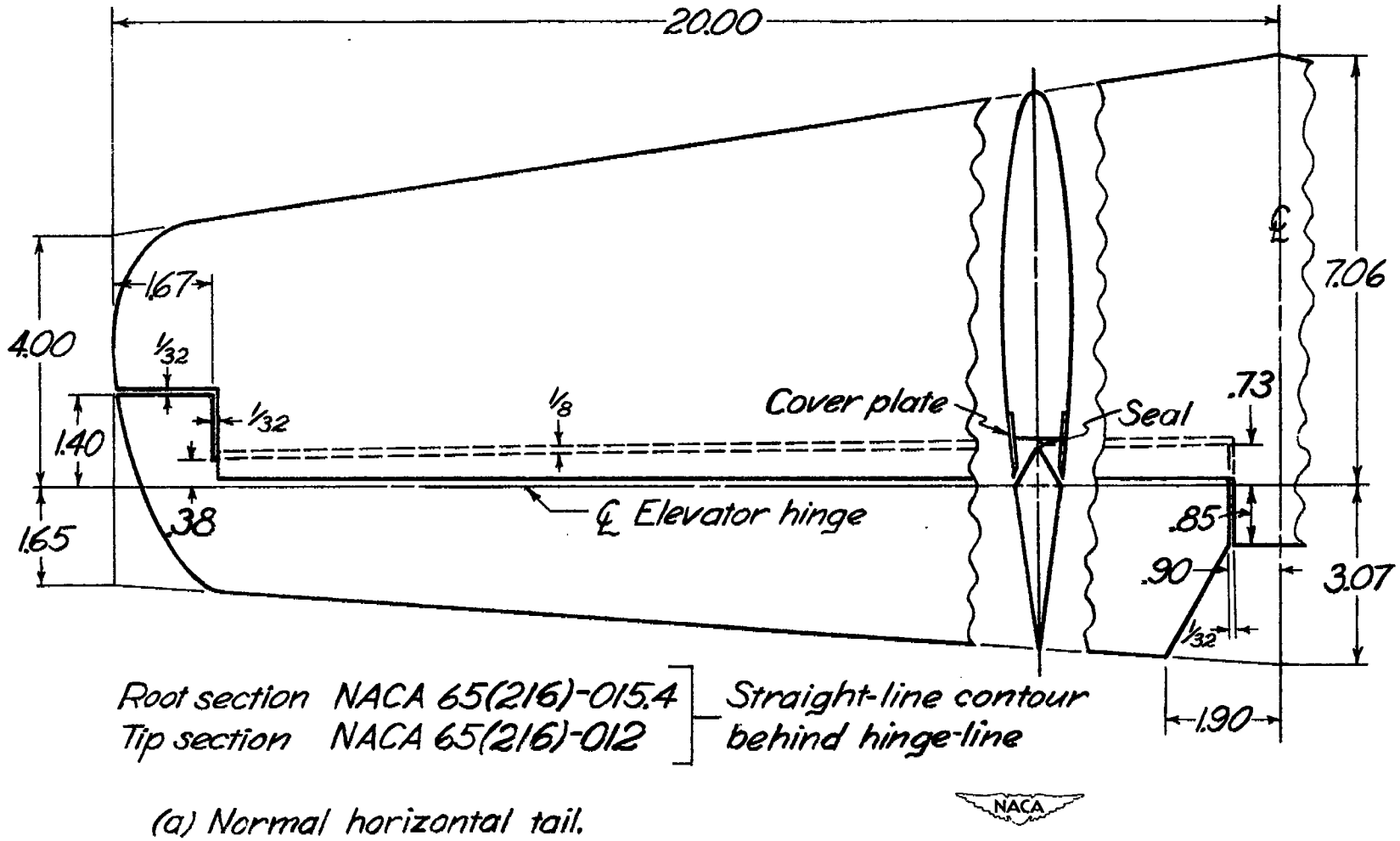

Figure 5.- Drawings of the horizontal tails used for tests of the single-propeller airplane model. (All dimensions are in inches.)

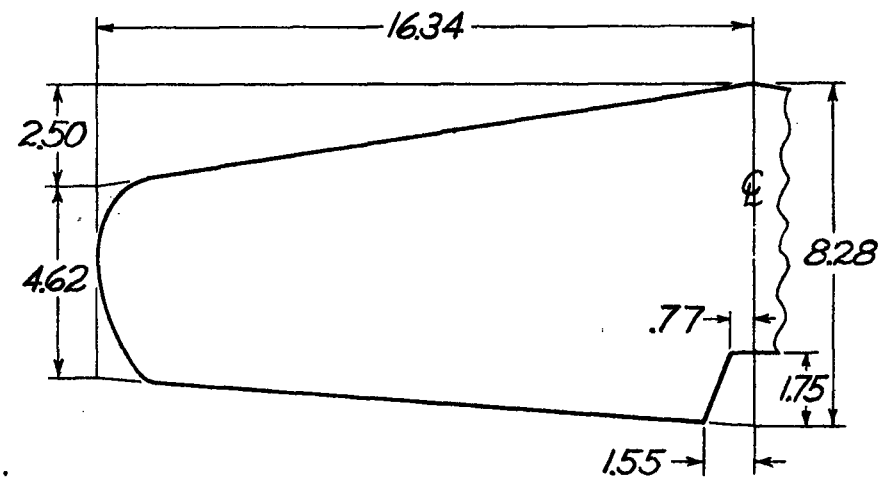

(b) Small horizontal tail.

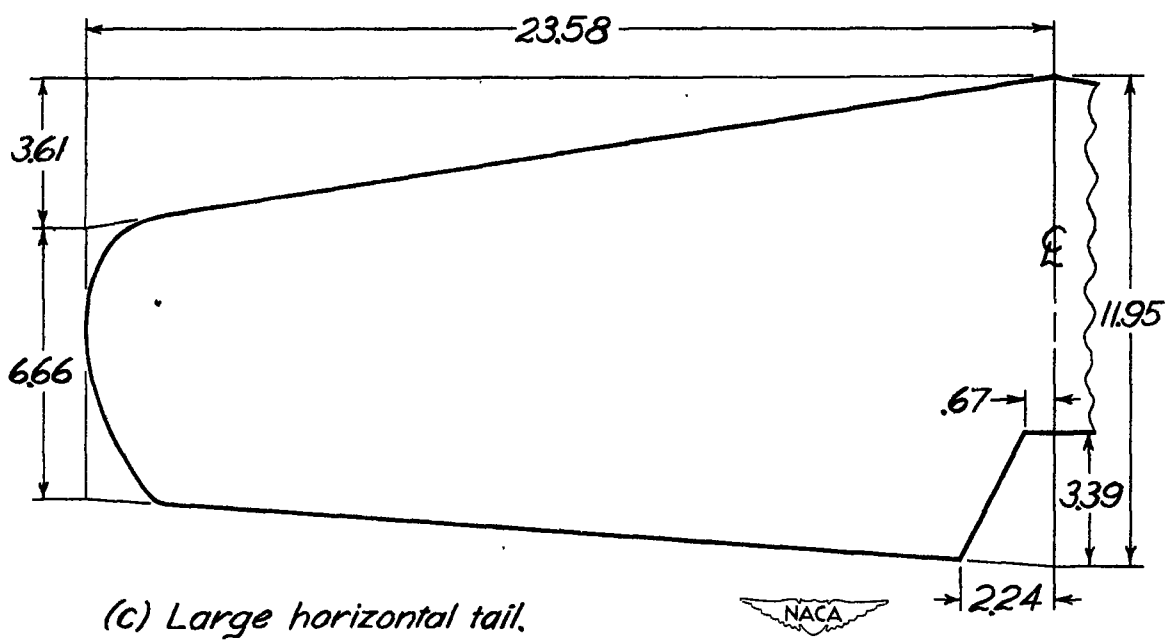

(c) Large horizontal tail.

Figure 5.- Concluded.

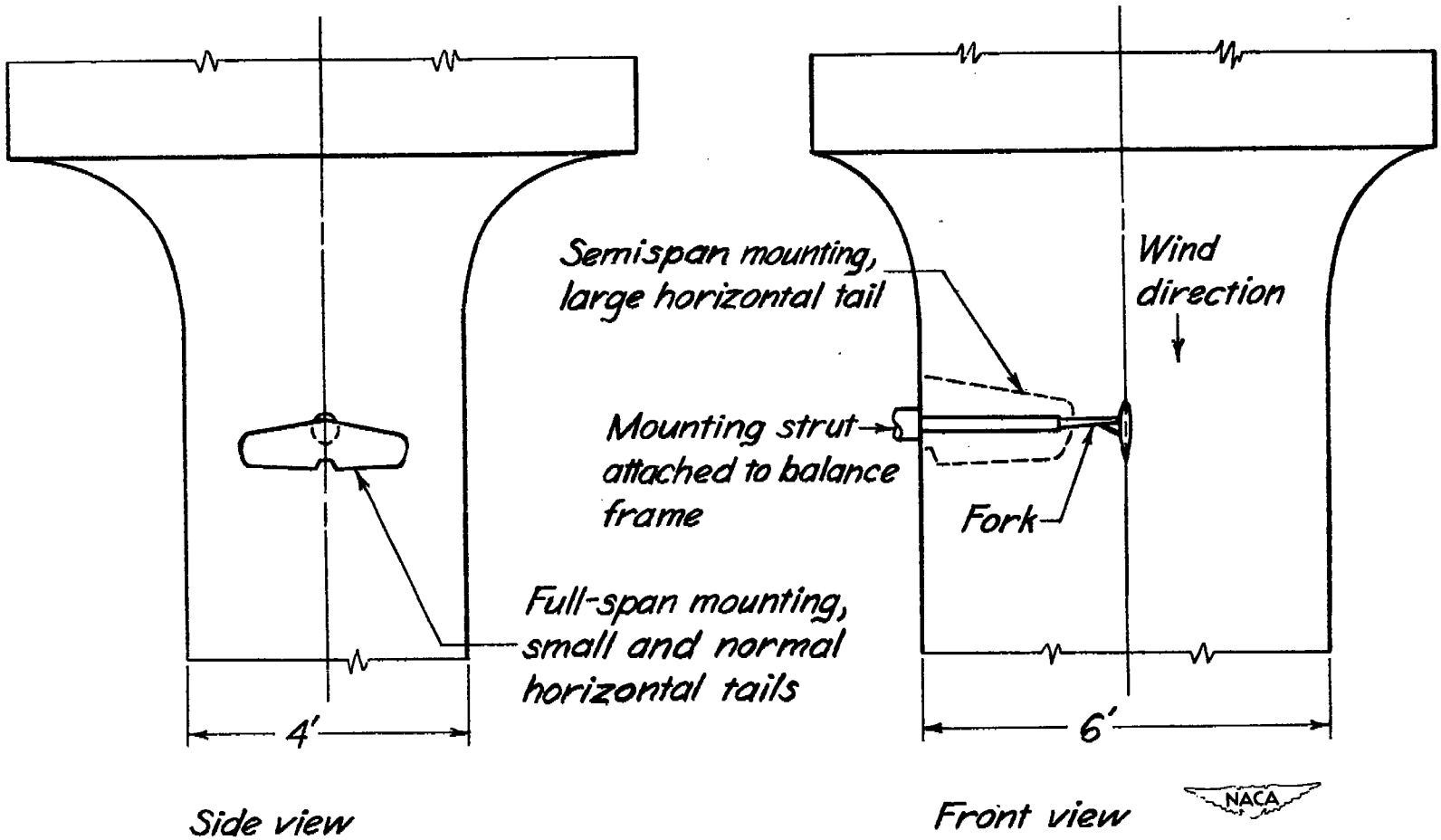

Figure 6.- Views of the test section of the Langley 4- by 6-foot vertical tunnel showing the mounting of the isolated horizontal-tail surfaces.

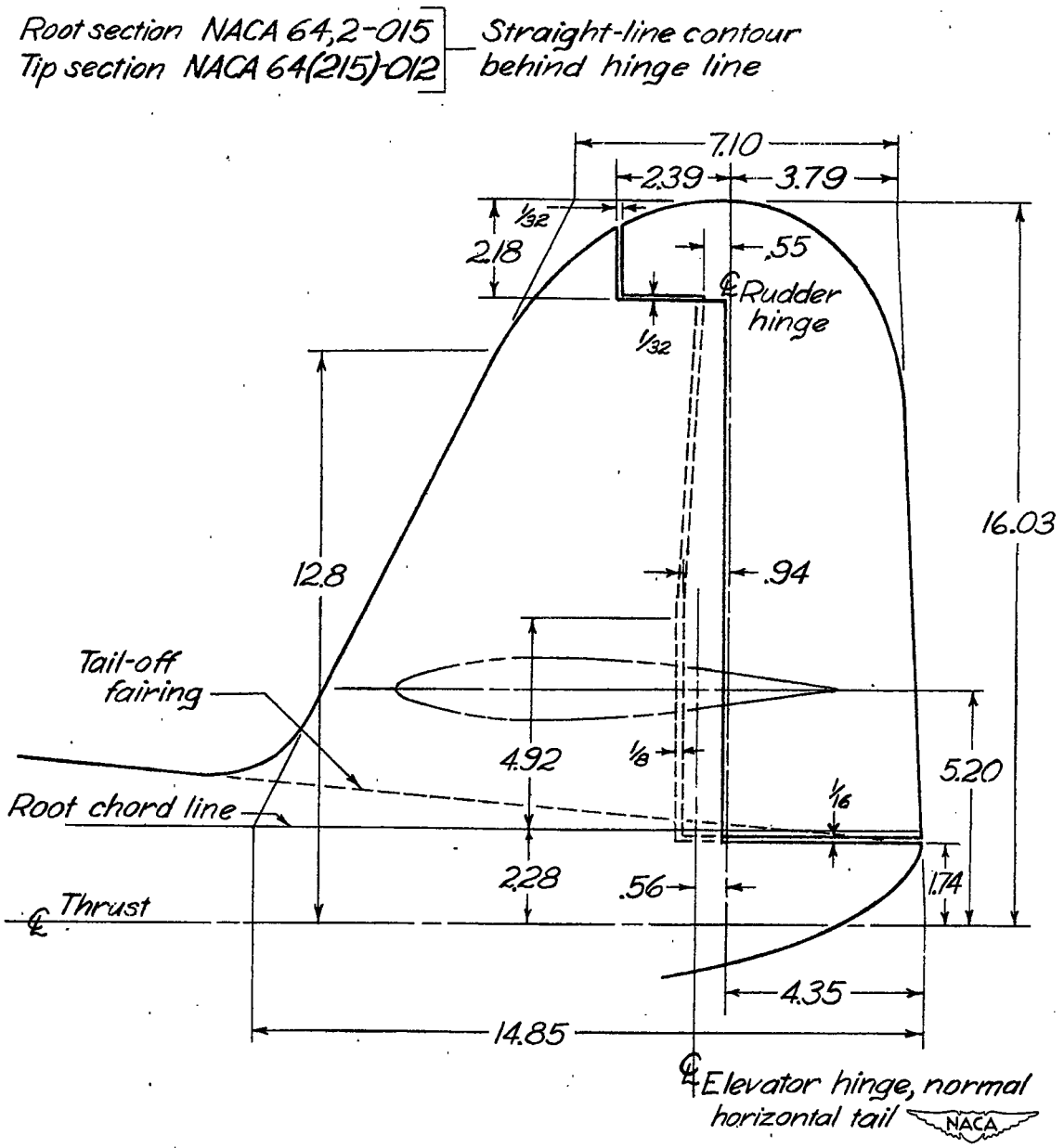

Figure 7.- Plan view of the vertical tail used for tests of the single-propeller airplane model. (All dimensions are in inches.)

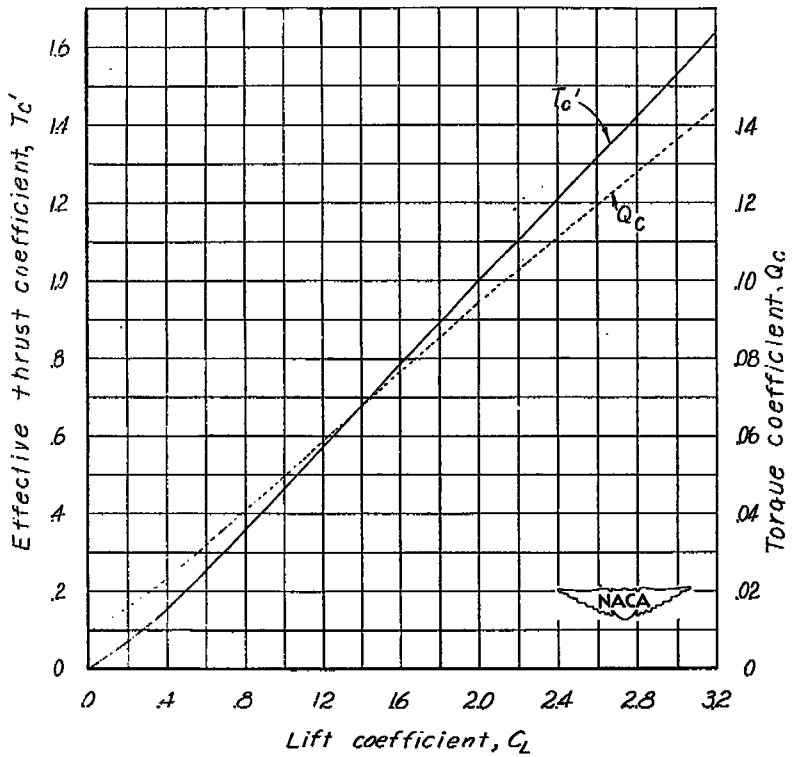

Figure 8.- Thrust and torque coefficients for the single-propeller airplane model.

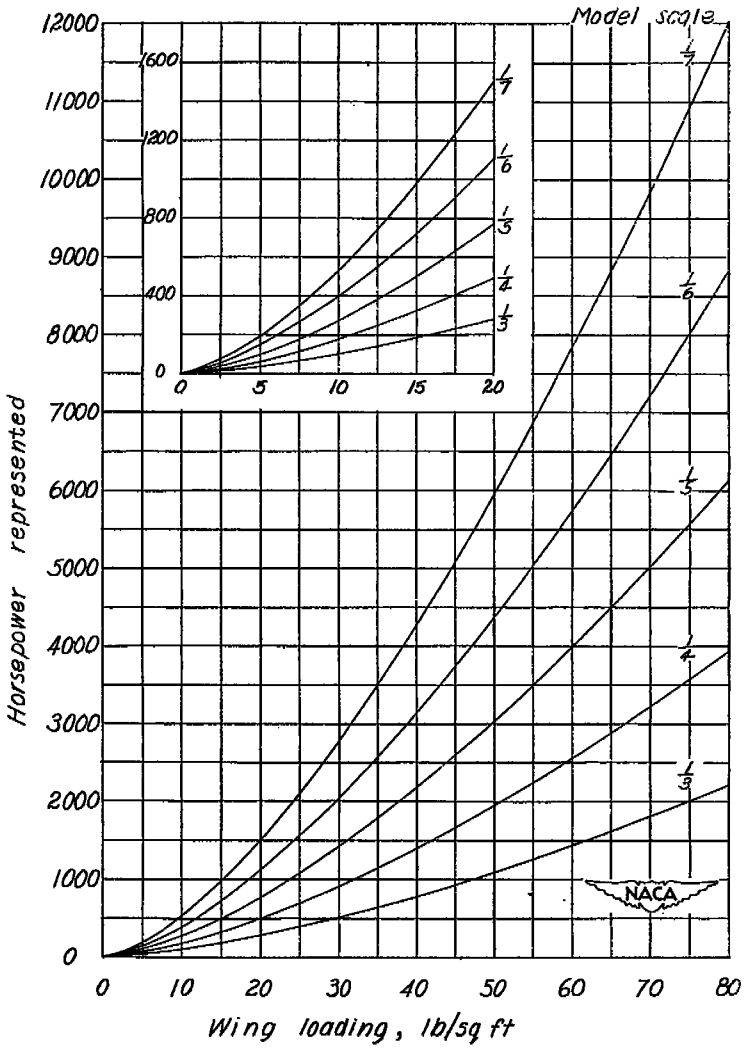

Figure 9.- Horsepower represented for various wing loadings and model scales.

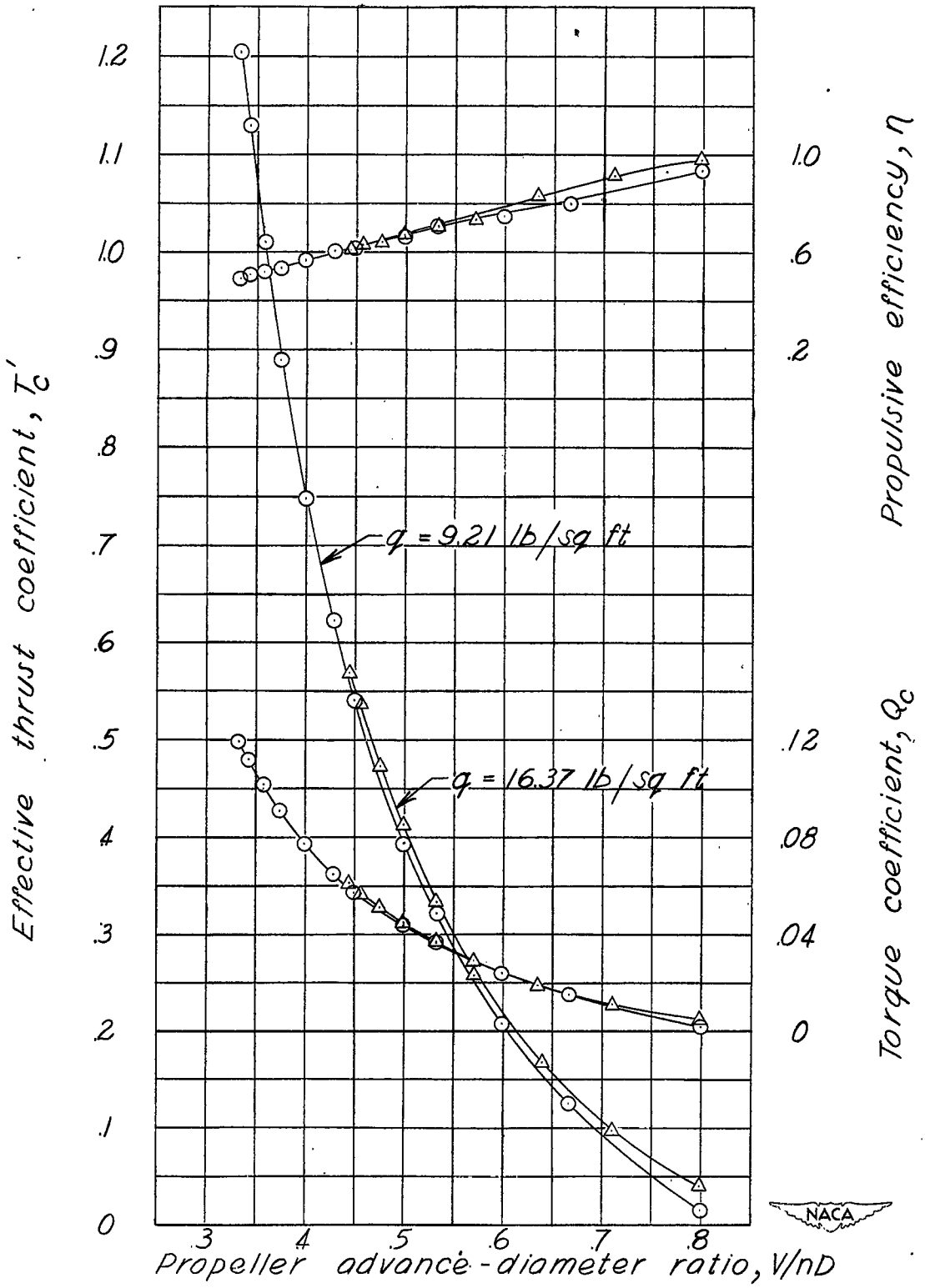

Figure 10.- Propeller calibration of the single-propeller airplane model. Cruising configuration; $\alpha = 0^{\circ}$.

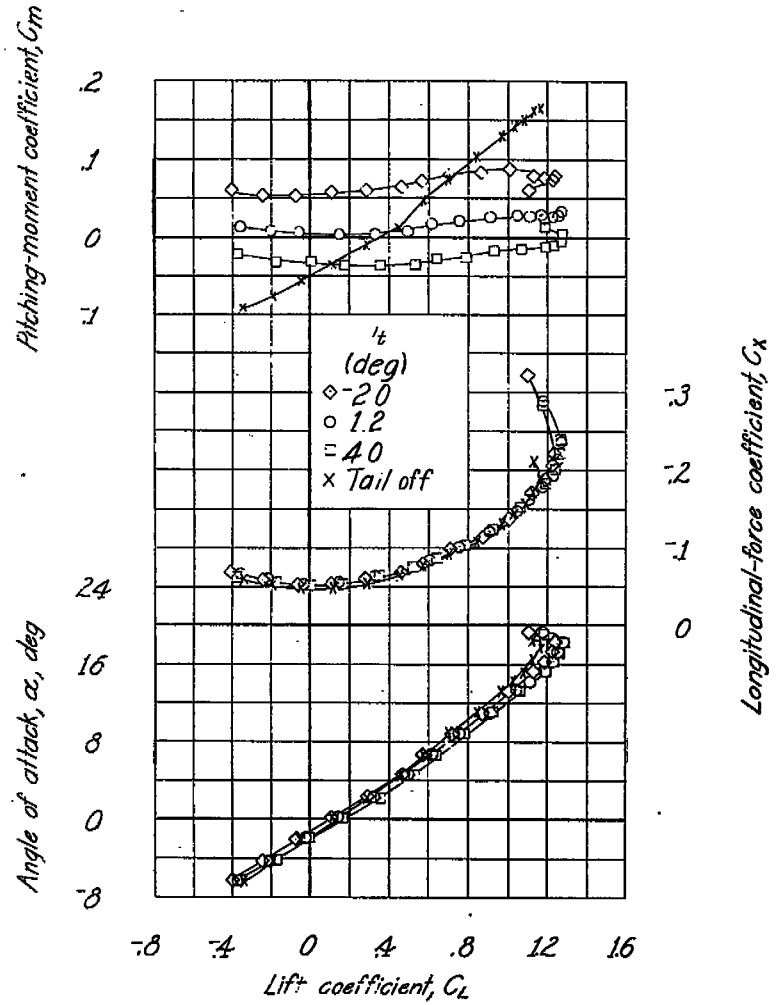

(a) Cruising configuration, windmilling propeller.

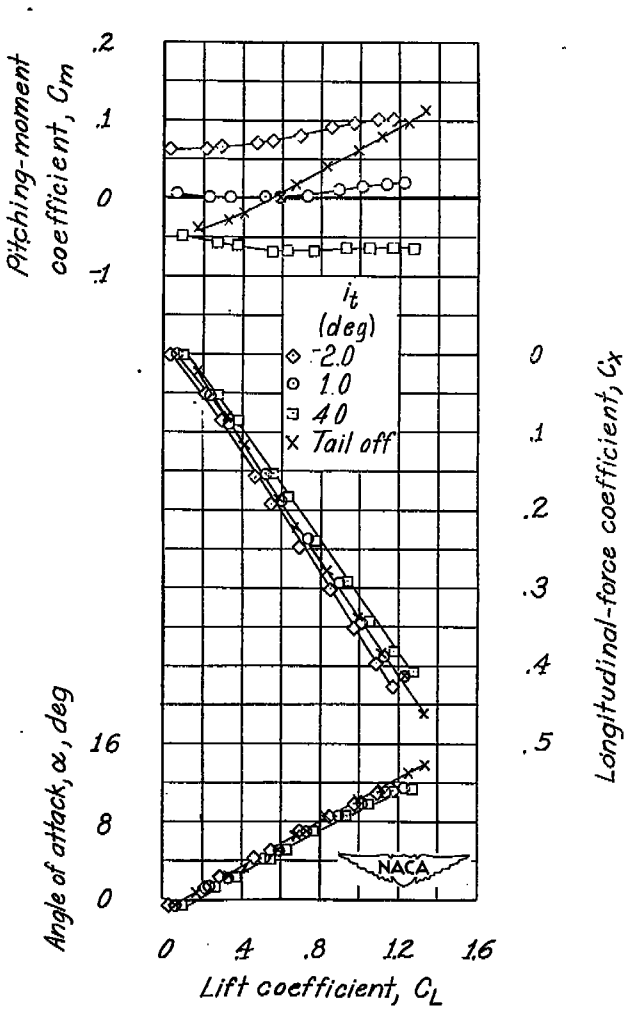

(b) Cruising configuration, power on.

Figure 11.- Effect of the small horizontal tail on the longitudinal characteristics of the single-propeller airplane model with the short tail length.

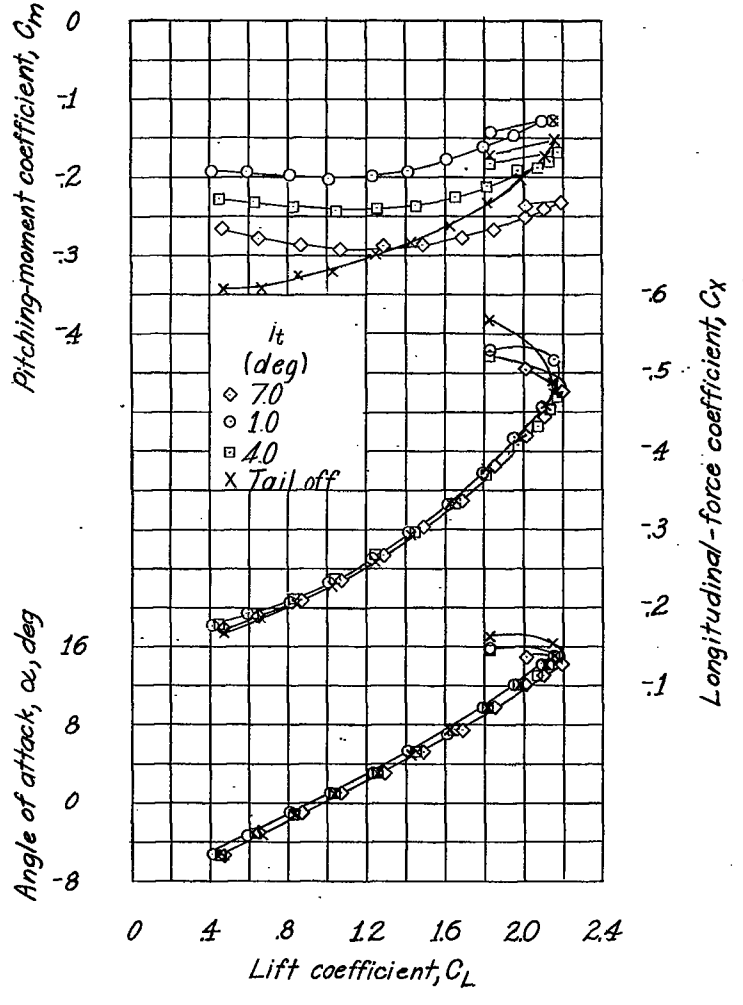

(c) Landing configuration, windmilling propeller.

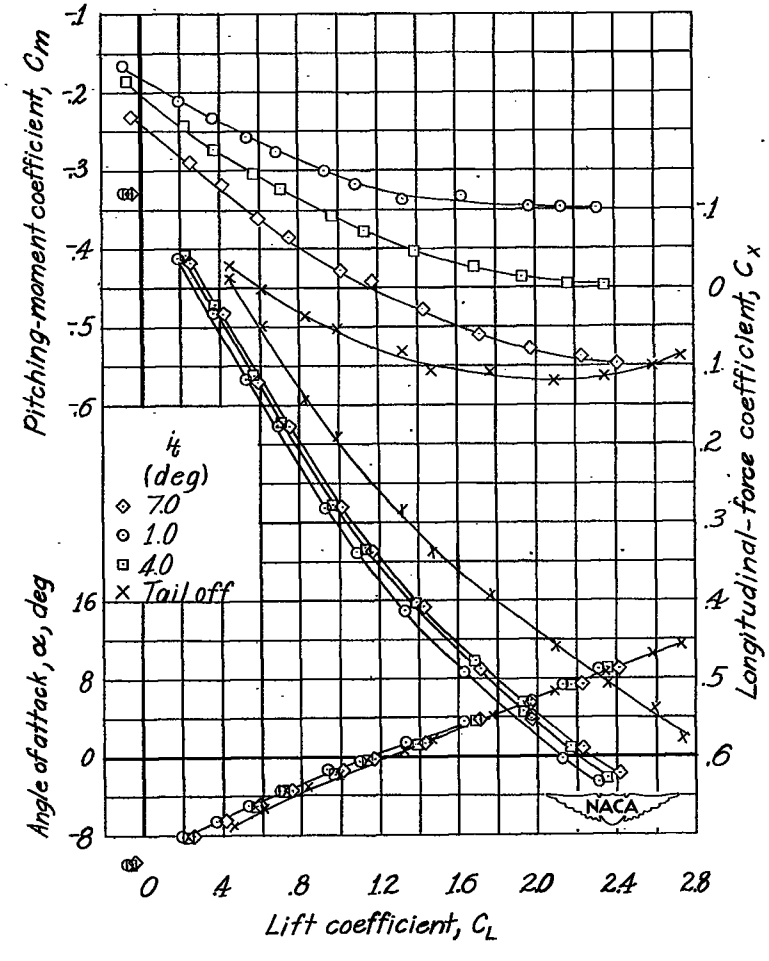

(d) Landing configuration, power on.

Figure 11.- Concluded.

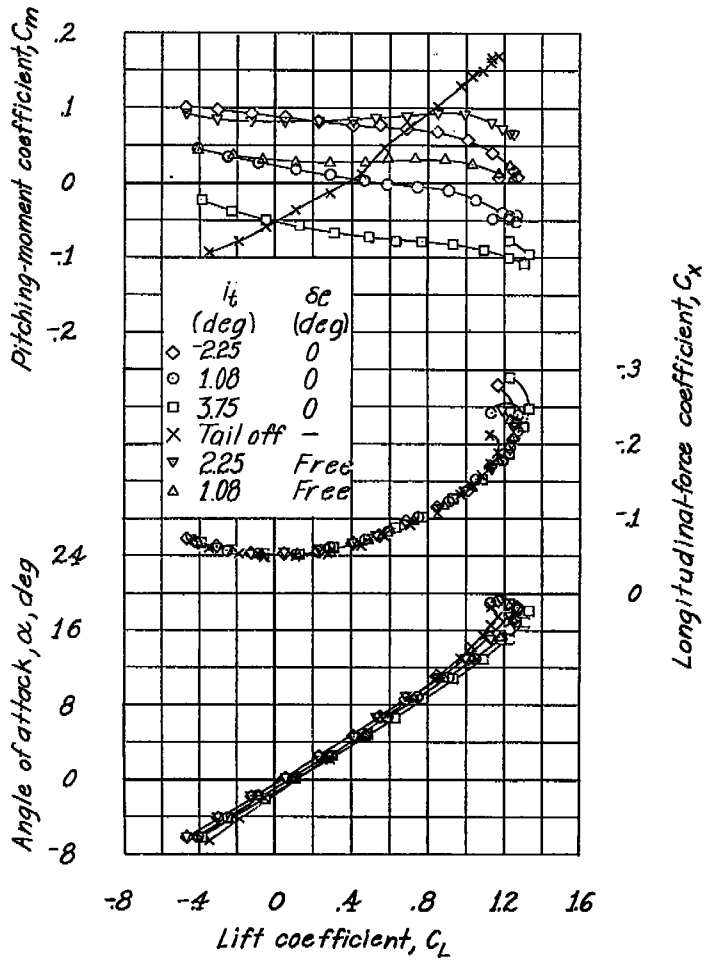

(a) Cruising configuration, windmilling propeller.

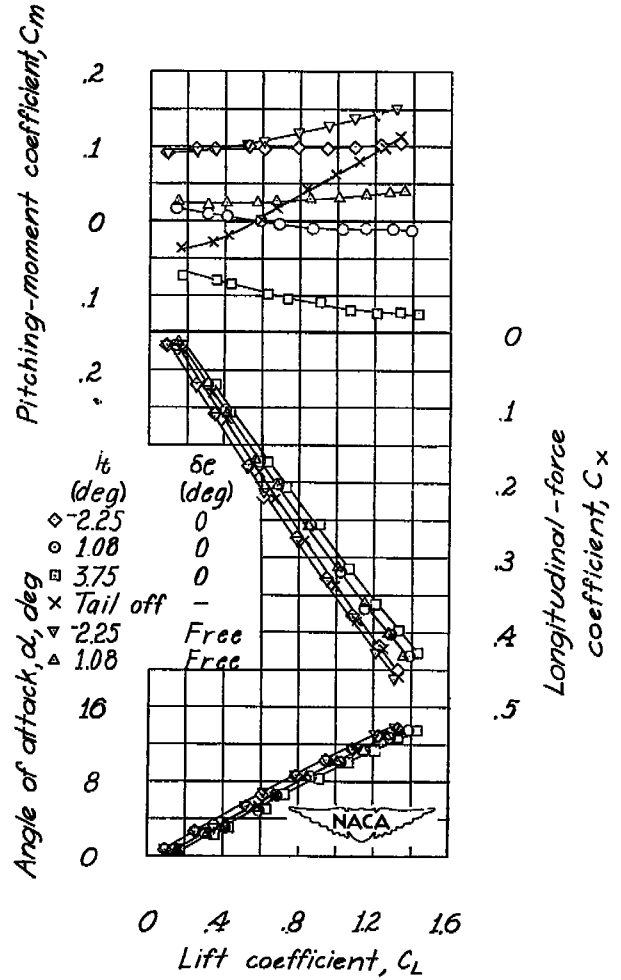

(b) Cruising configuration, power on.

Figure 12.- Effect of the normal horizontal tail and free elevator on the longitudinal characteristics of the single-propeller airplane model with the short tail length.

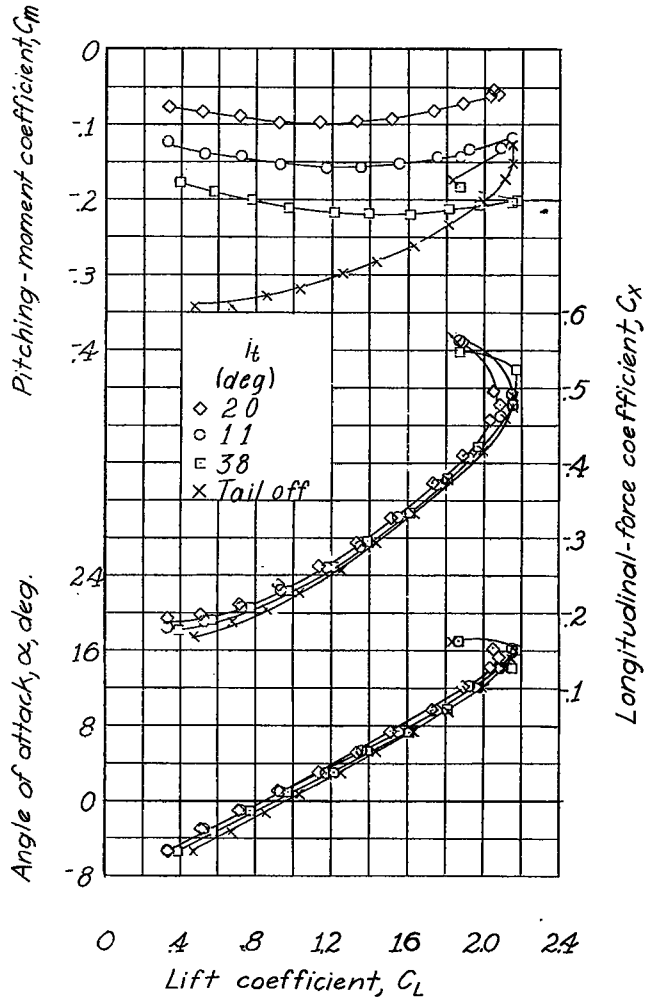

(c) Landing configuration, windmilling propeller.

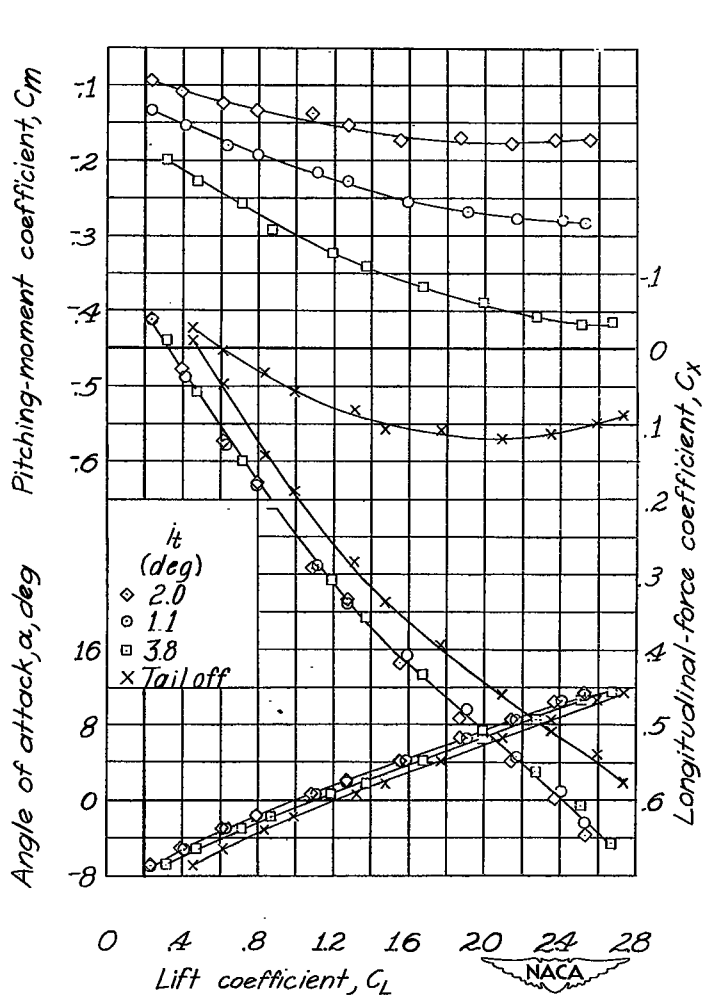

(d) Landing configuration, power on.

Figure 12.- Concluded.

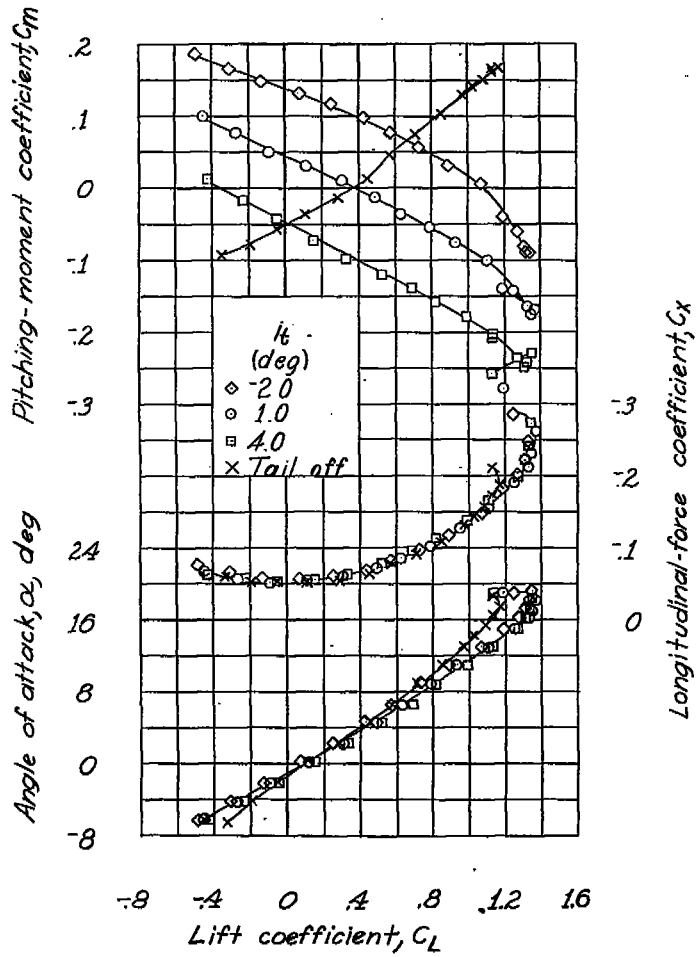

(a) Cruising configuration, windmilling propeller.

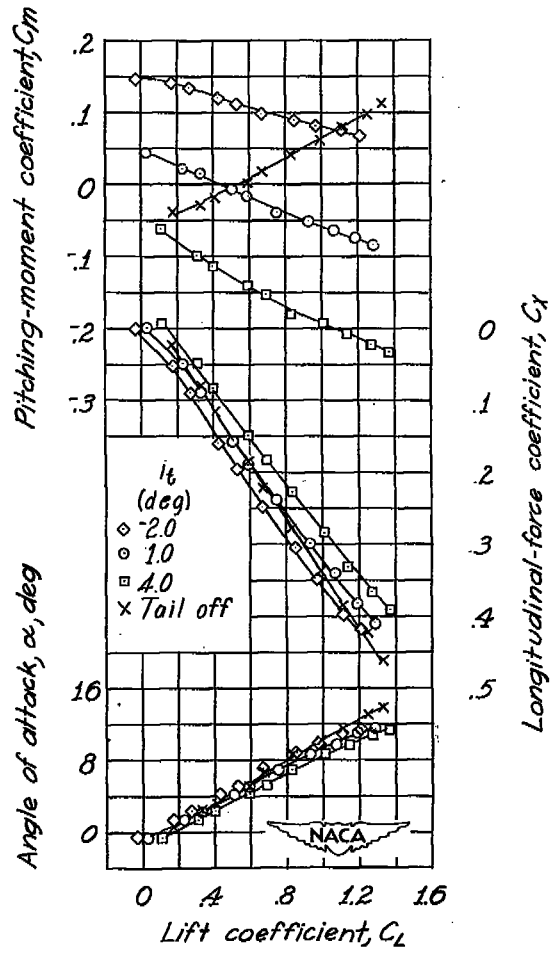

(b) Cruising configuration, power on.

Figure 13.- Effect of the large horizontal tail on the longitudinal characteristics of the single-propeller airplane model with the short tail length.

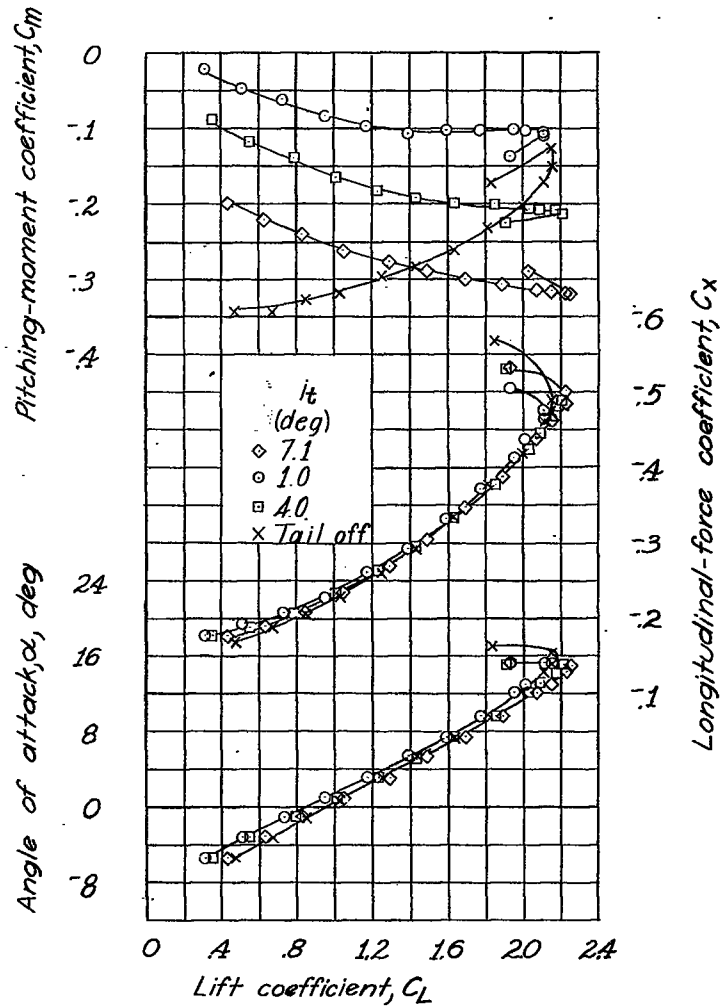

(c) Landing configuration, windmilling propeller.

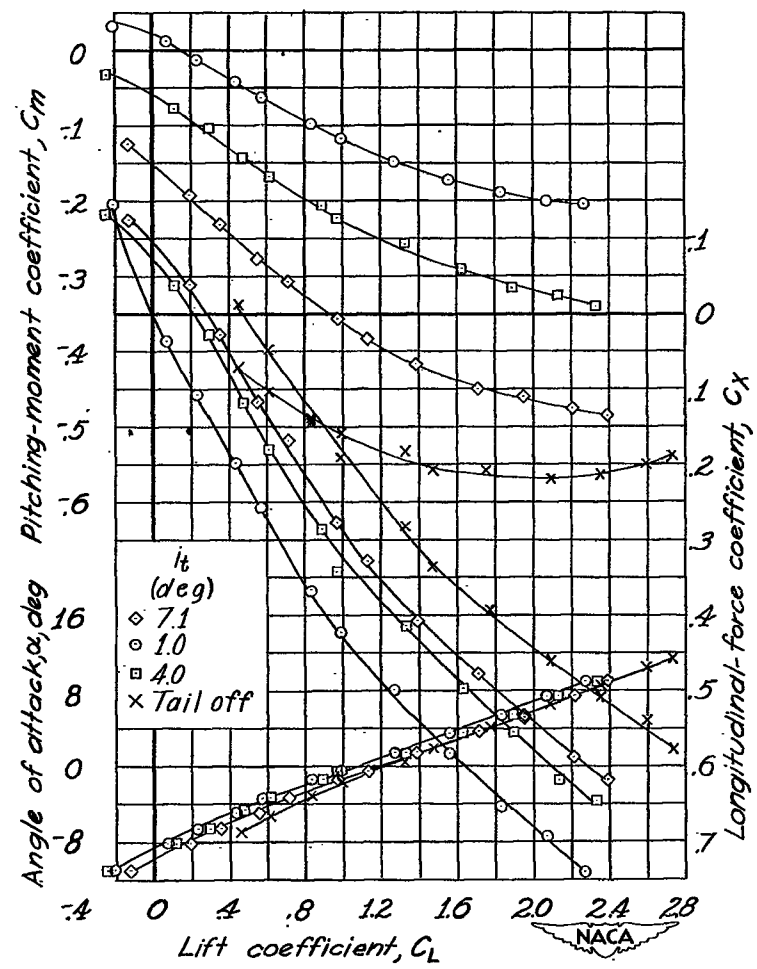

(d) Landing configuration, power on.

Figure 13.- Concluded.

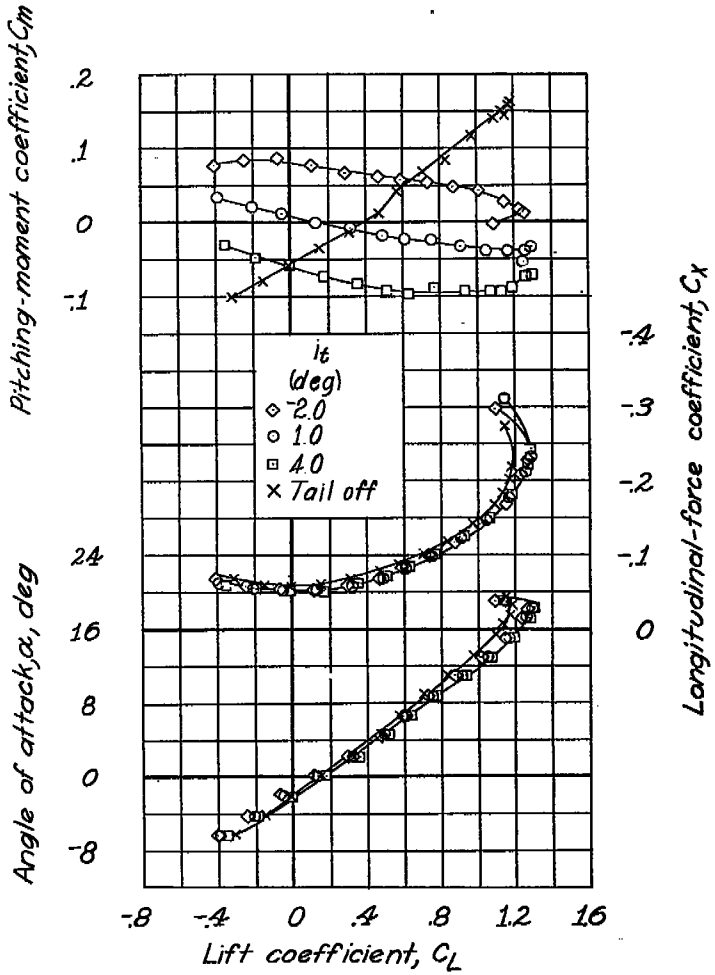

(a) Cruising configuration, windmilling propeller.

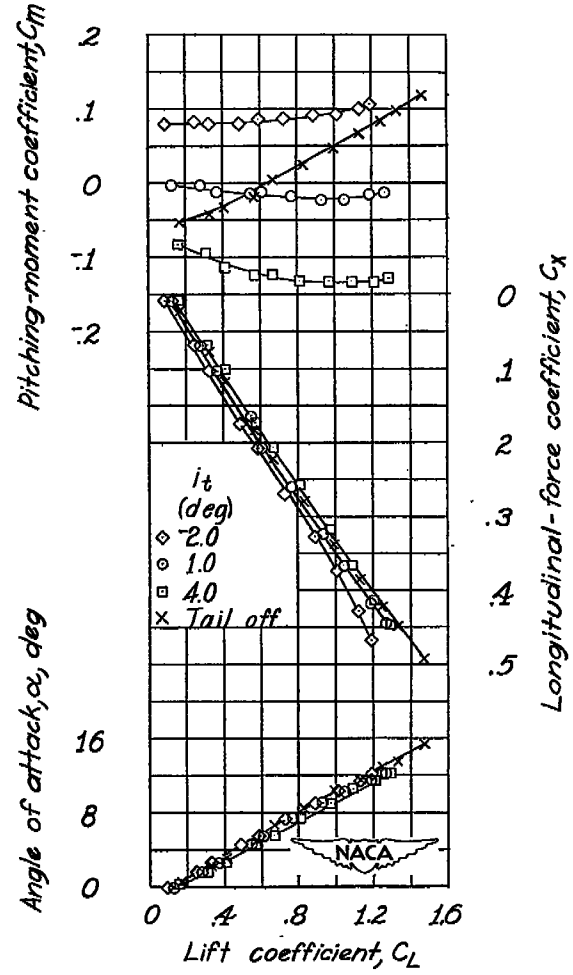

(b) Cruising configuration, power on.

Figure 14.- Effect of the small horizontal tail on the longitudinal characteristics of the single-propeller airplane model with the normal tail length.

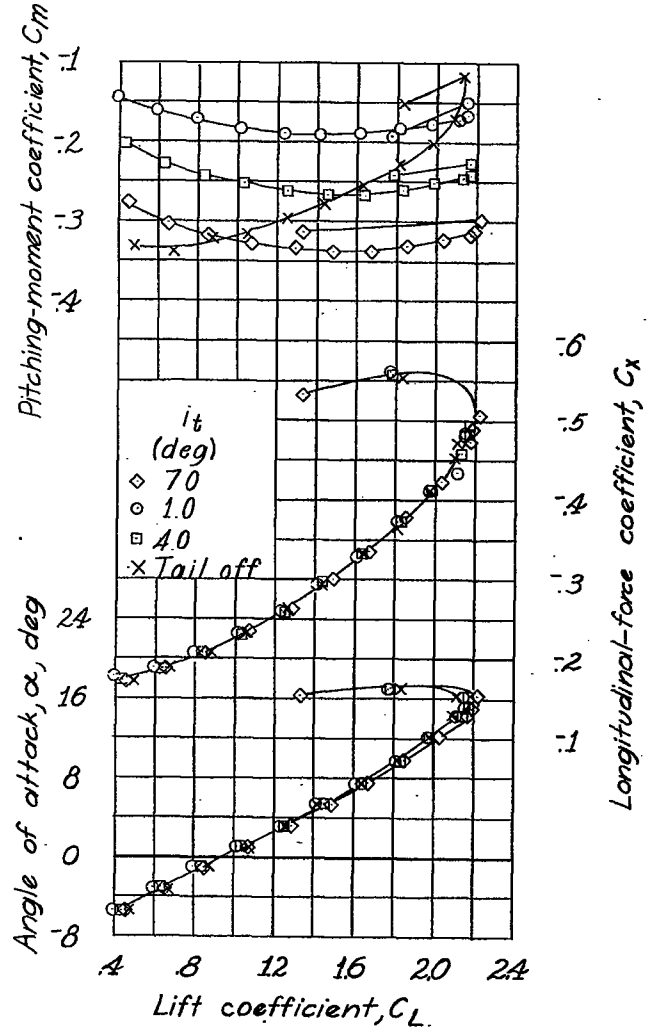

(c) Landing configuration, windmilling propeller.

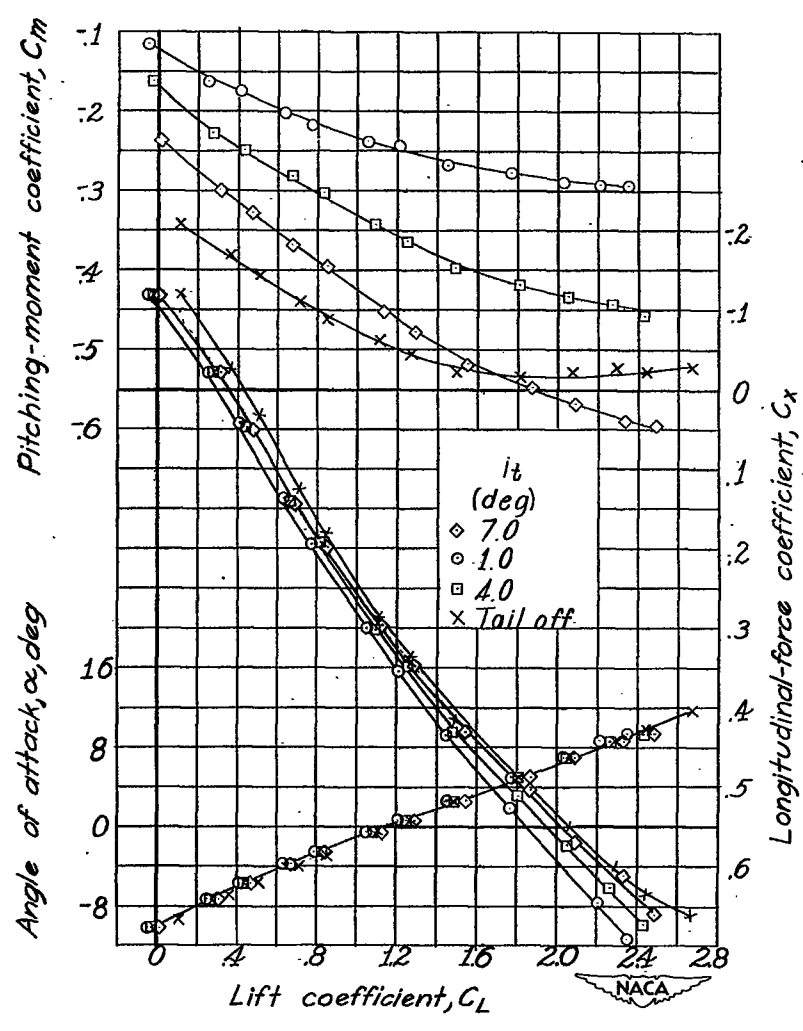

(d) Landing configuration, power on.

Figure 14.- Concluded.

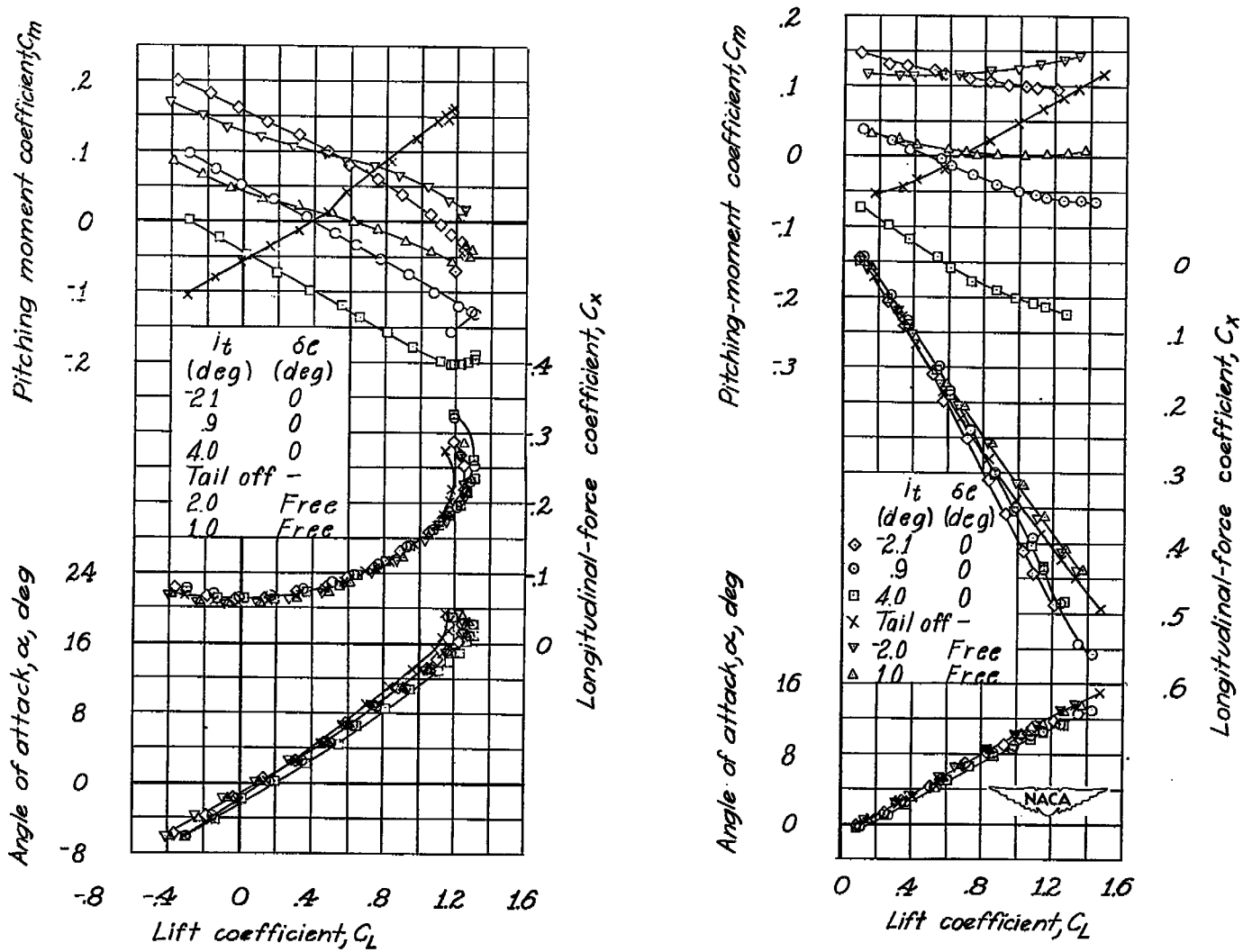

(a) Cruising configuration, windmilling propeller.

(b) Cruising configuration, power on.

Figure 15.- Effect of the normal horizontal tail and free elevator on the longitudinal characteristics of the single-propeller airplane model with normal tail length.

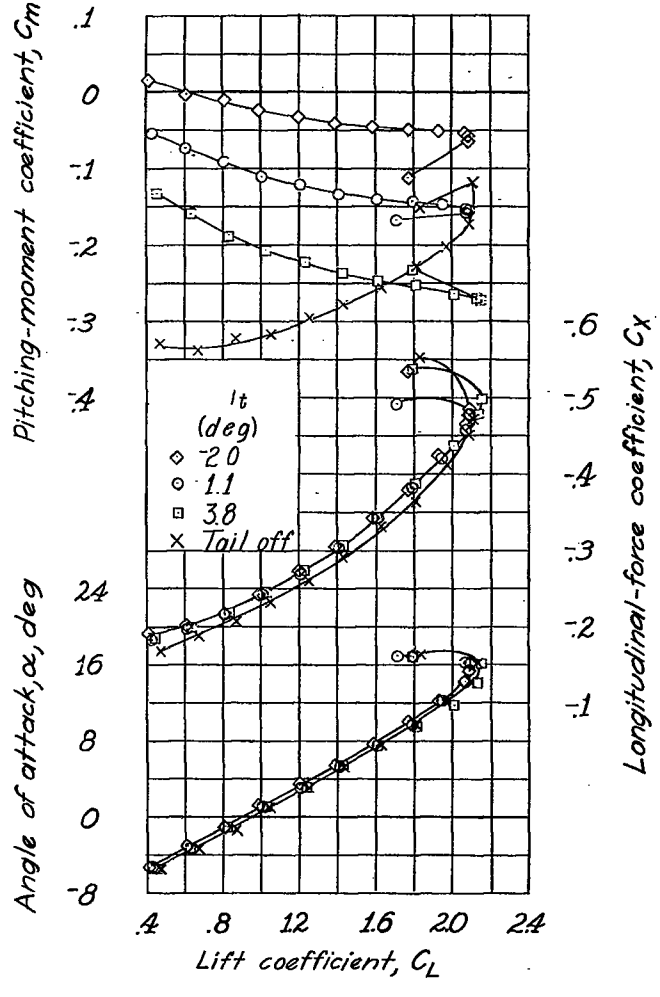

(c) Landing configuration, windmilling propeller.

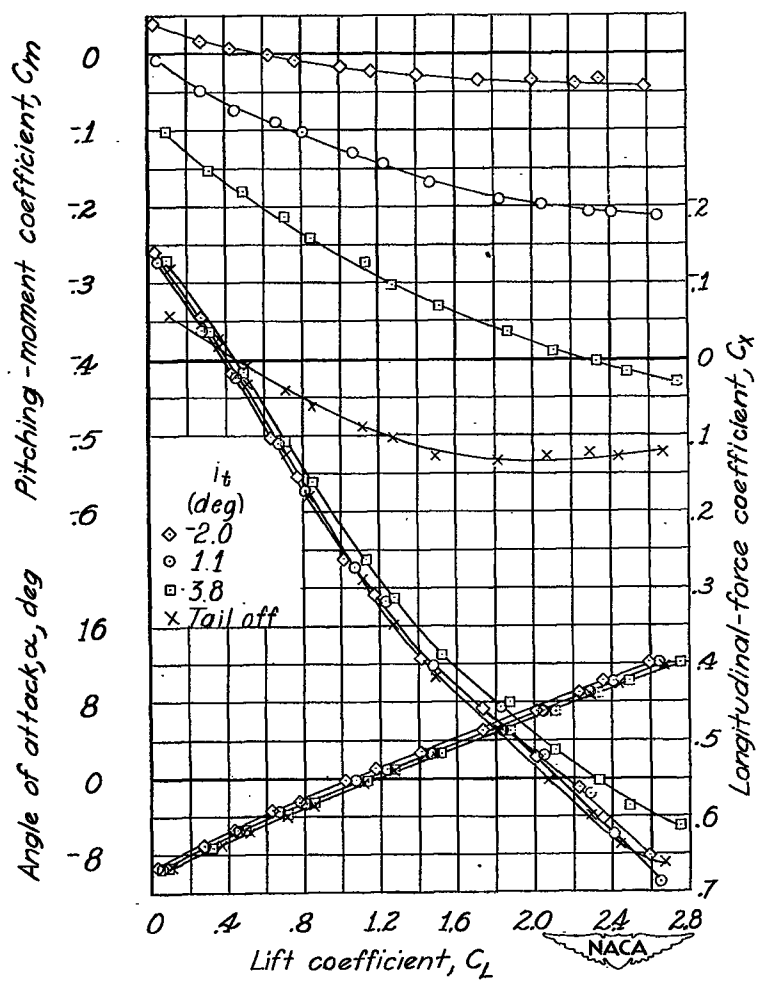

(d) Landing configuration, power on.

Figure 15.- Concluded.

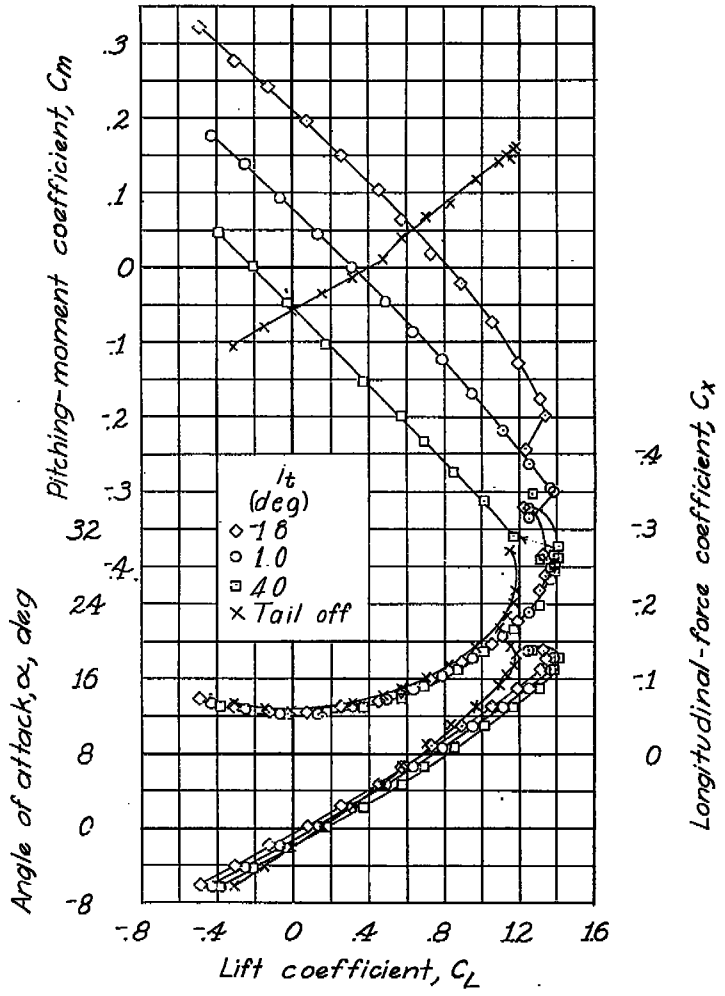

(a) Cruising configuration, windmilling propeller.

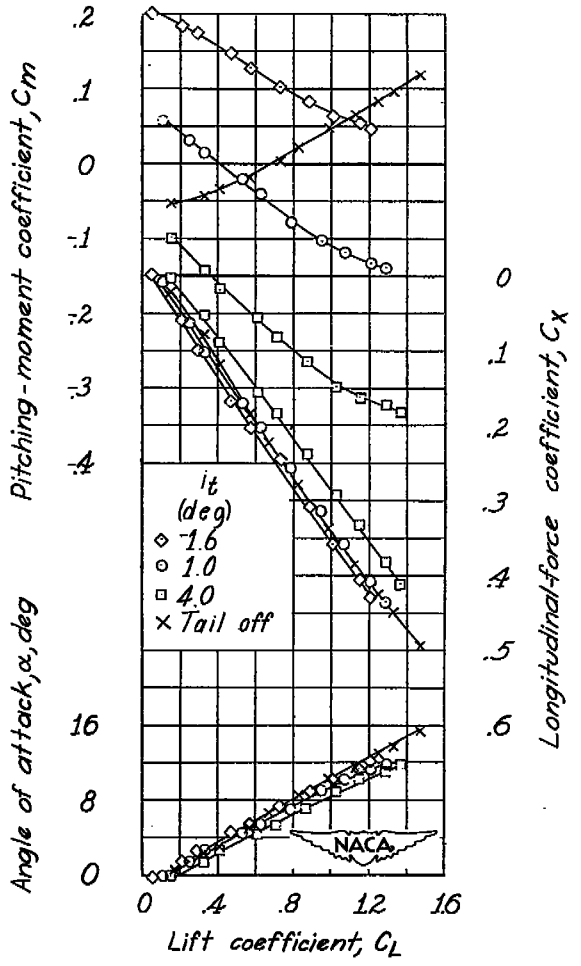

(b) Cruising configuration, power on.

Figure 16.- Effect of the large horizontal tail on the longitudinal characteristics of the single-propeller airplane model with the normal tail length.

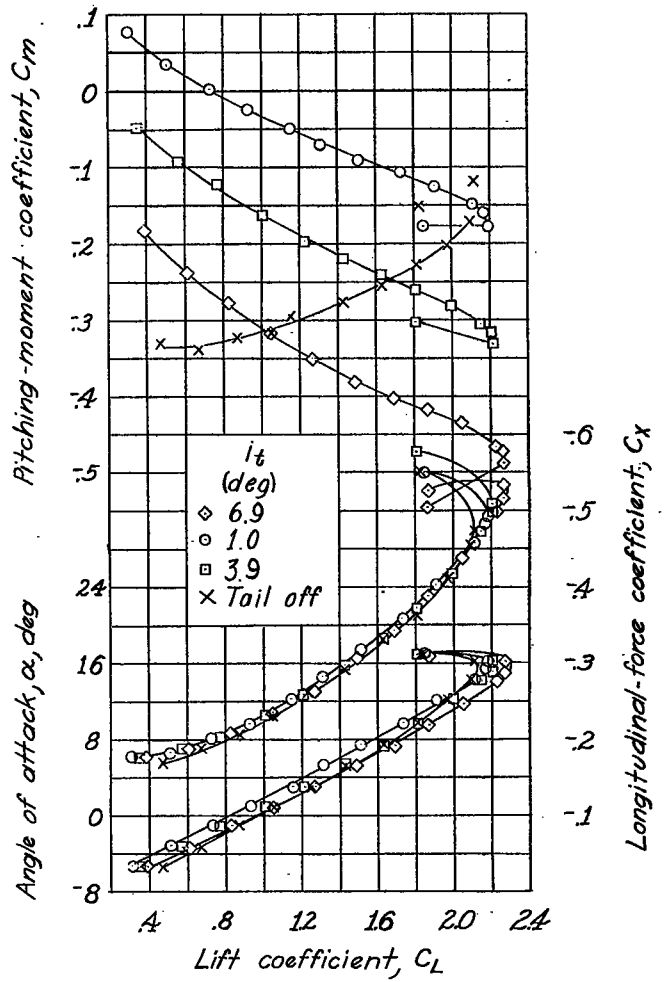

(c) Landing configuration, windmilling propeller.

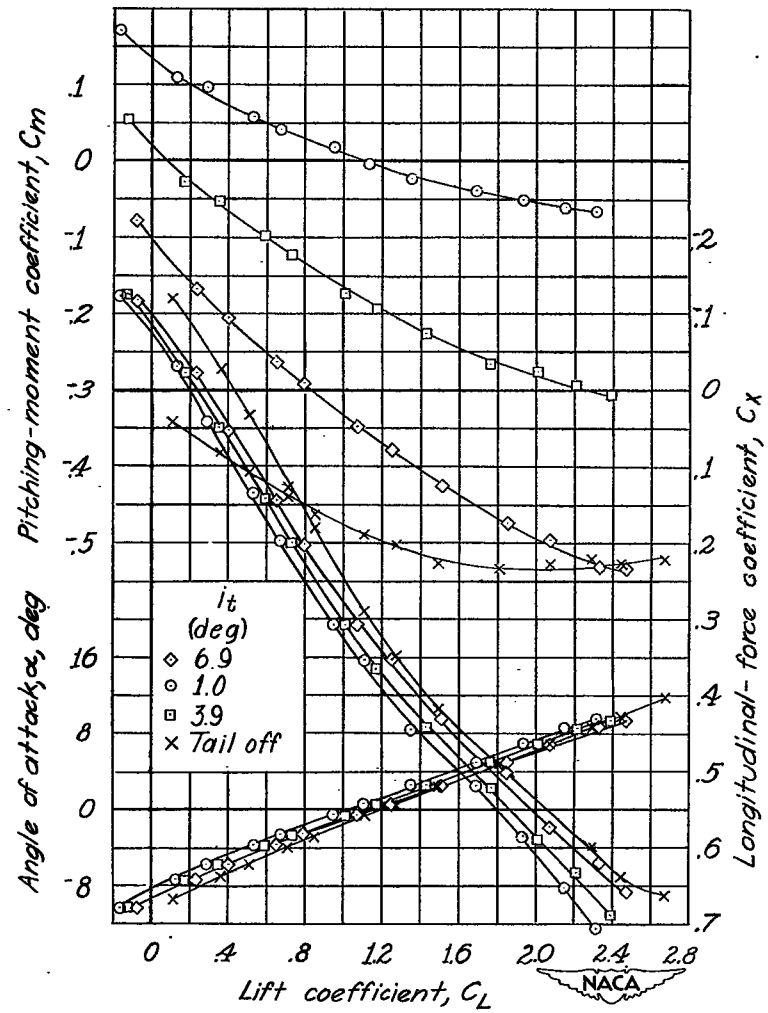

(d) Landing configuration, power on.

Figure 16.- Concluded.

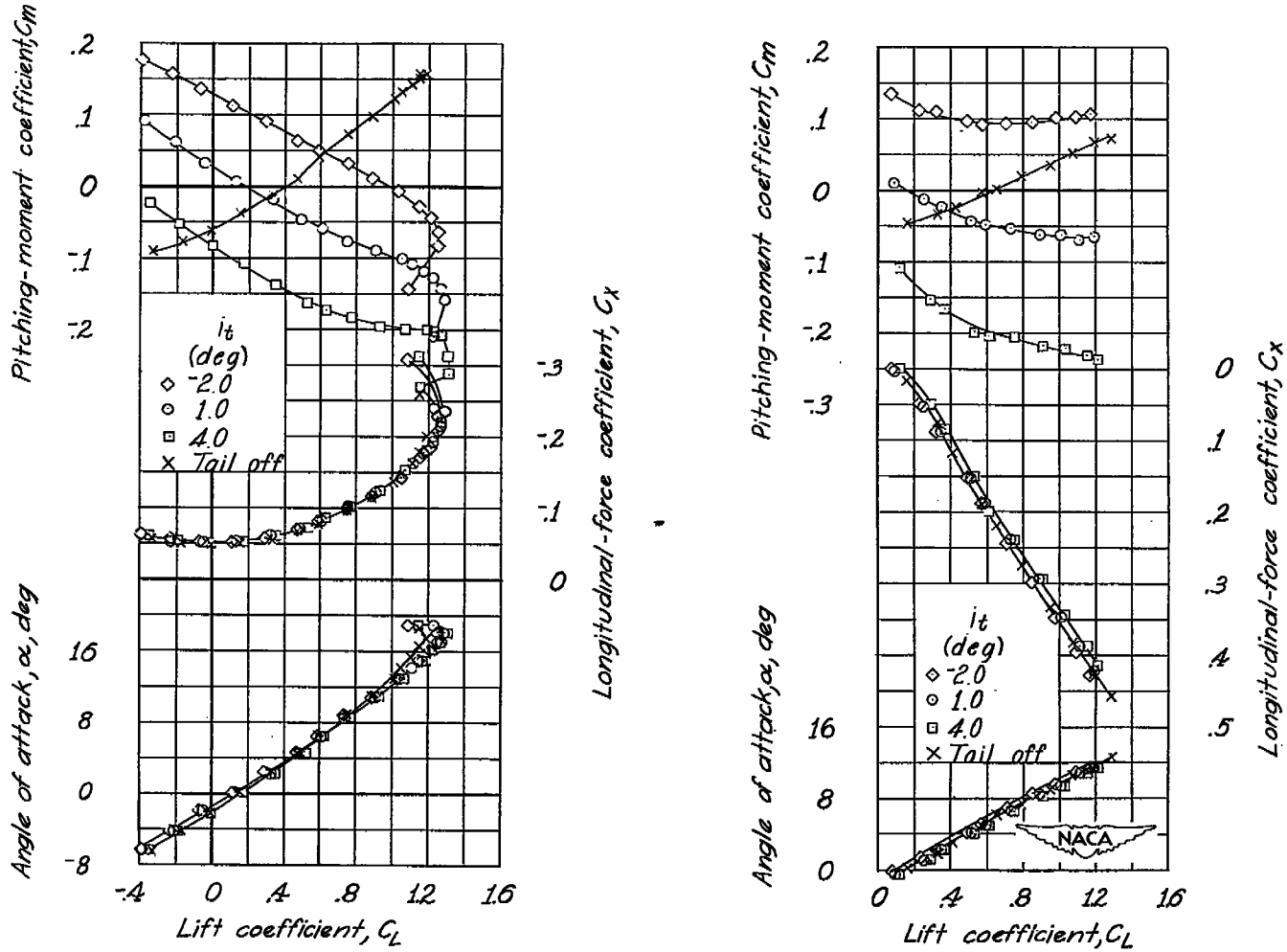

(a) Cruising configuration, windmilling propeller.

(b) Cruising configuration, power on.

Figure 17.- Effect of the small horizontal tail on the longitudinal characteristics of the single-propeller airplane model with the long tail length.

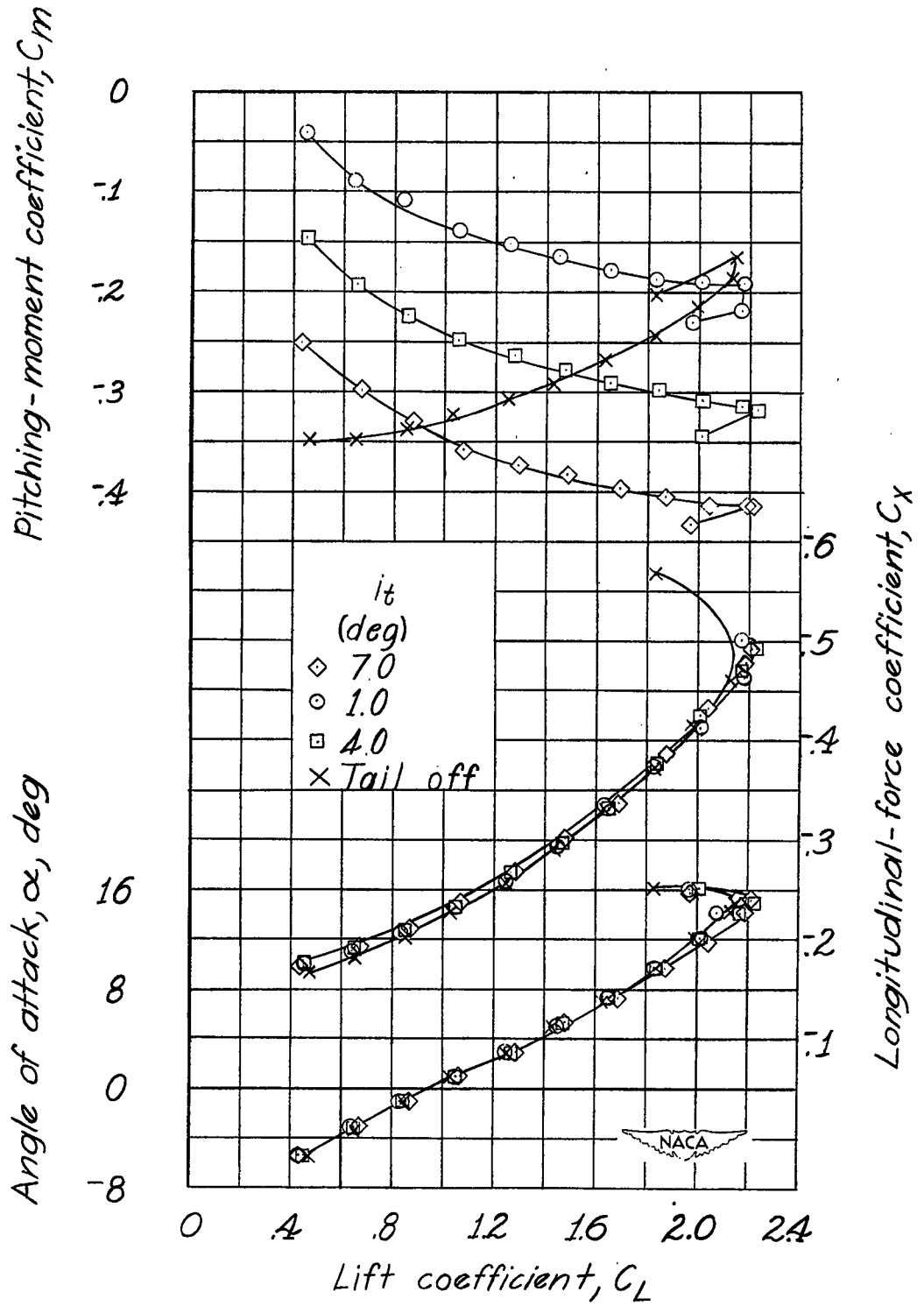

(c) Landing configuration, windmilling propeller.

Figure 17.- Continued.

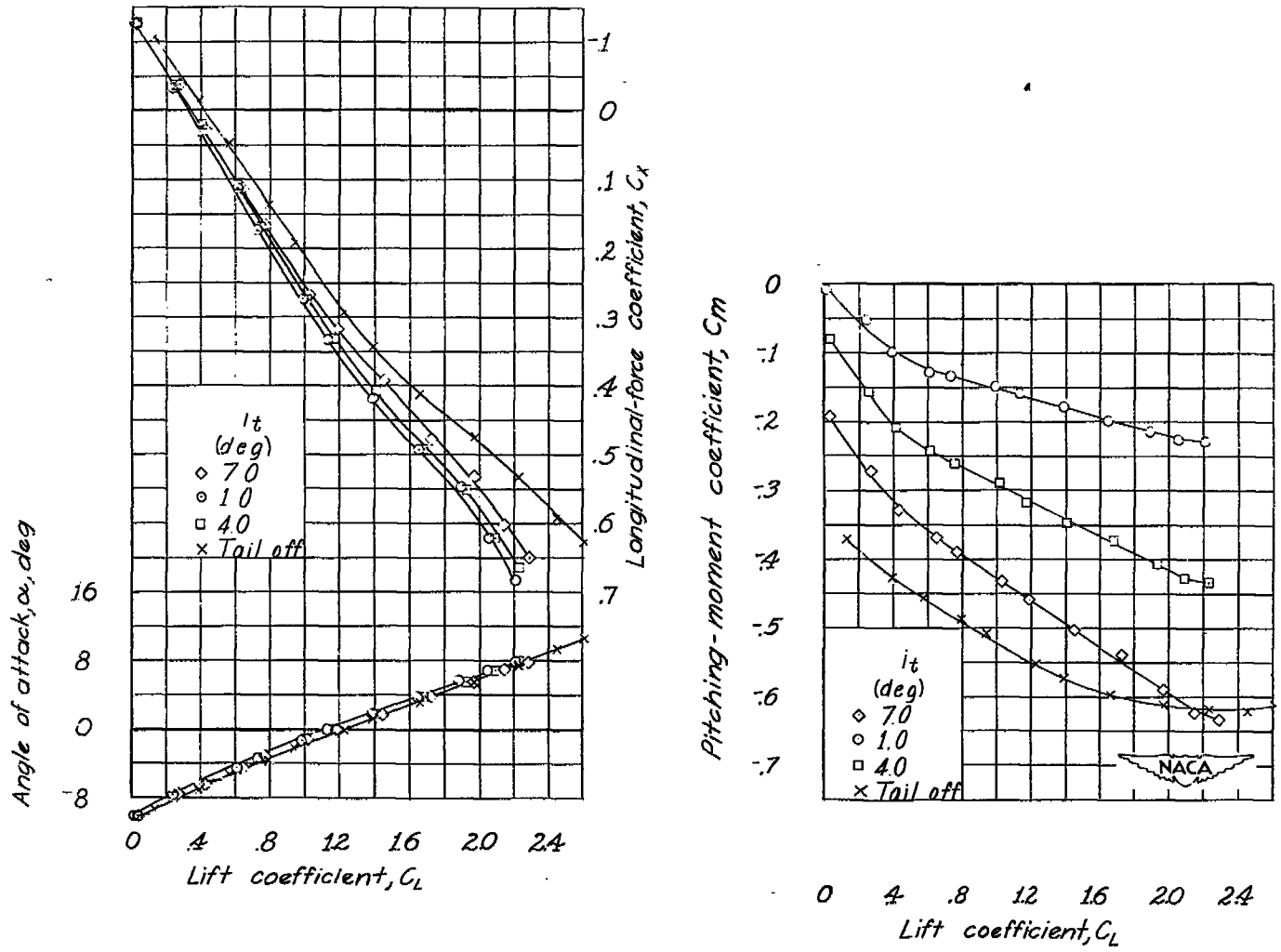

(d) Landing configuration, power on.

Figure 17.- Concluded.

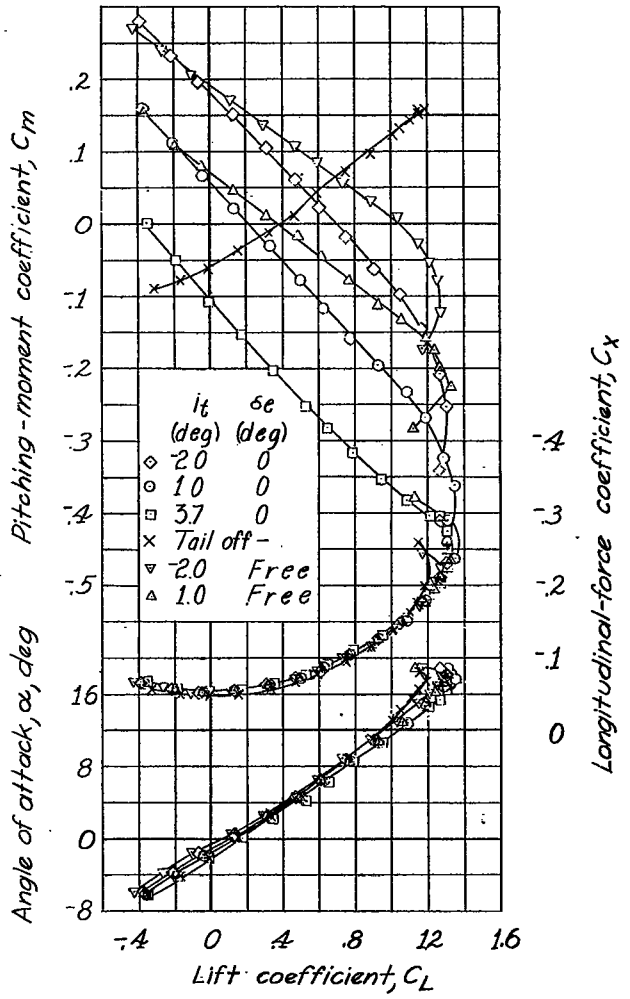

(a) Cruising configuration, windmilling propeller.

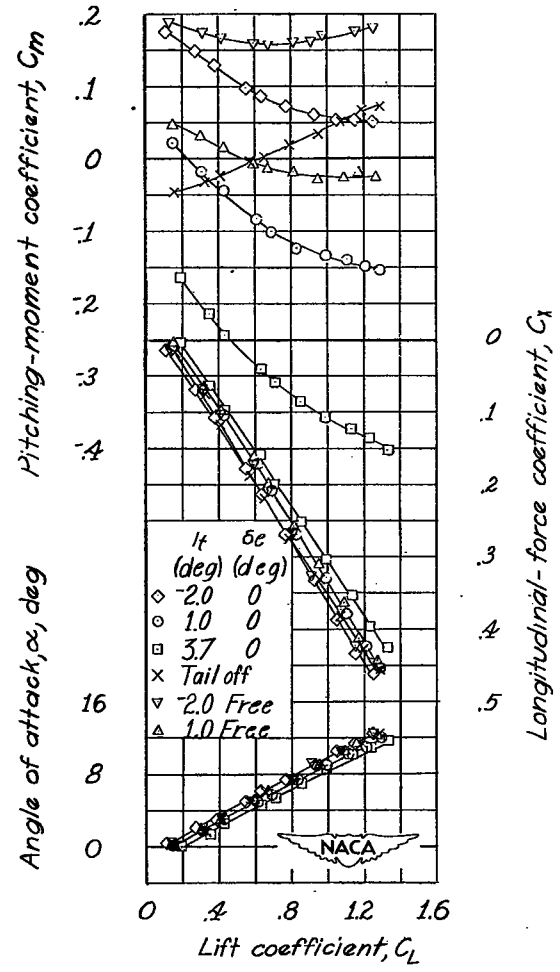

(b) Cruising configuration, power on.

Figure 18.- Effect of the normal horizontal tail and free elevator on the longitudinal characteristics of the single-propeller airplane model with the long tail length.

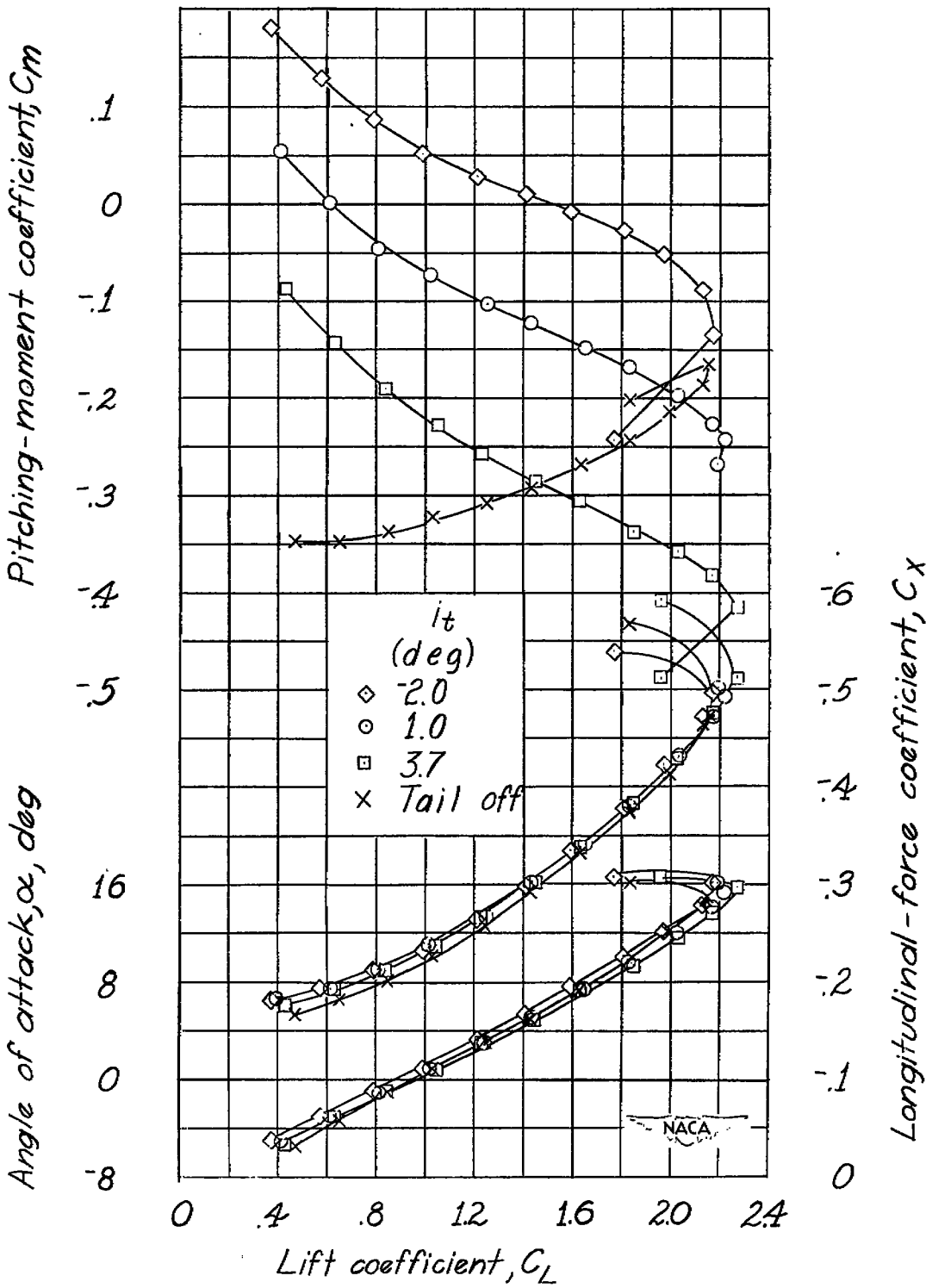

(c) Landing configuration, windmilling propeller.

Figure 18.- Continued.

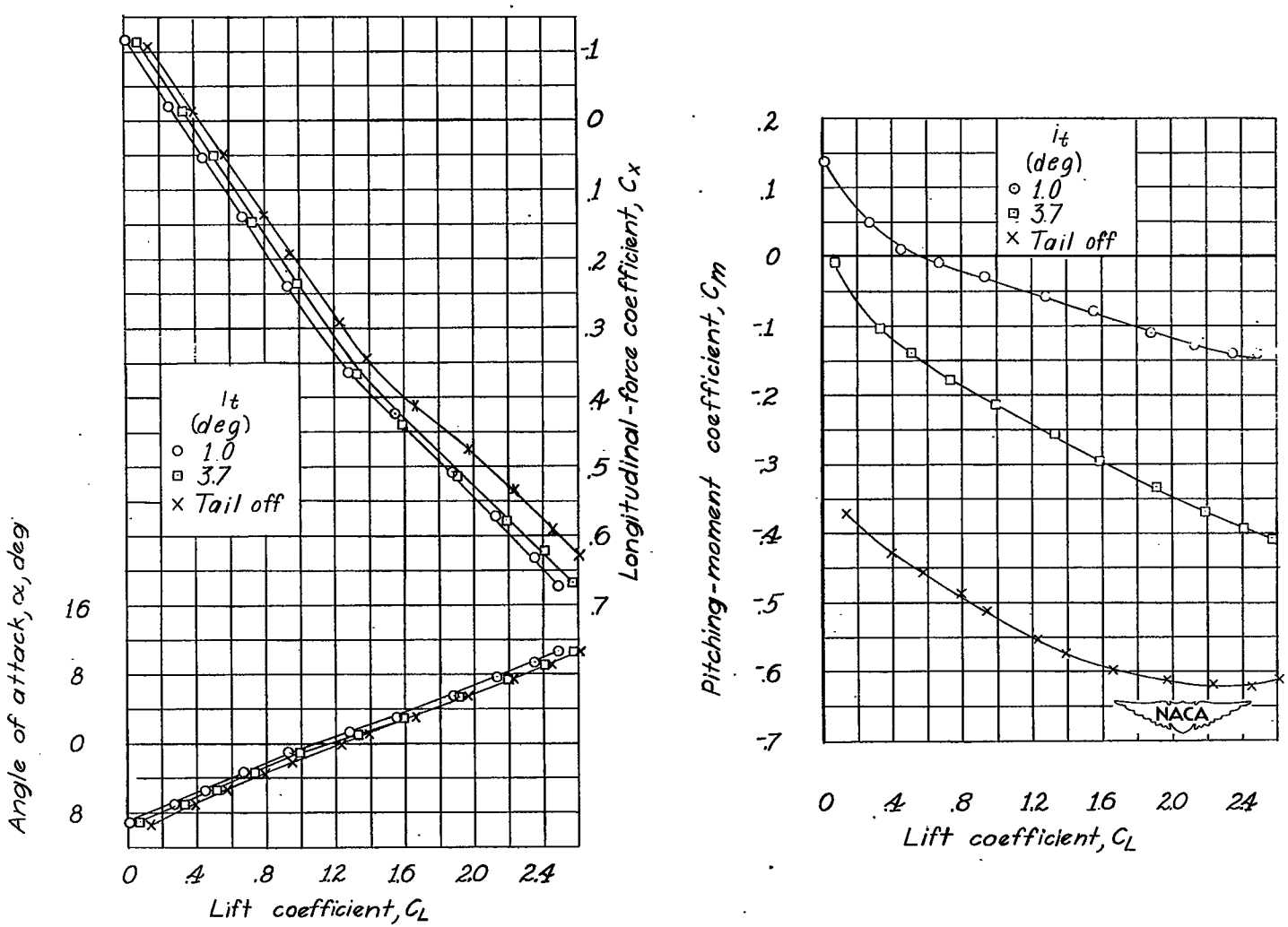

(d) Landing configuration, power on.

Figure 18.- Concluded.

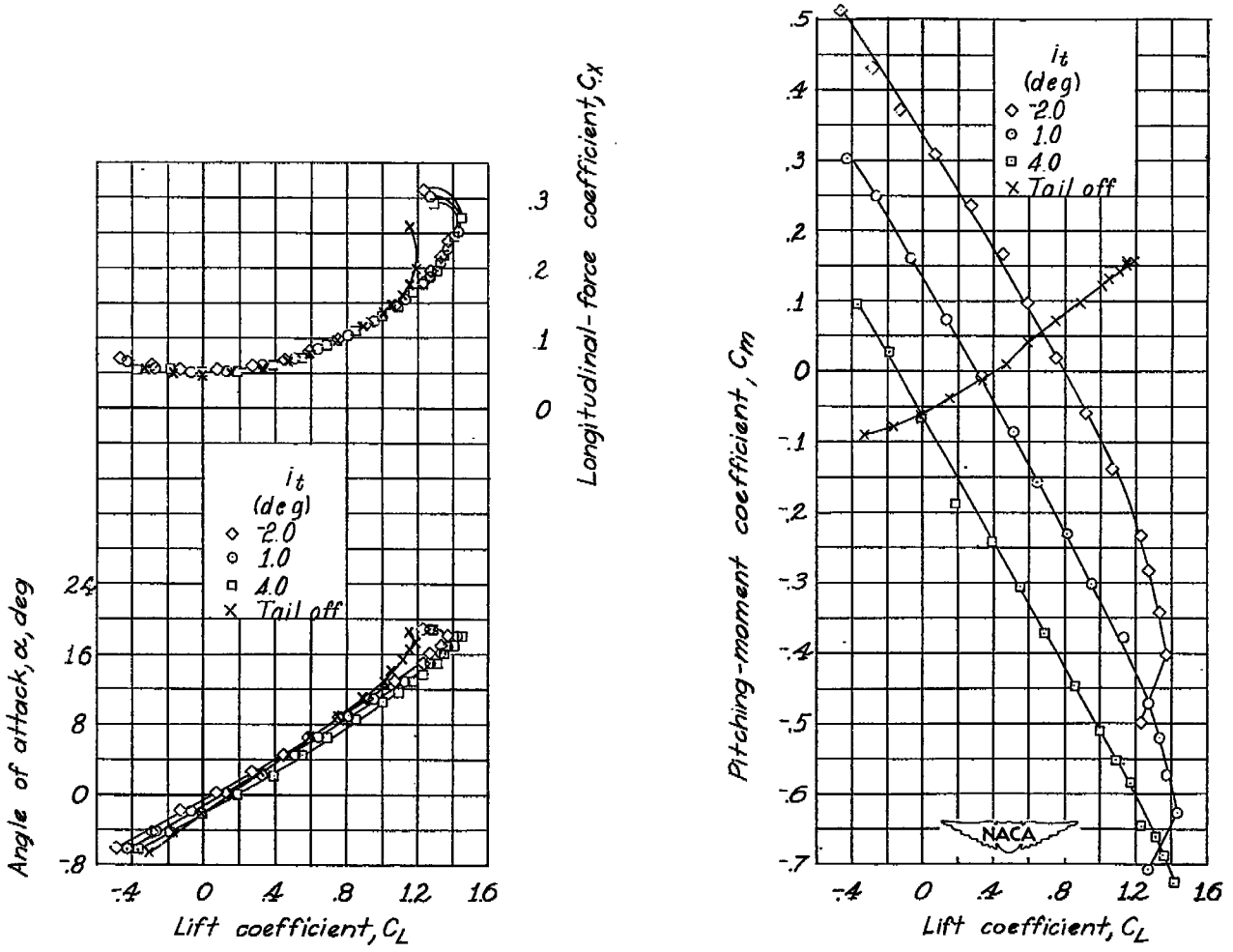

(a) Cruising configuration, windmilling propeller.

Figure 19.- Effect of the large horizontal tail on the longitudinal characteristics of the single-propeller airplane model with the long tail length.

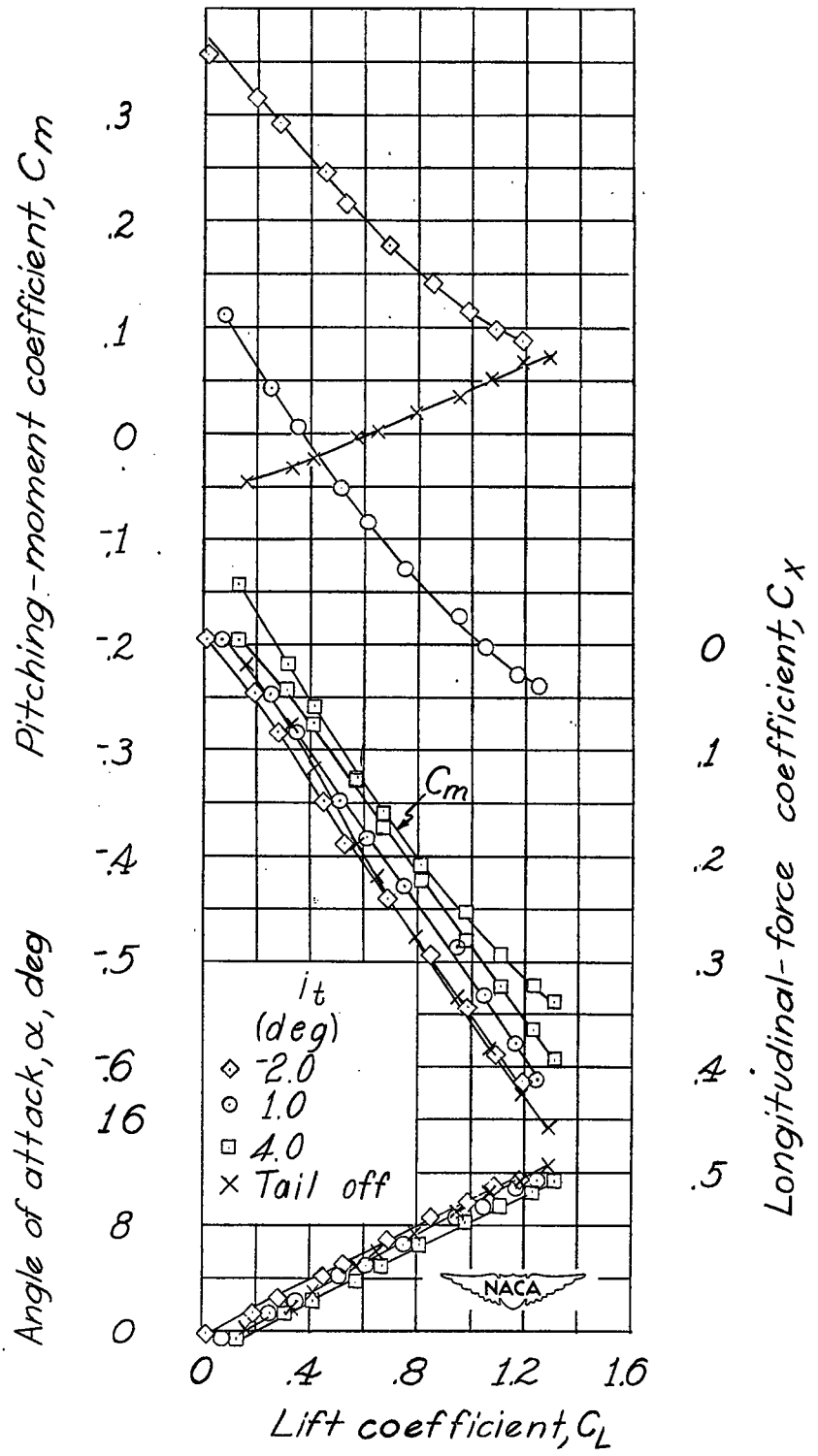

(b) Cruising configuration, power on.

Figure 19.- Continued.

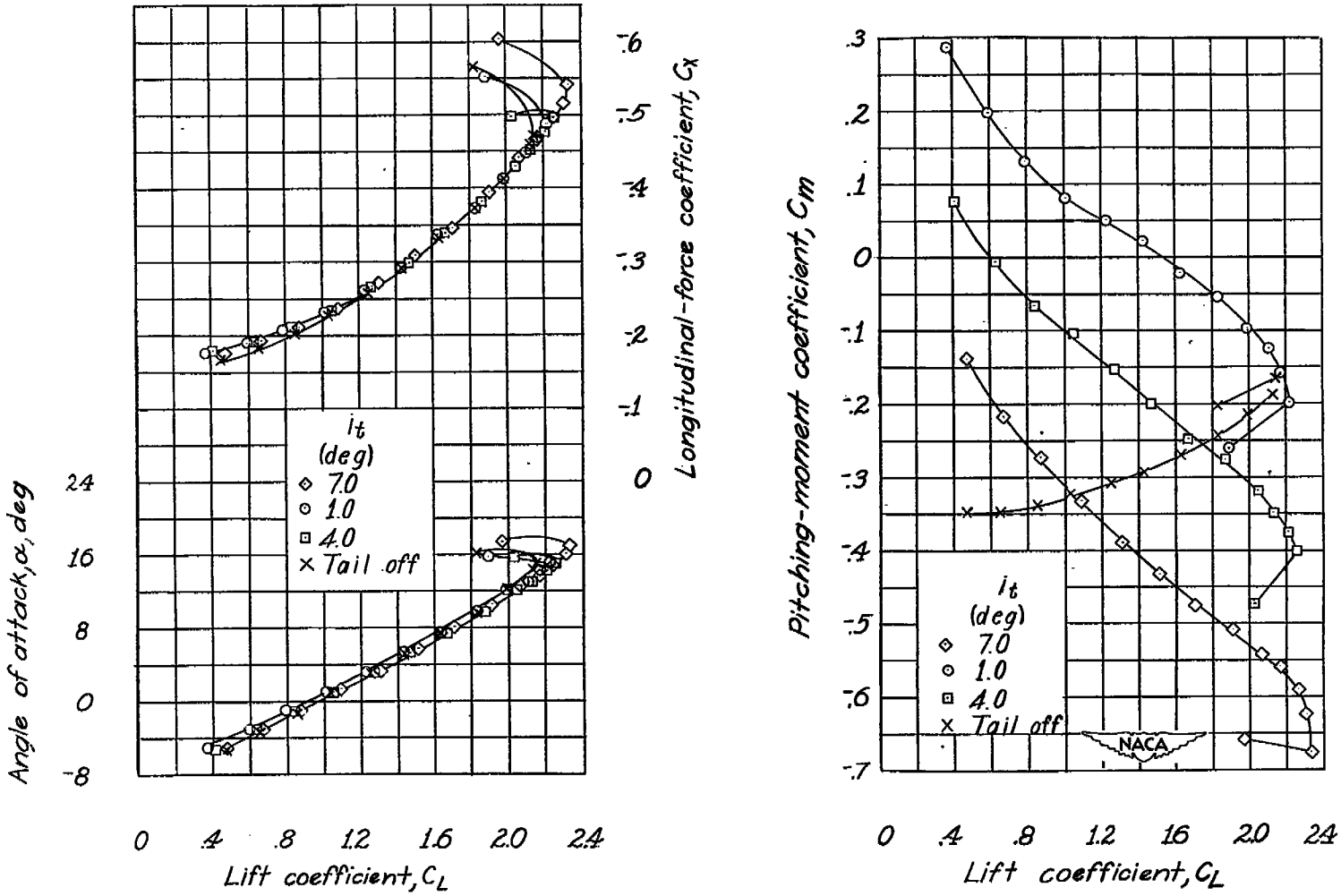

(c) Landing configuration, windmilling propeller.

Figure 19.- Continued.

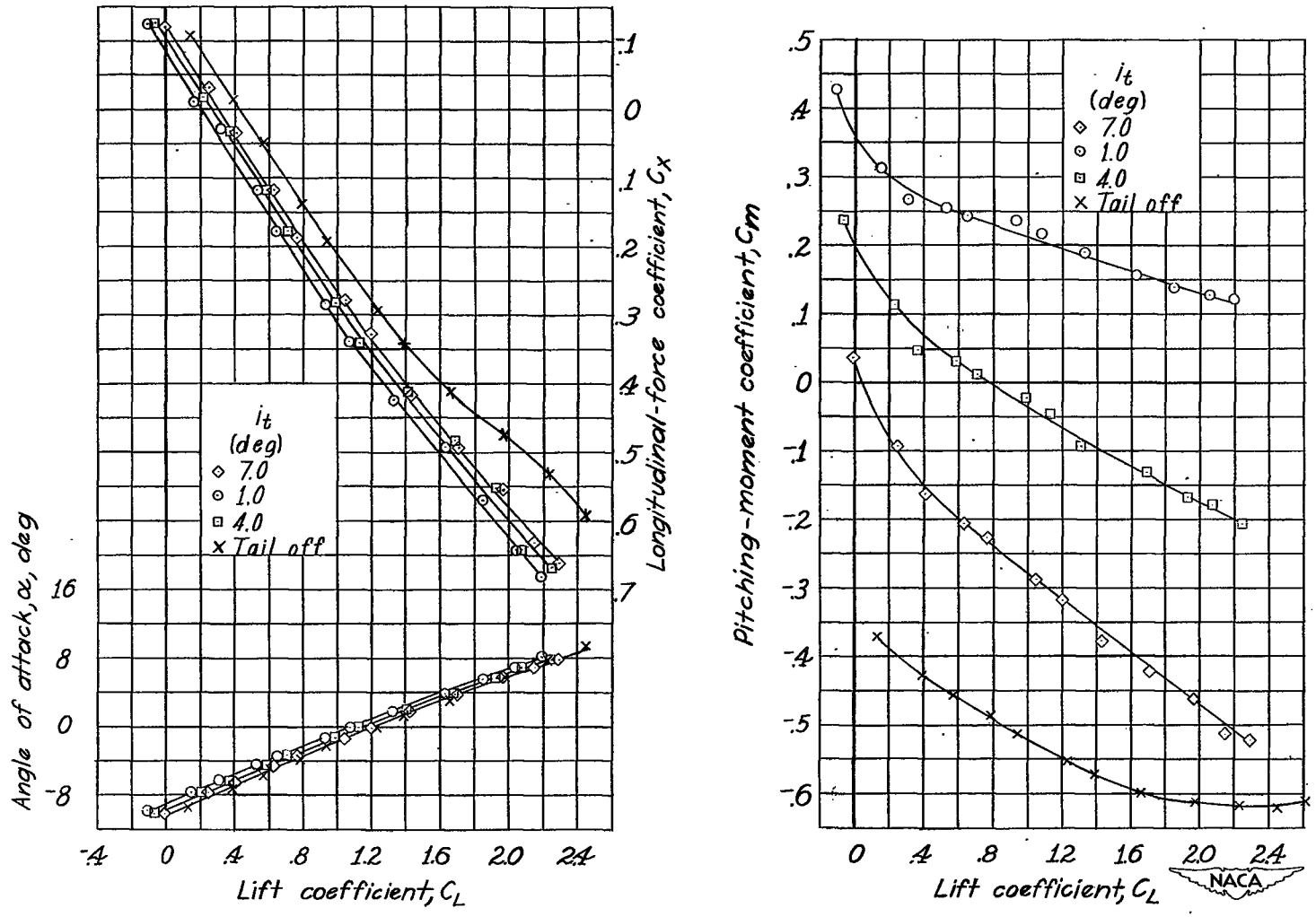

(d) Landing configuration, power on.

Figure 19.- Concluded.

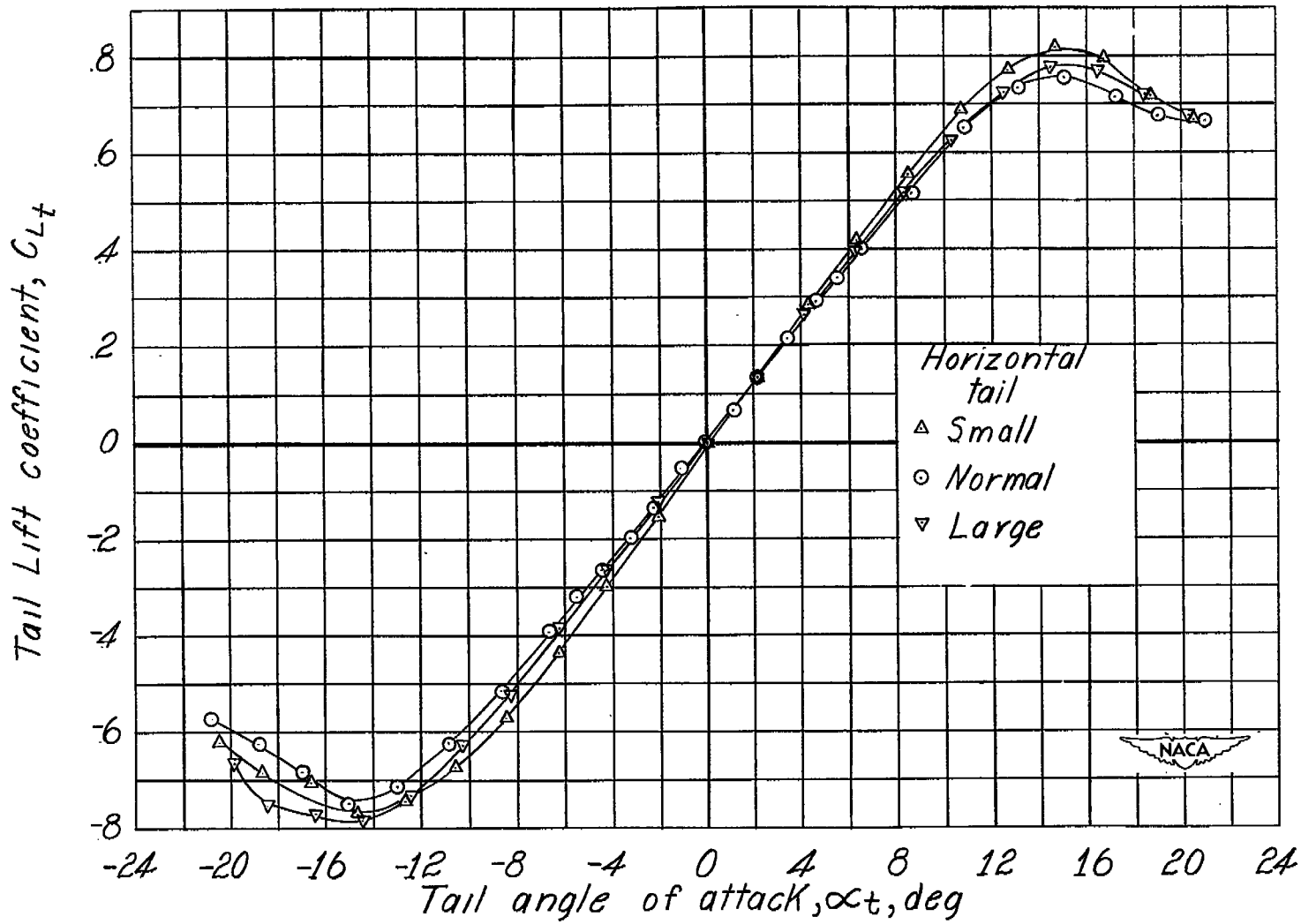

Figure 20.- Lift curves of the three isolated horizontal tails used in tests of the single-propeller airplane model.

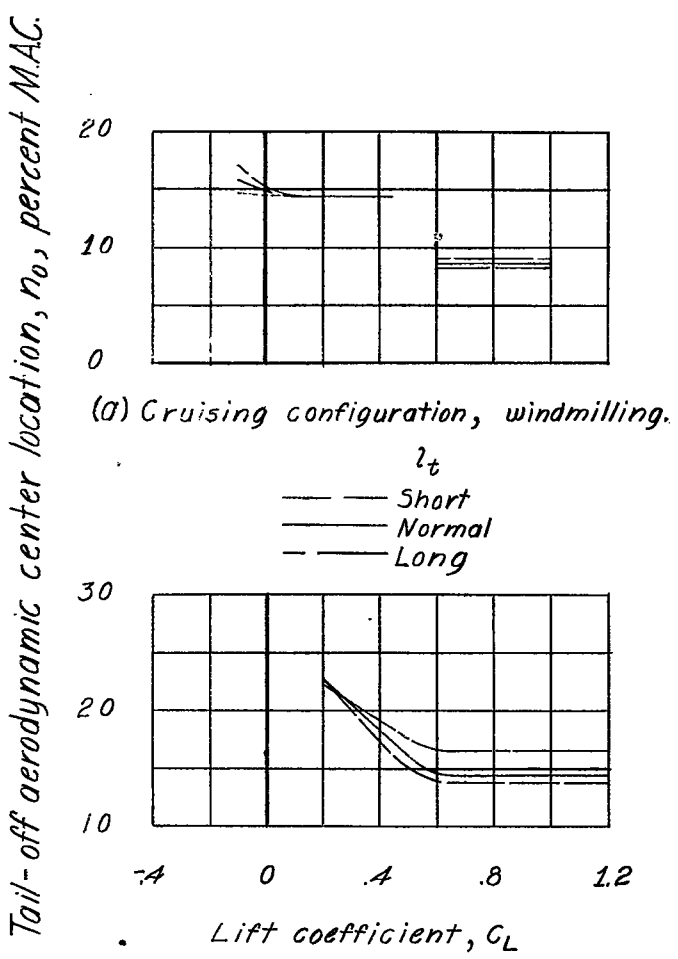

(b) Cruising configuration, power on.

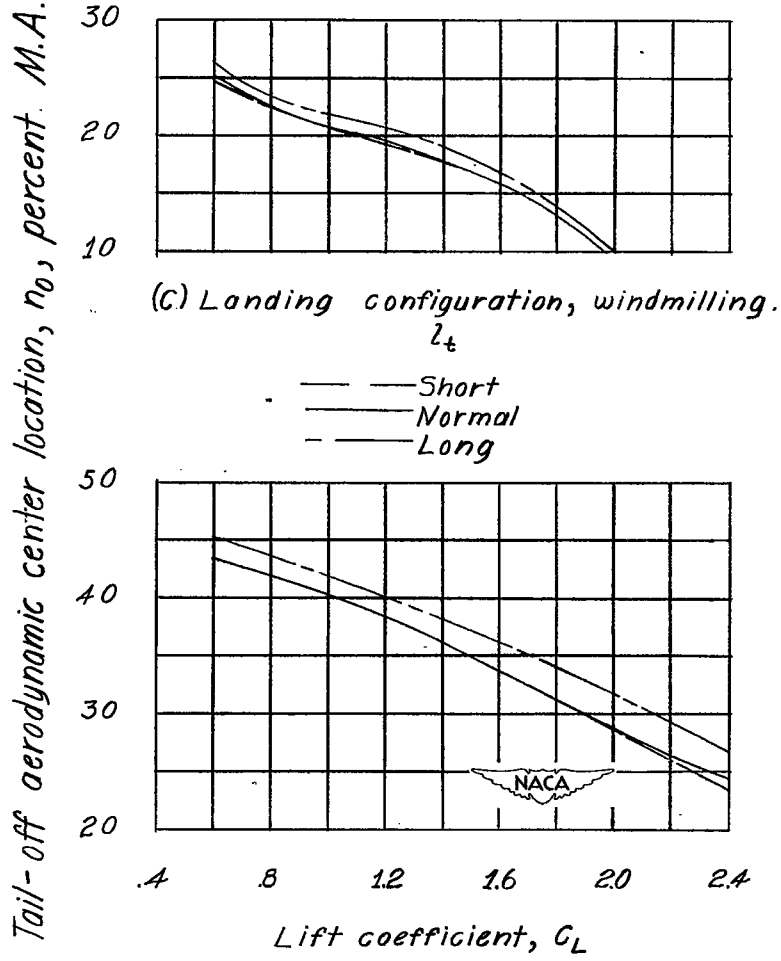

(d) Landing configuration, power on.

Figure 21.- Effect of tail length on the tail-off aerodynamic-center location of the single-propeller airplane model.

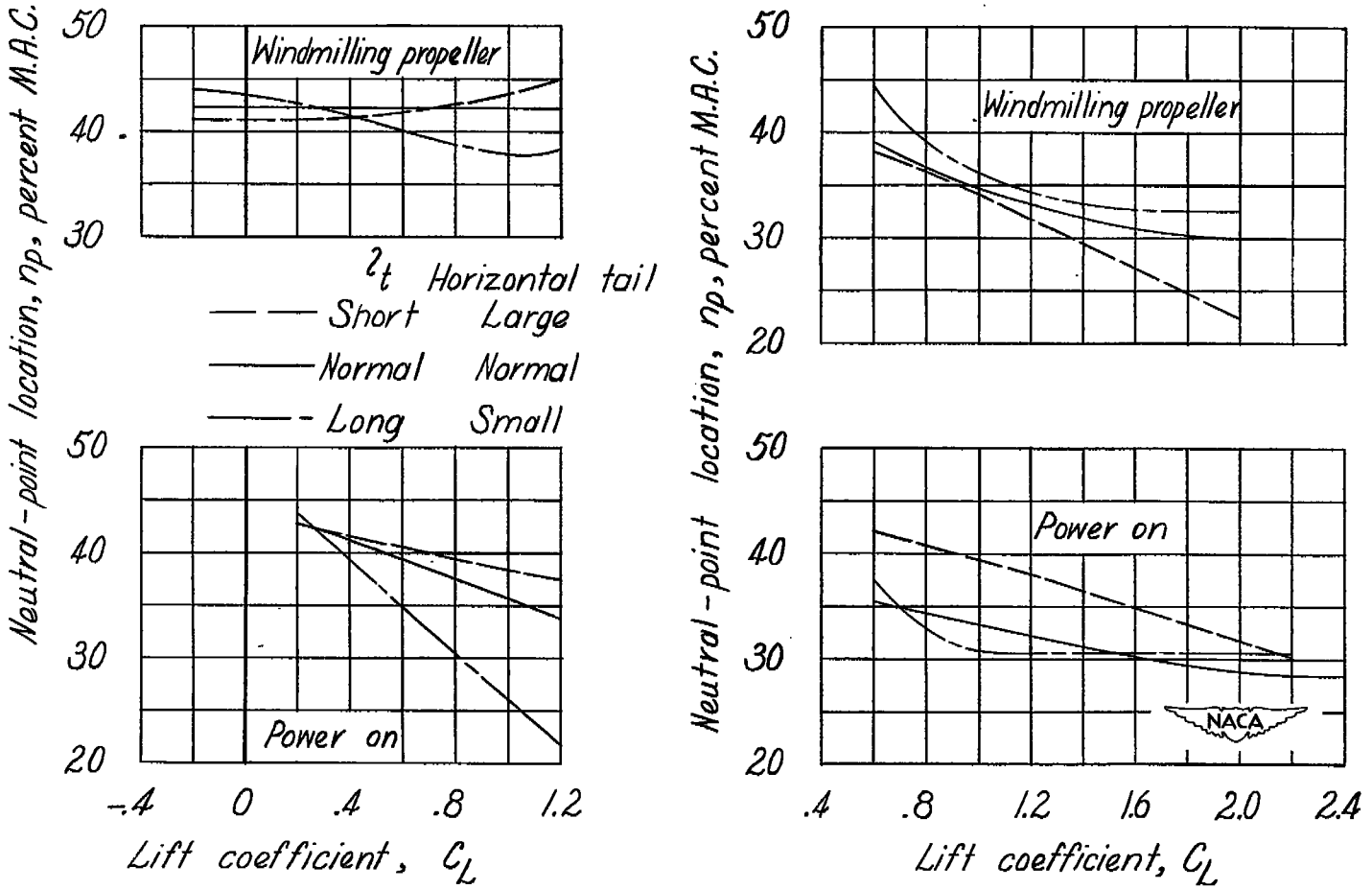

(a) Cruising configuration.

(b) Landing configuration.

Figure 22.- Effect of tail length on the neutral-point location of the single-propeller airplane model with constant tail volume.

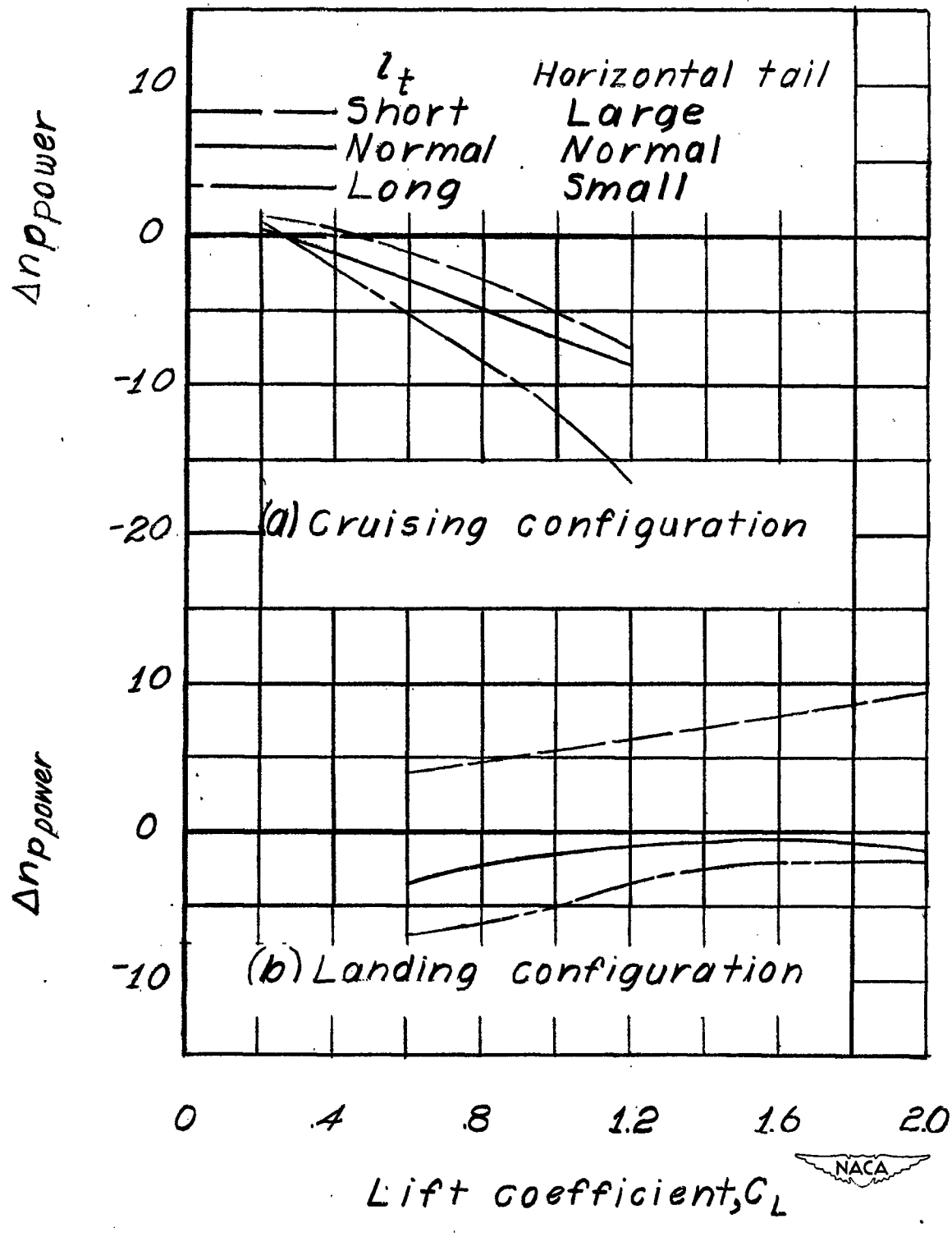

Figure 23.- Effect of tail length on the change in neutral-point location caused by power for the single-propeller airplane model with constant tail volume.

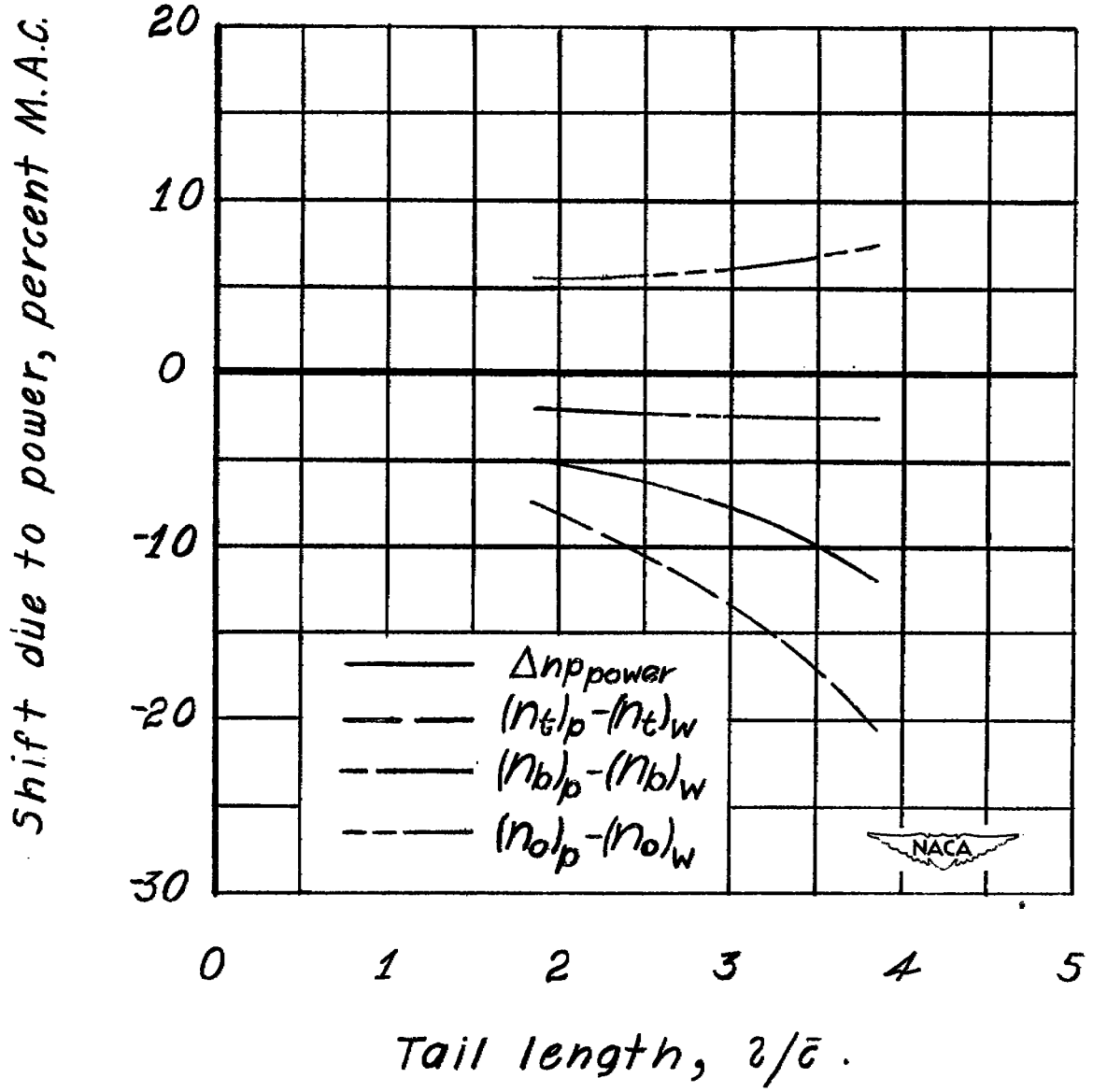

Figure 24.- Variation with tail length of the effect of power on the terms of the neutral-point equation for the single-propeller airplane model with constant tail volume. Cruising configuration, $C_L = 1.0$.

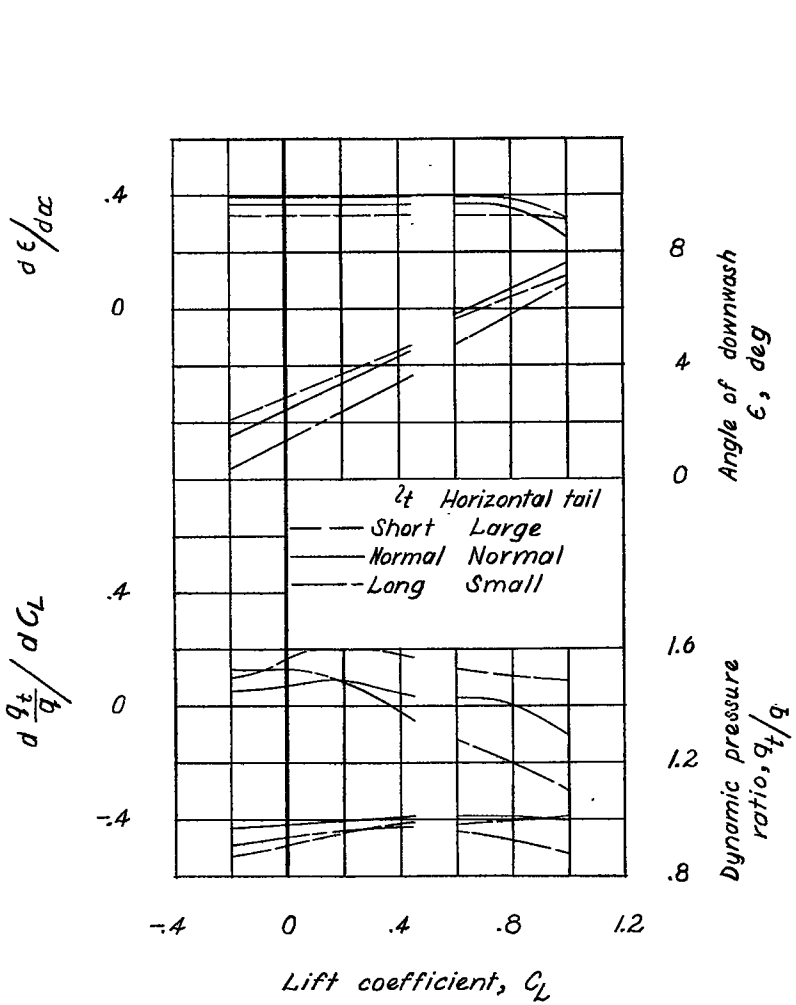

(a) Cruising configuration, windmilling propeller.

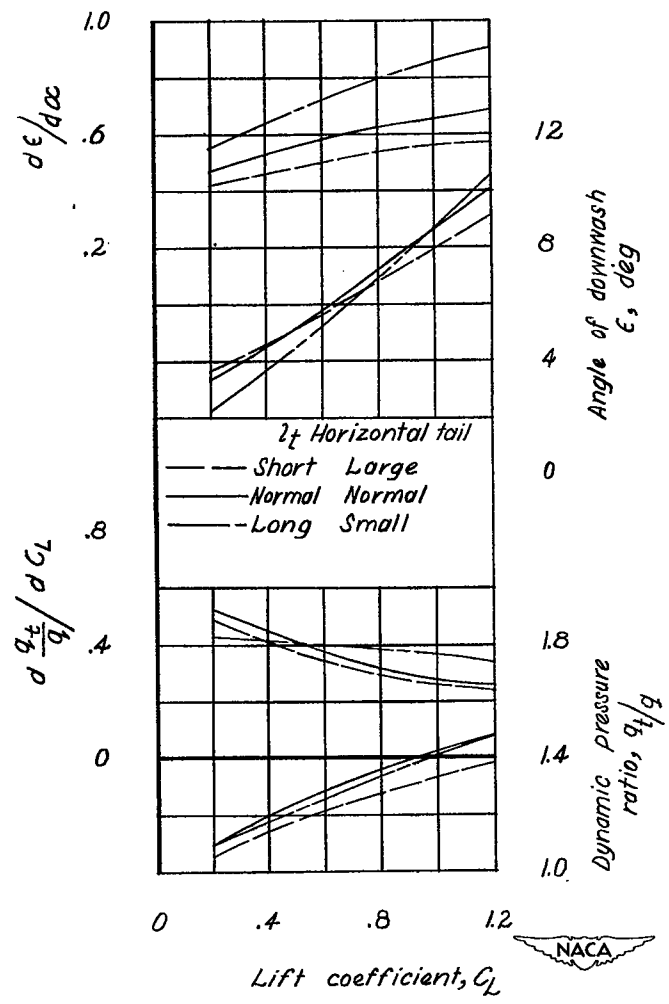

(b) Cruising configuration, power on.

Figure 25.- Effect of tail length on the longitudinal stability parameters of the single-propeller airplane model with constant tail volume.

(c) Landing configuration, windmilling propeller.

(d) Landing configuration, power on.

Figure 25.- Concluded.

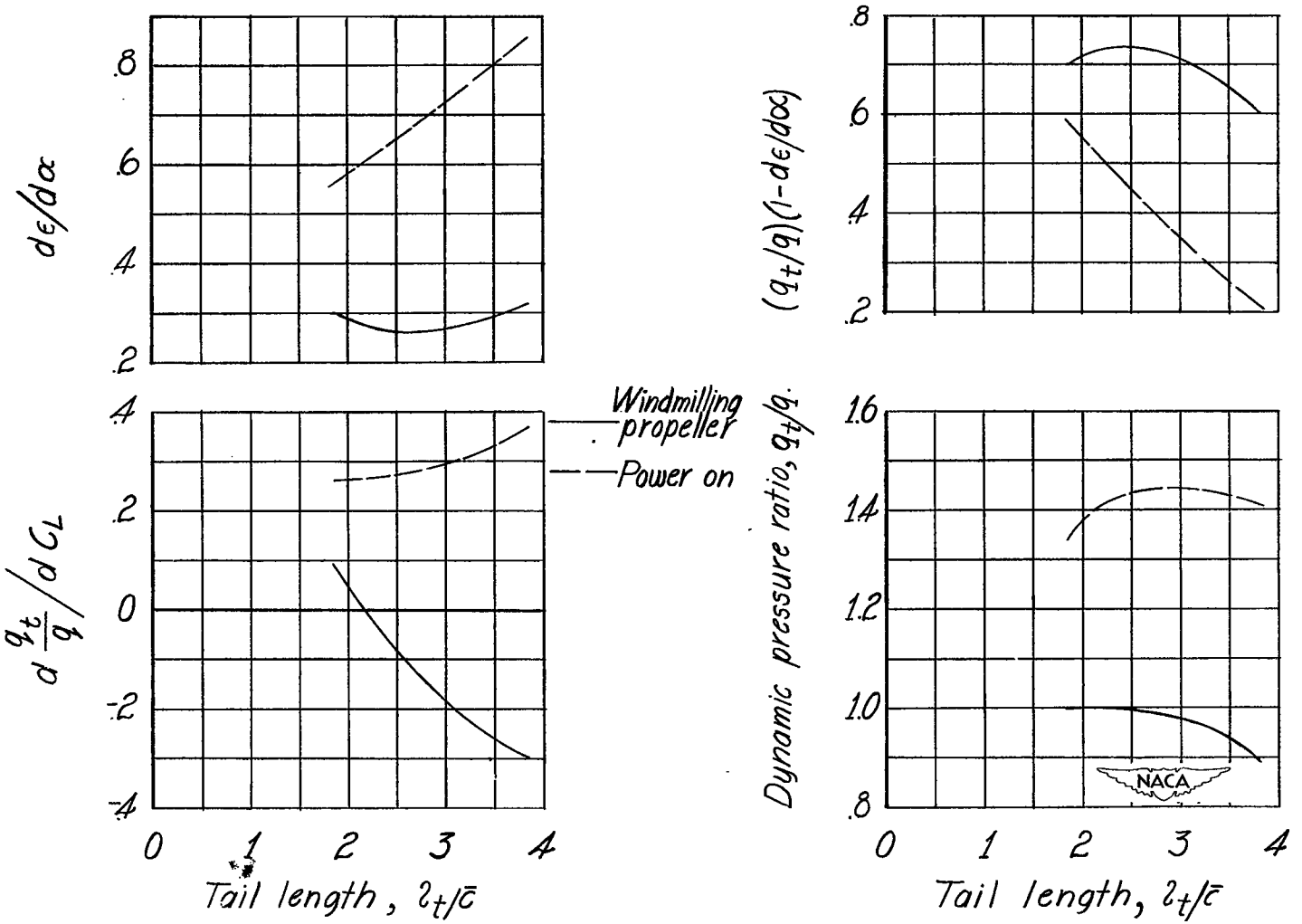

Figure 26.- Effect of power on the variation of the longitudinal stability parameters with tail length for the single-propeller airplane model with constant tail volume. Cruising configuration, $C_L = 1.0$.

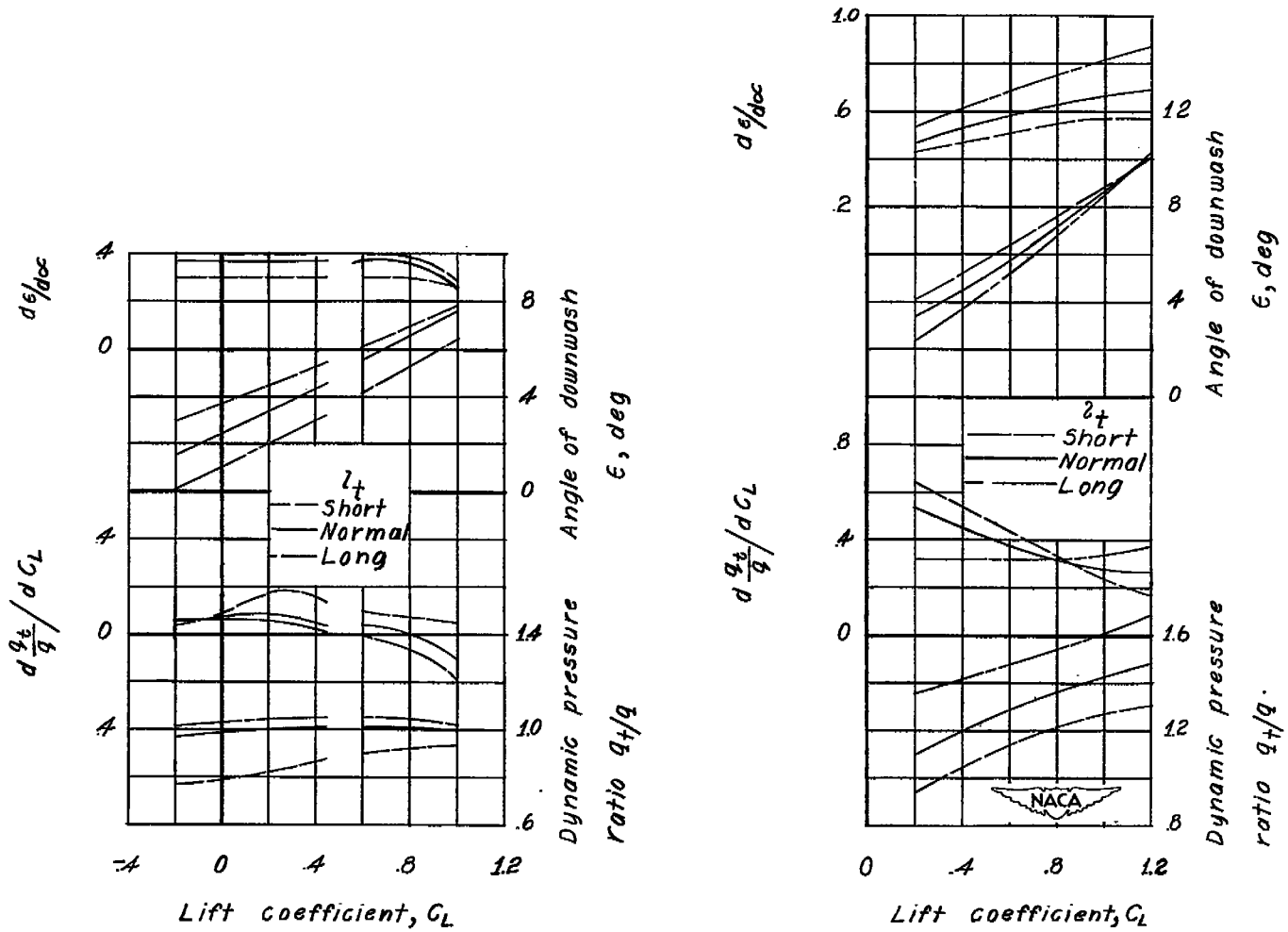

(a) Cruising configuration, windmilling propeller.

(b) Cruising configuration, power on.

Figure 27.- Effect of tail length on the longitudinal stability parameters of the single-propeller airplane model with constant tail area. Normal horizontal tail.

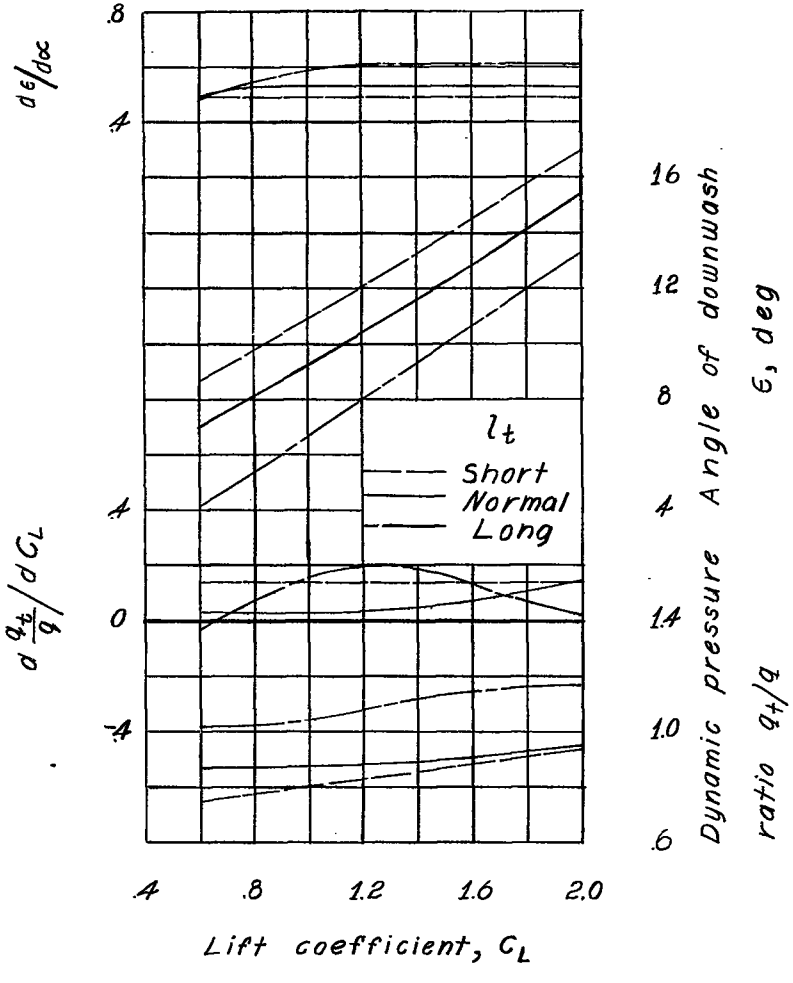

(c) Landing configuration, windmilling propeller.

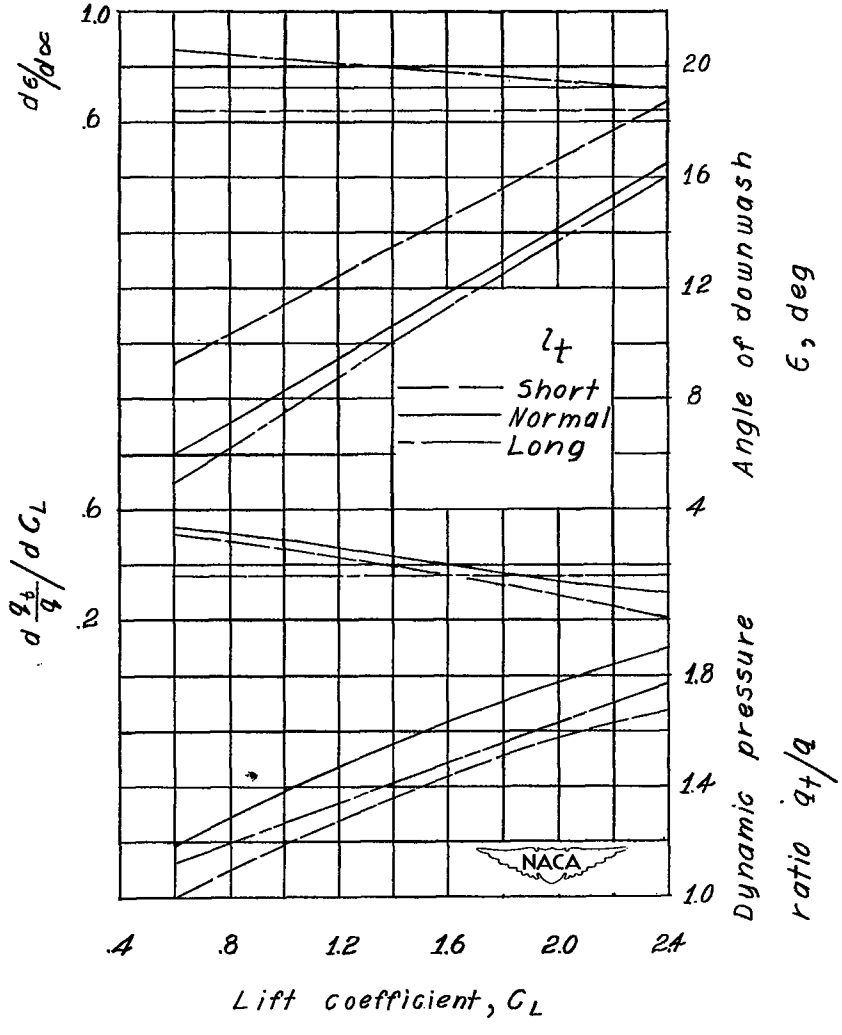

(d) Landing configuration, power on.

Figure 27.- Concluded.

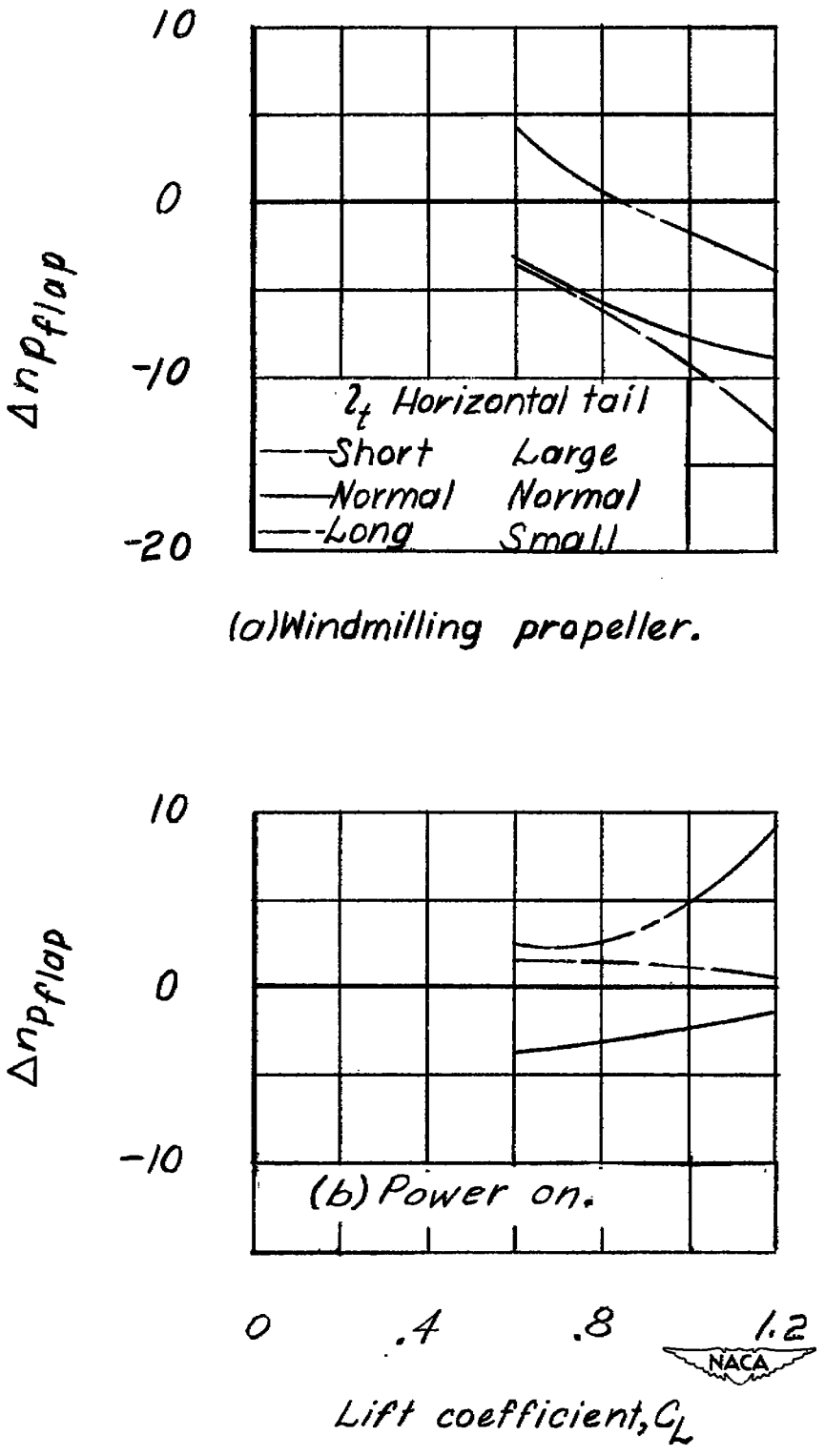

Figure 28.- Effect of tail length on the change in neutral-point location caused by flap deflection for the single-propeller airplane model with constant tail volume.

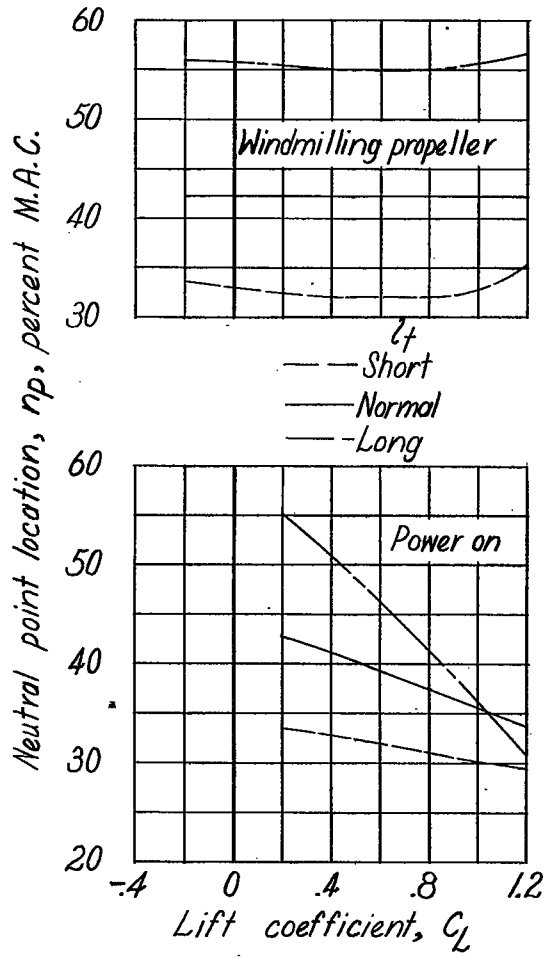

(a) Cruising configuration.

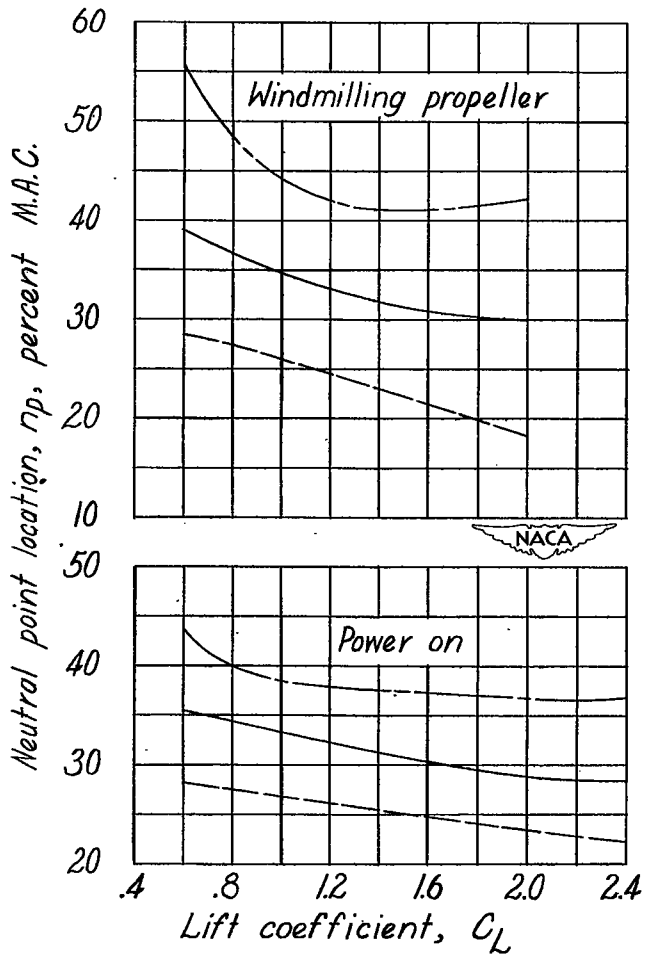

(b) Landing configuration.

Figure 29.- Effect of tail length on the neutral-point location of the single-propeller airplane model with constant tail area. Normal horizontal tail.

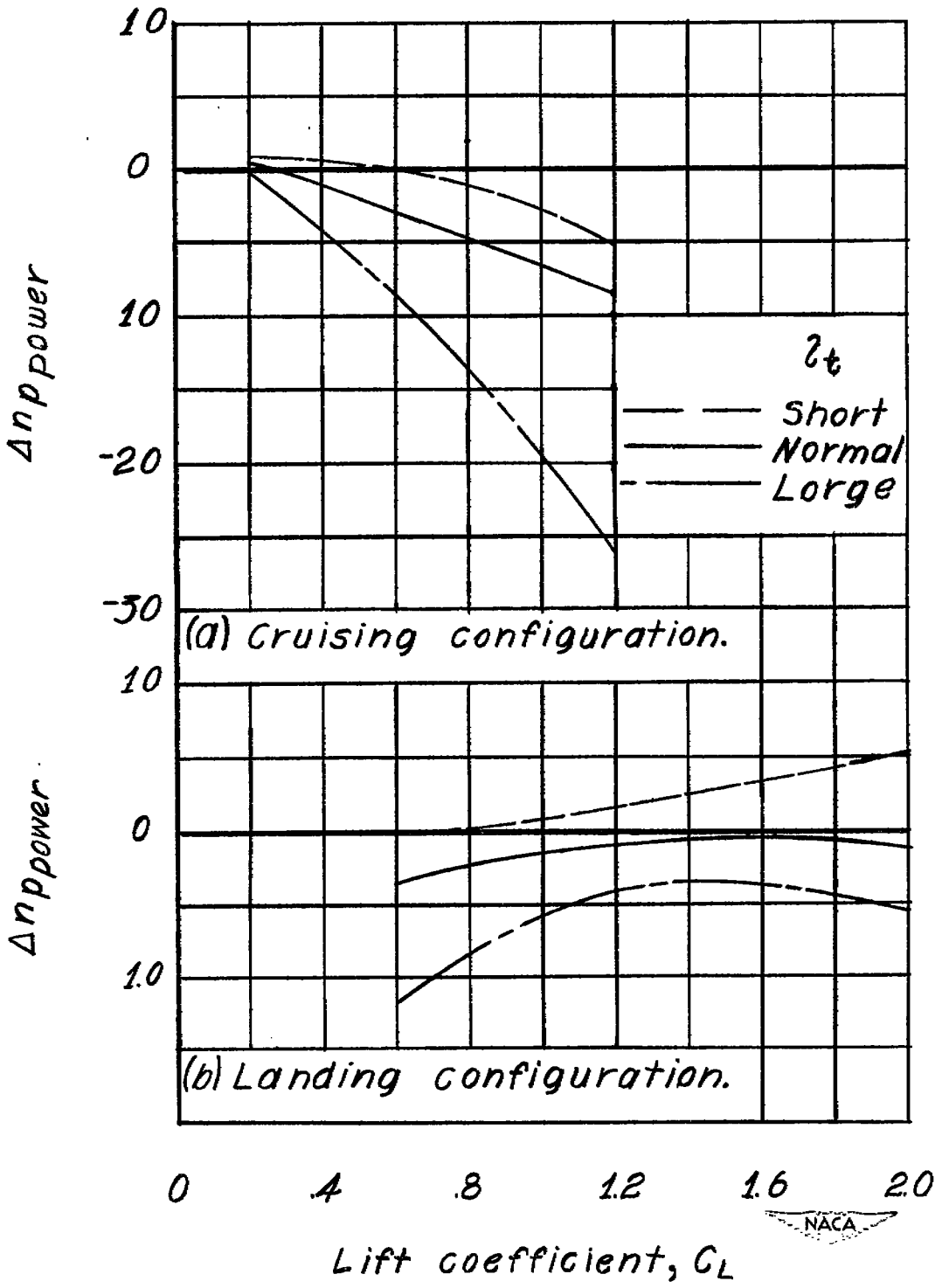

Figure 30.- Effect of tail length on the change in neutral-point location caused by power for the single-propeller airplane model with constant tail area. Normal horizontal tail.

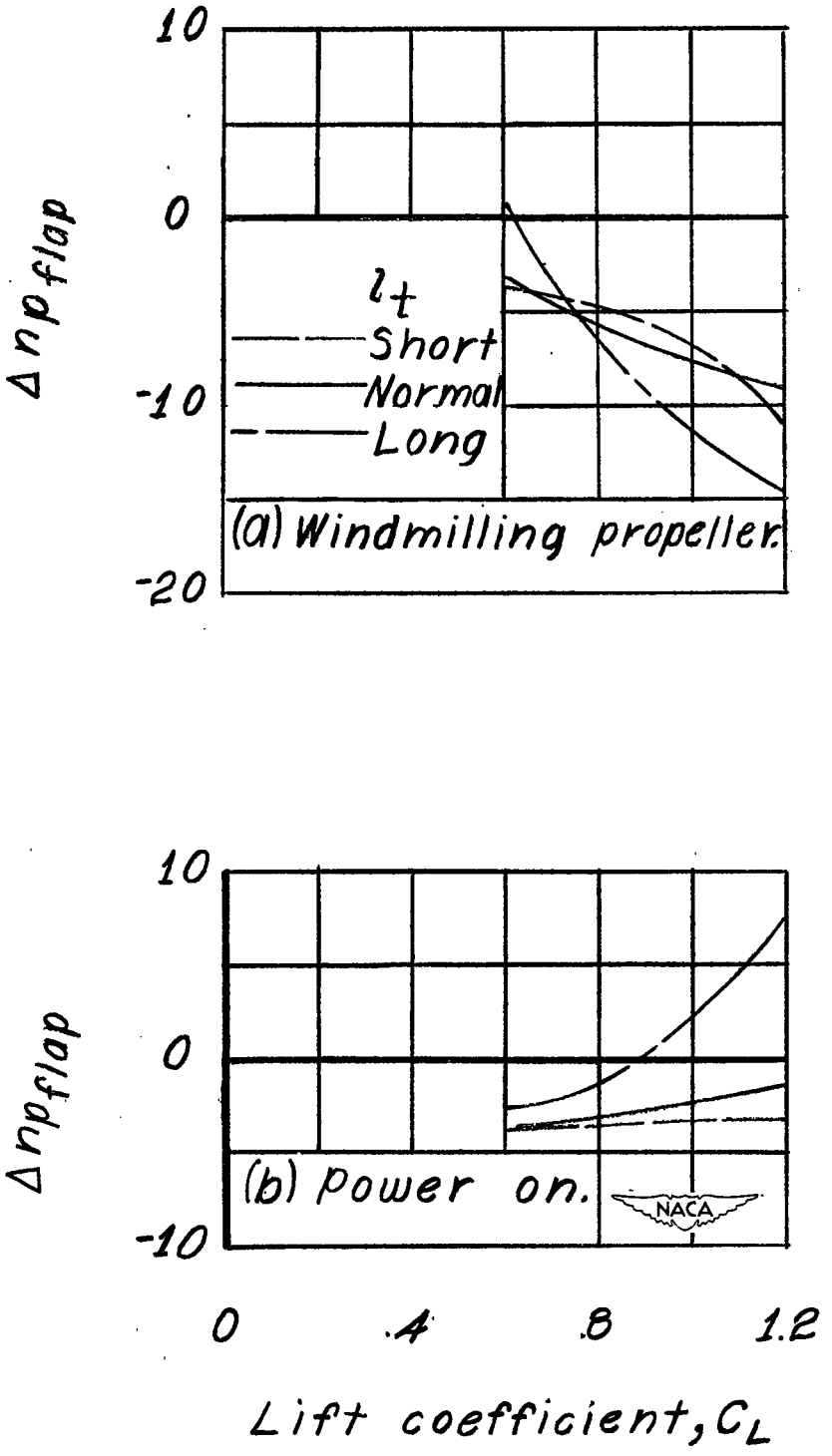

Figure 31.- Effect of tail length on the change in neutral-point location caused by flap deflection for the single-propeller airplane model with constant tail area. Normal horizontal tail.

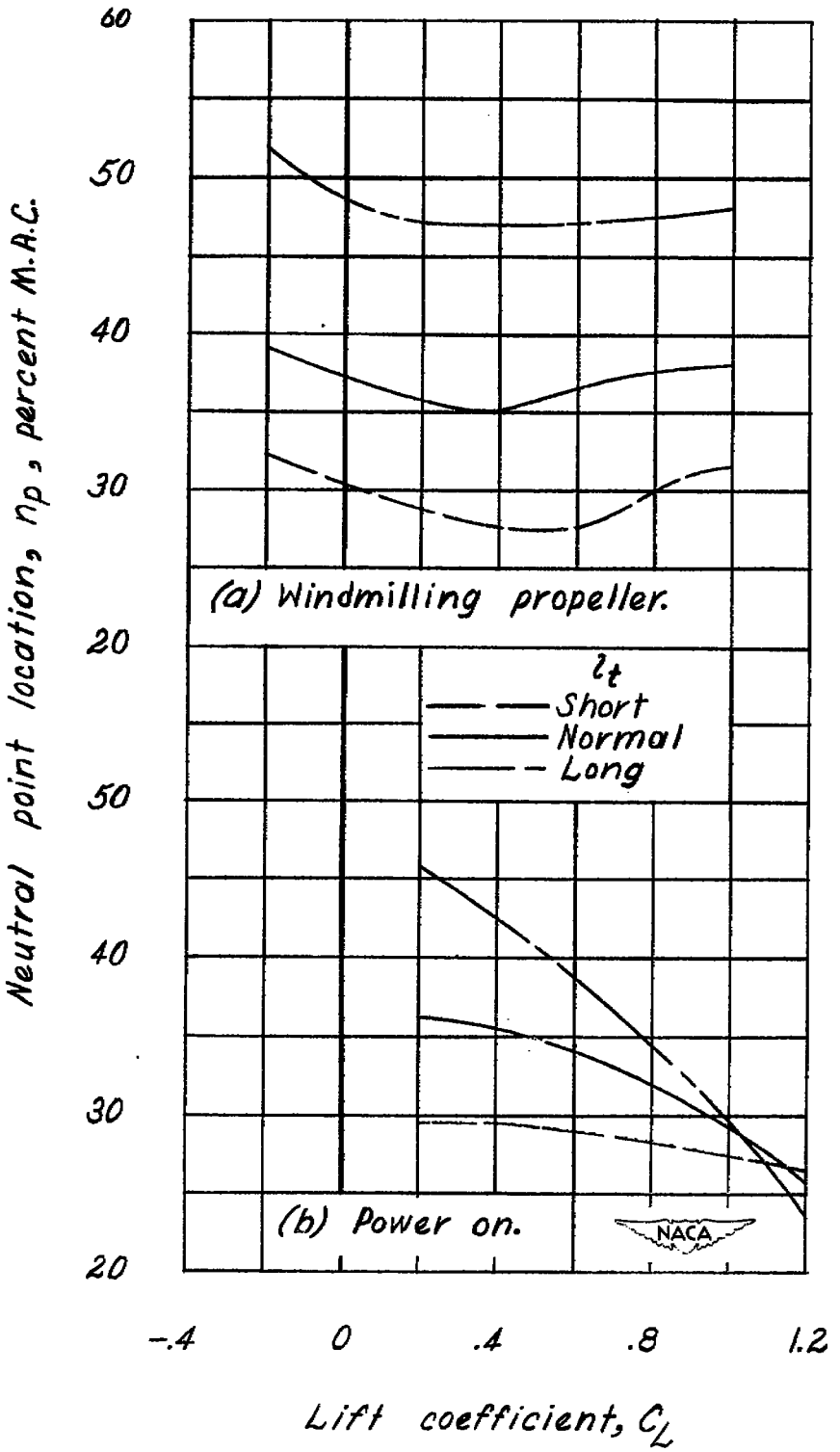

Figure 32.- Effect of tail length on the elevator-free neutral-point location of the single-propeller airplane model with constant tail area. Normal horizontal tail, cruising configuration.

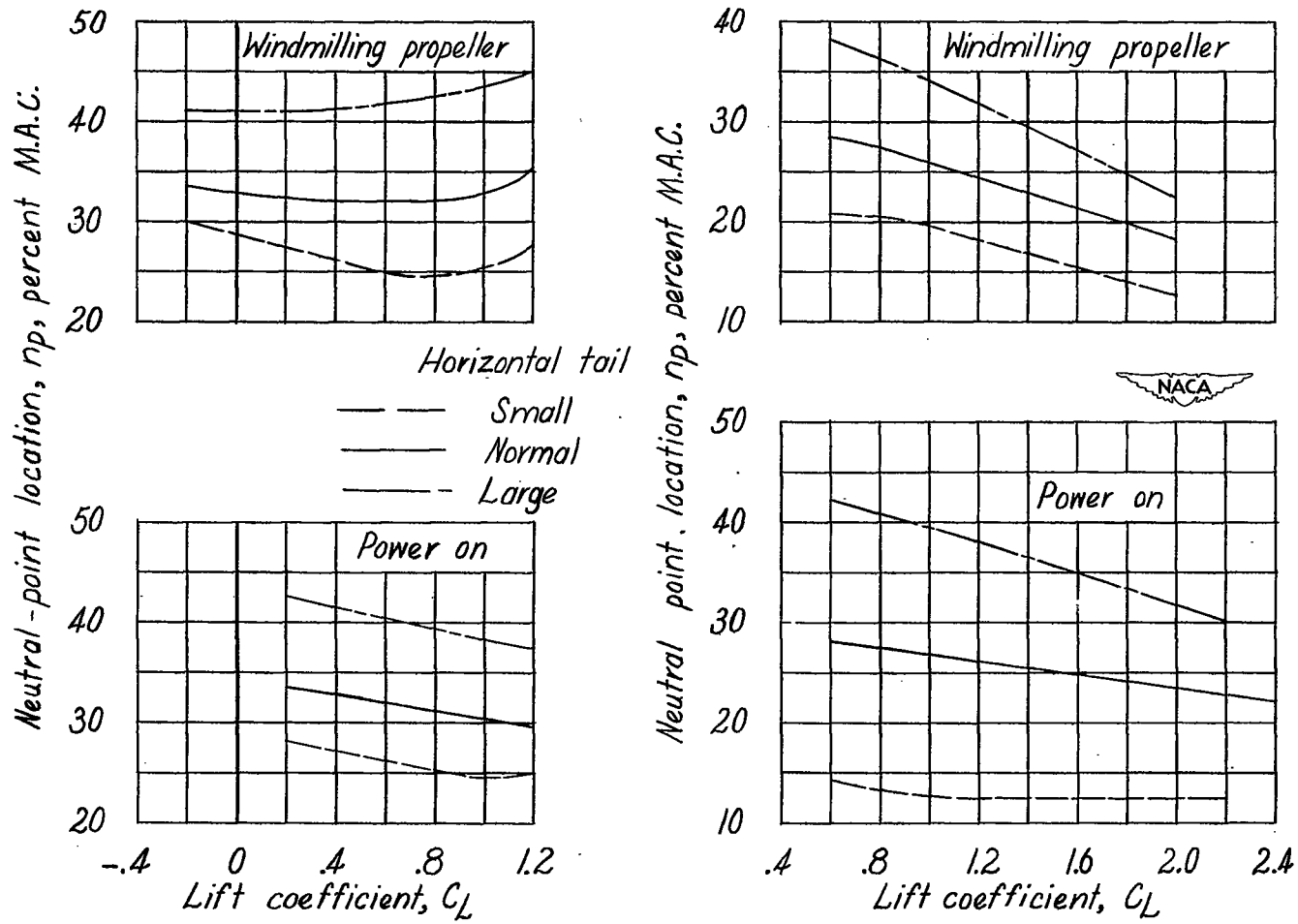

(a) Cruising configuration.

(b) Landing configuration.

Figure 33.- Effect of horizontal-tail area on the neutral-point location of the single-propeller airplane model with the short tail length.

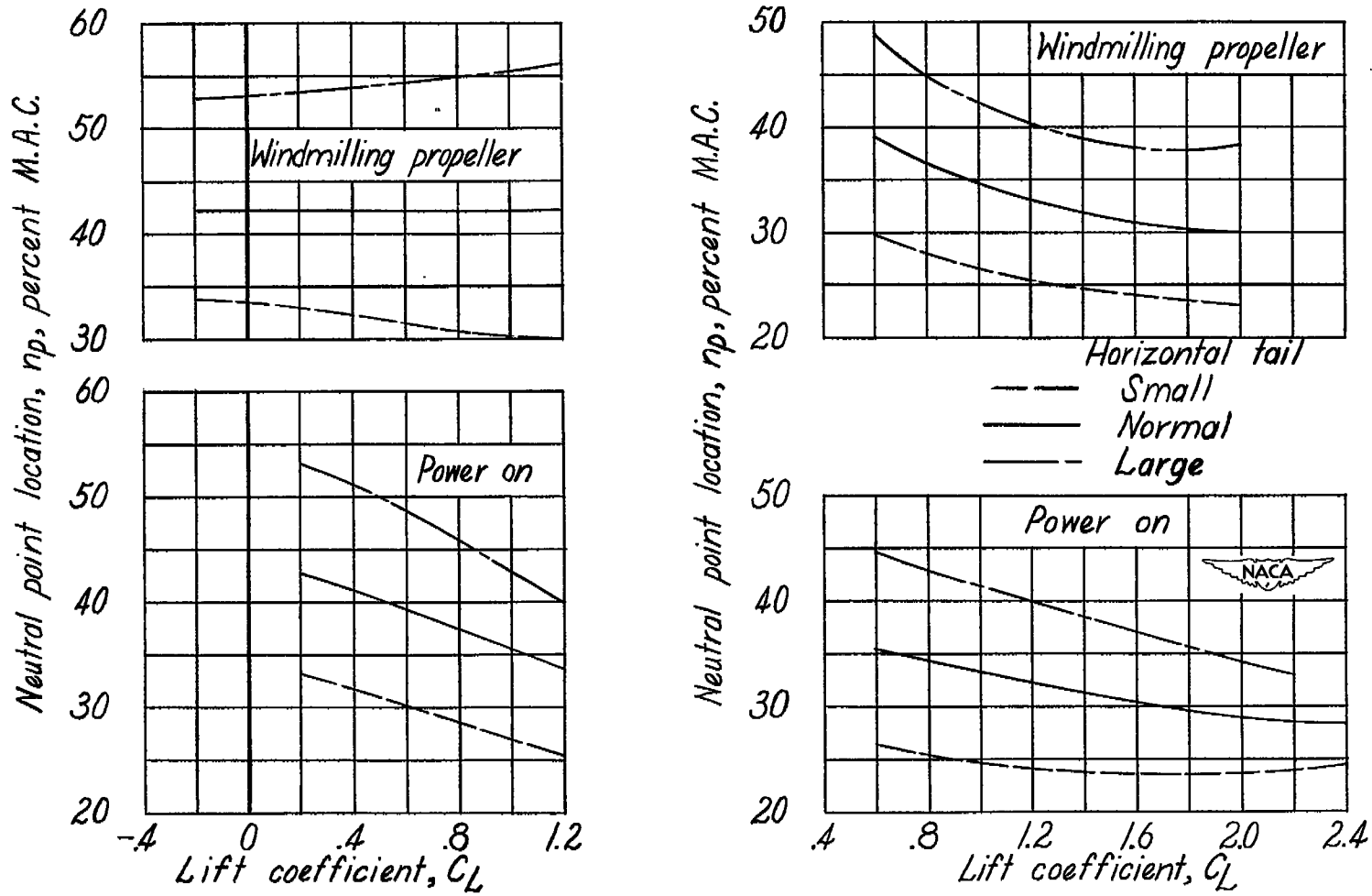

(a) Cruising configuration.

(b) Landing configuration.

Figure 34.- Effect of horizontal-tail area on the neutral-point location of the single-propeller airplane model with the normal tail length.

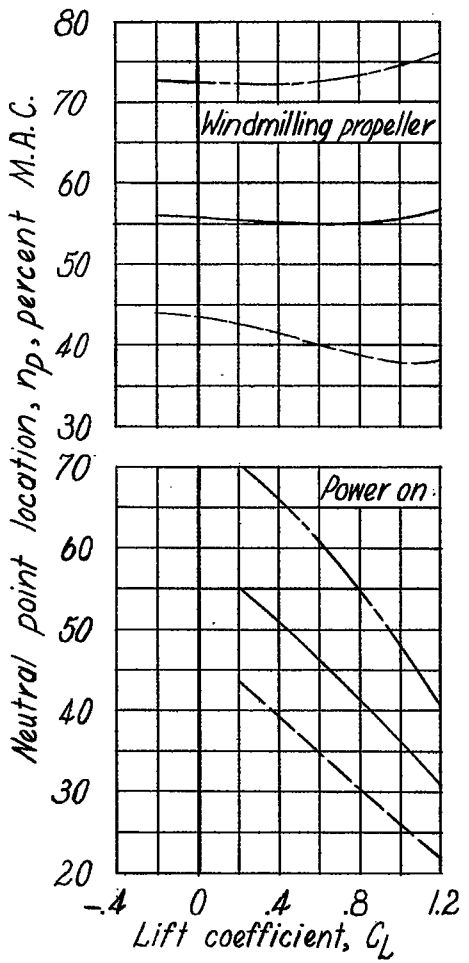

(a) Cruising configuration.

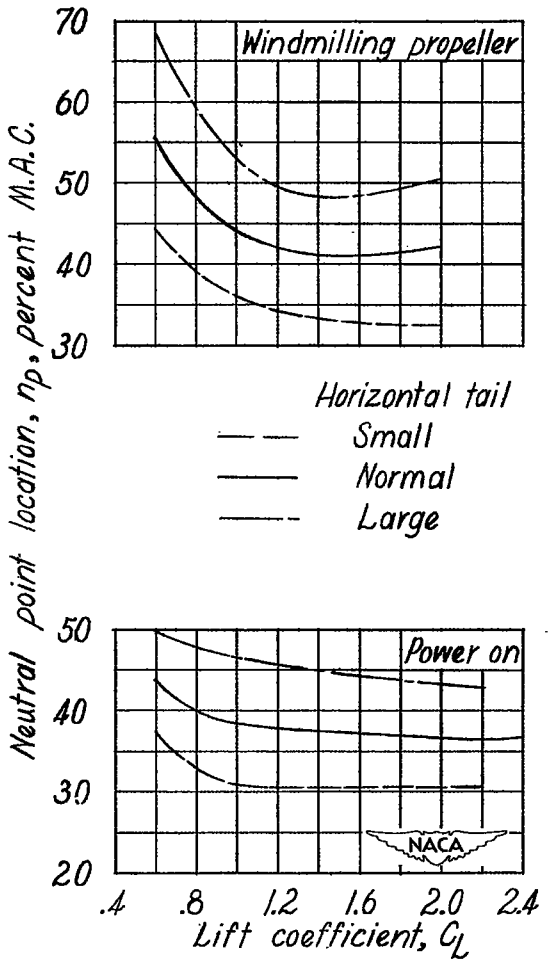

(b) Landing configuration.

Figure 35.- Effect of horizontal-tail area on the neutral-point location of the single-propeller airplane model with the long tail length.

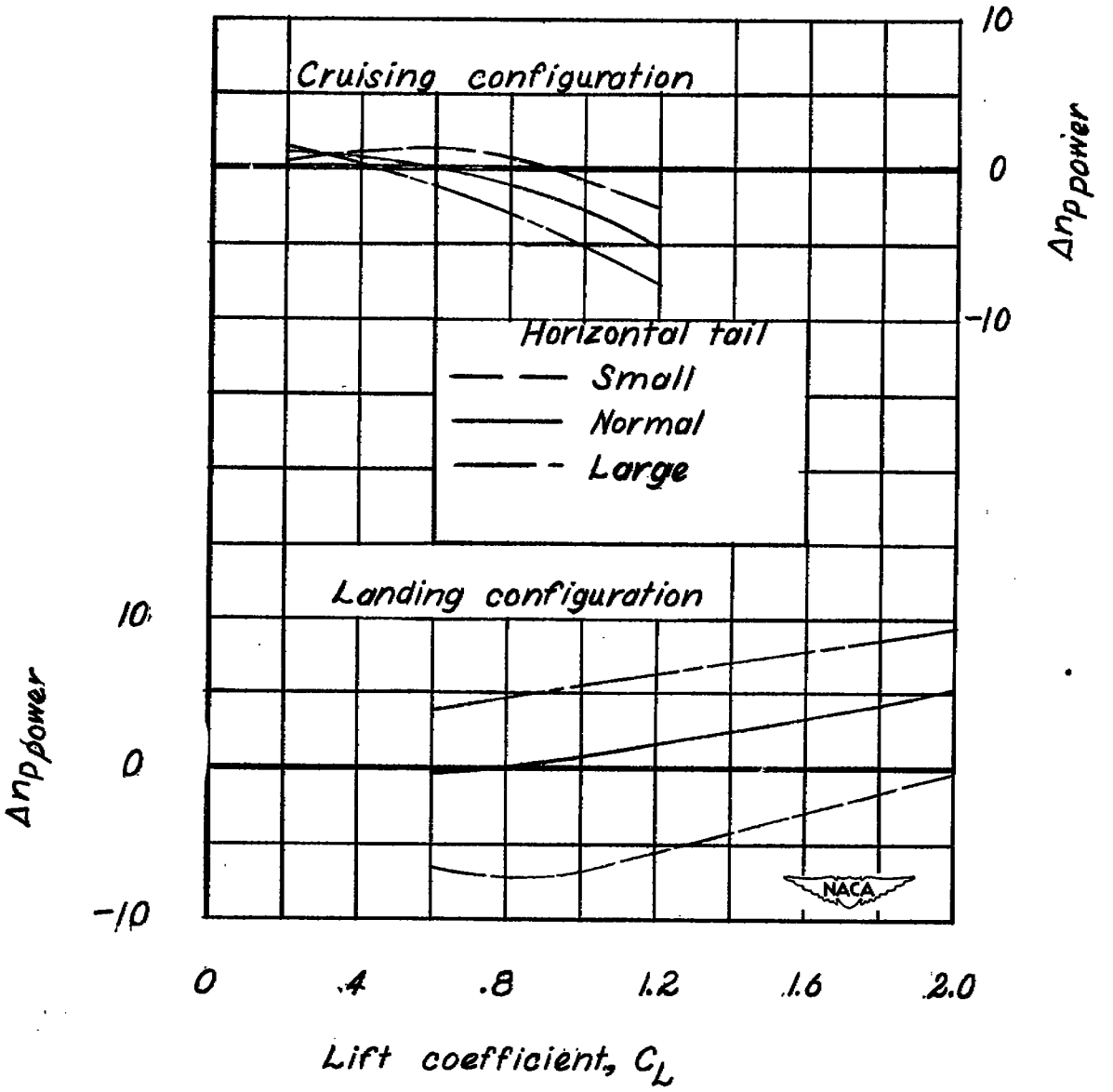

(a) Short tail length.

Figure 36.- Effect of horizontal-tail area on the change in neutral-point location caused by power for the single-propeller airplane model.

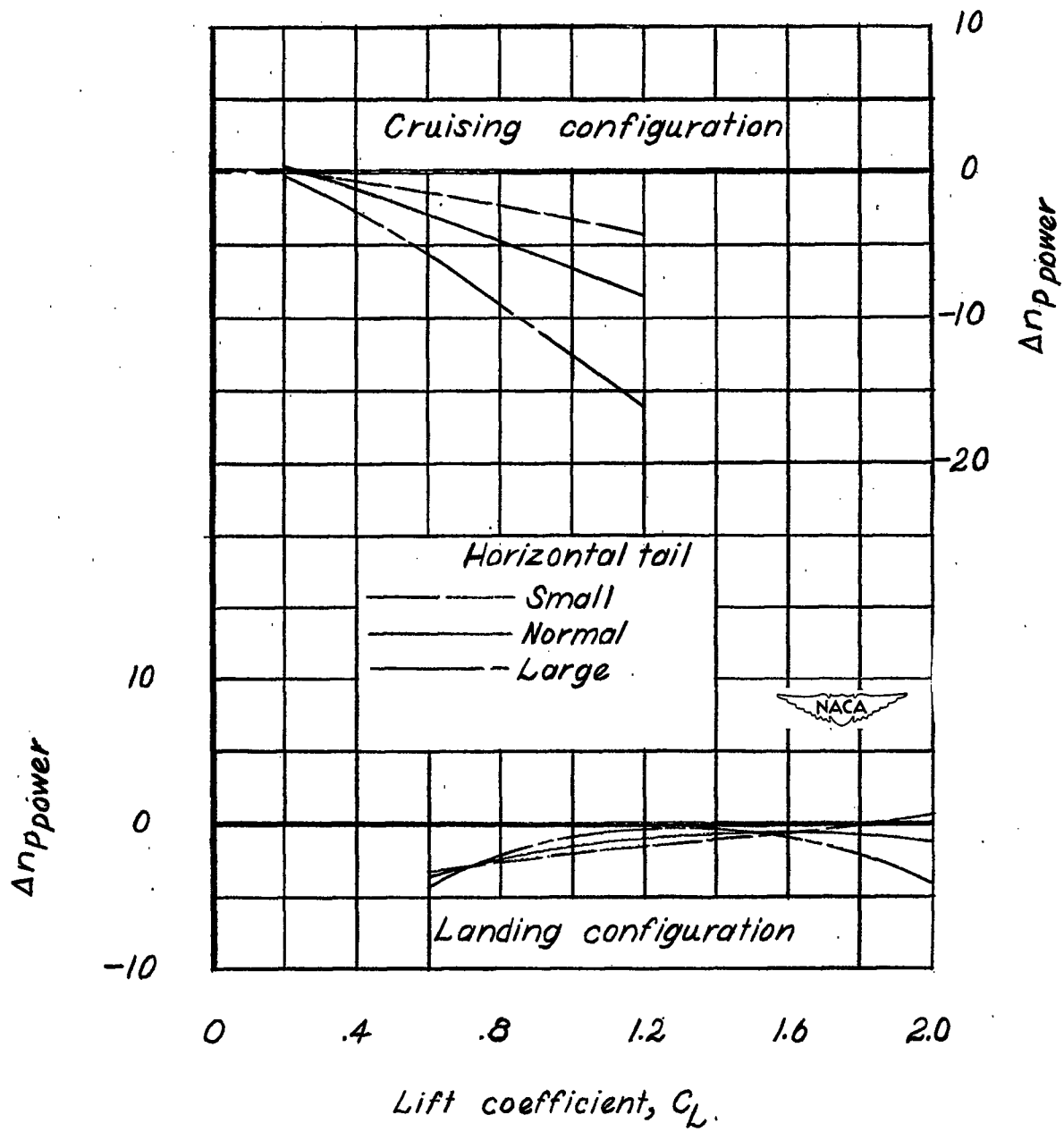

(b) Normal tail length.

Figure 36.- Continued.

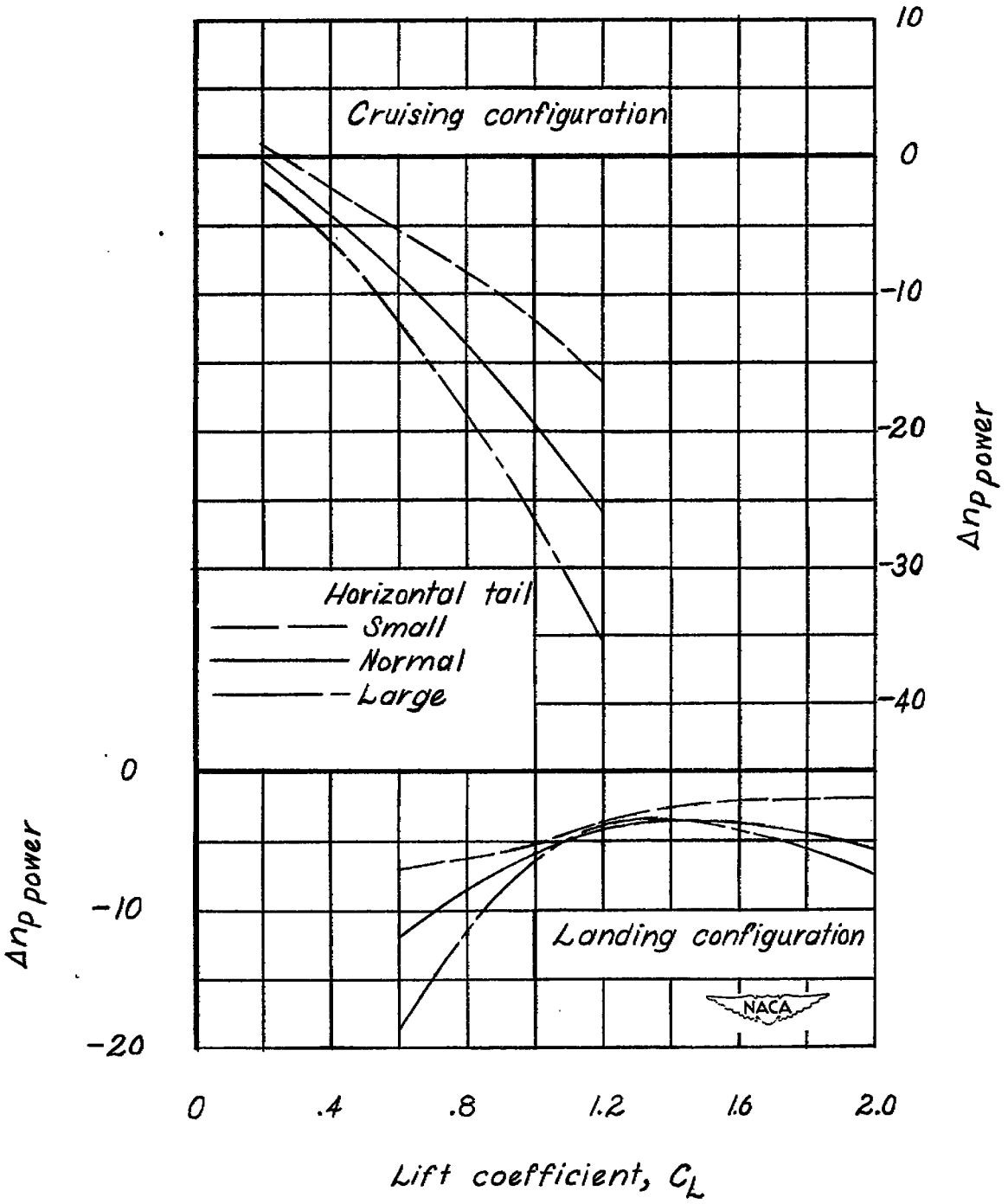

(c) Long tail length.

Figure 36.- Concluded.

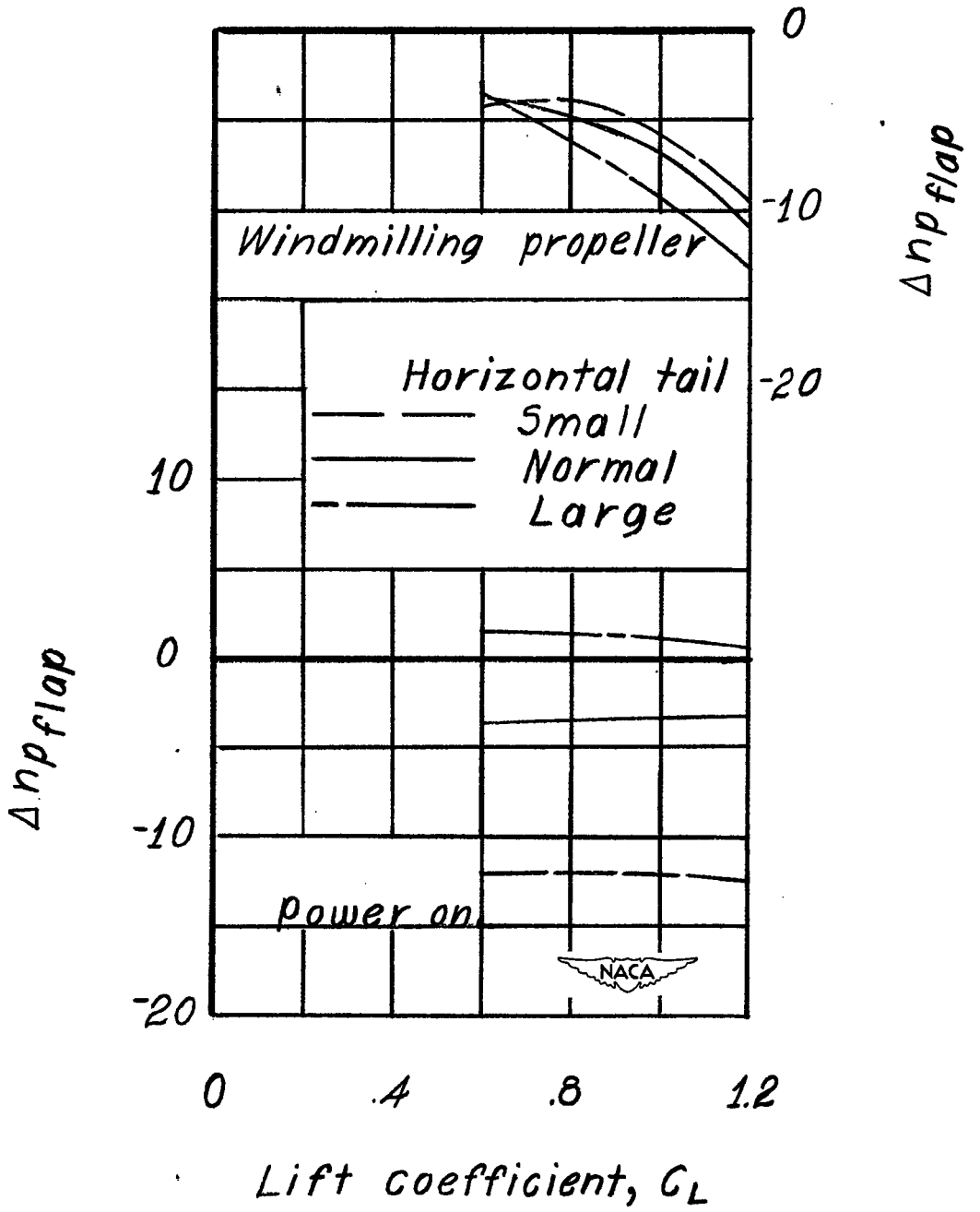

(a) Short tail length.

Figure 37.- Effect of horizontal-tail area on the change in neutral-point location caused by flap deflection for the single-propeller airplane model.

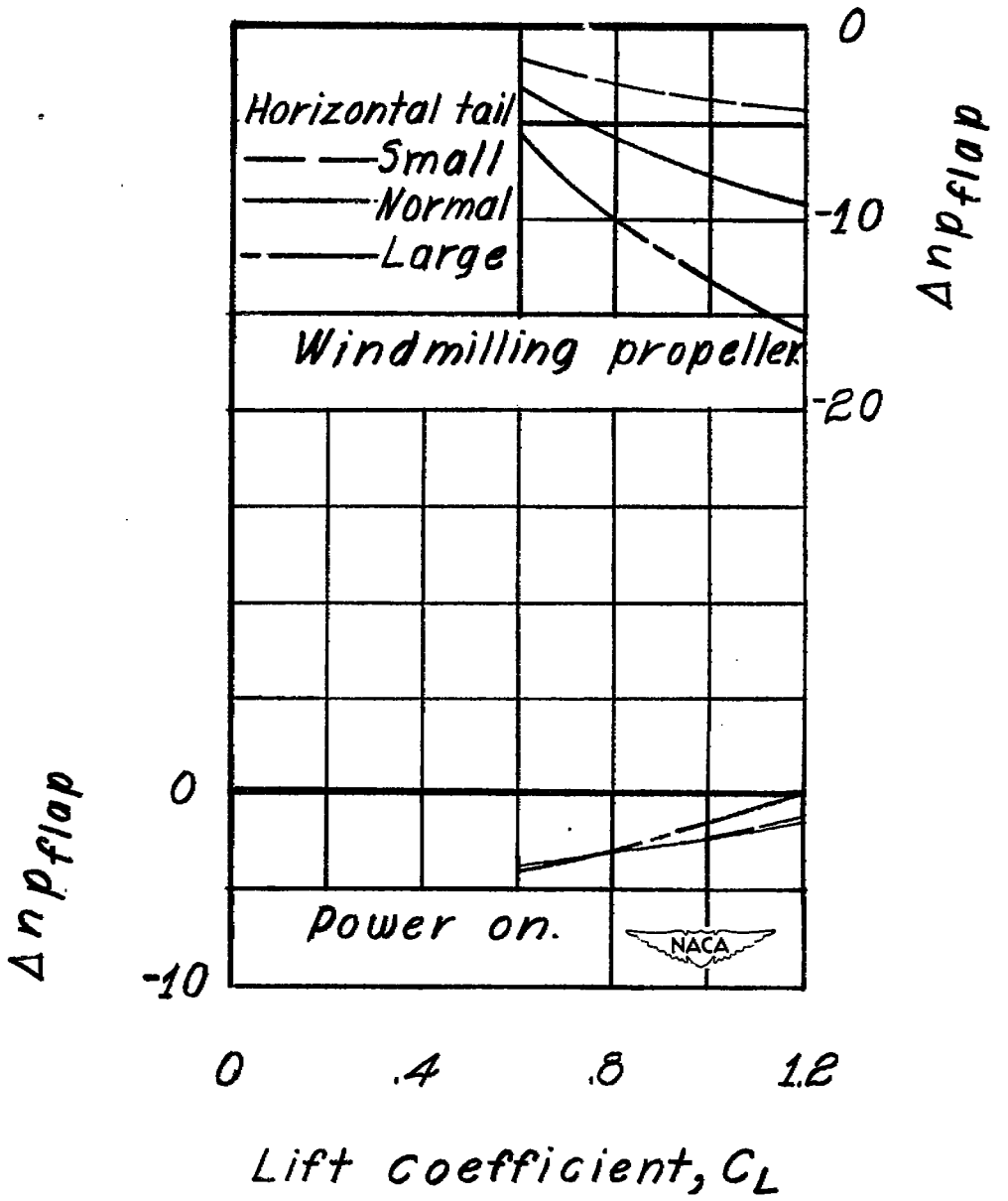

(b) Normal tail length.

Figure 37.- Continued.

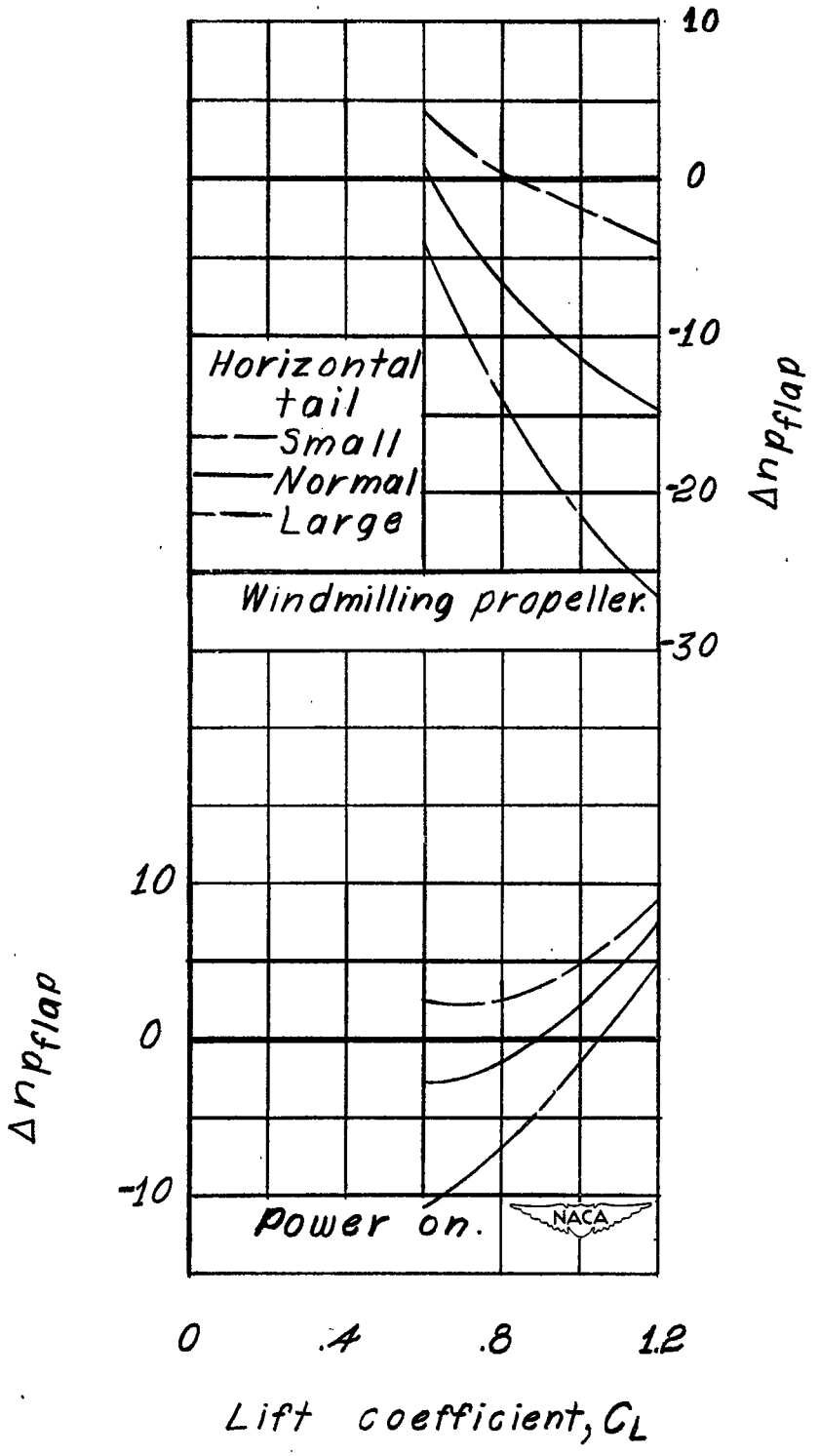

(c) Long tail length.

Figure 37.- Concluded.

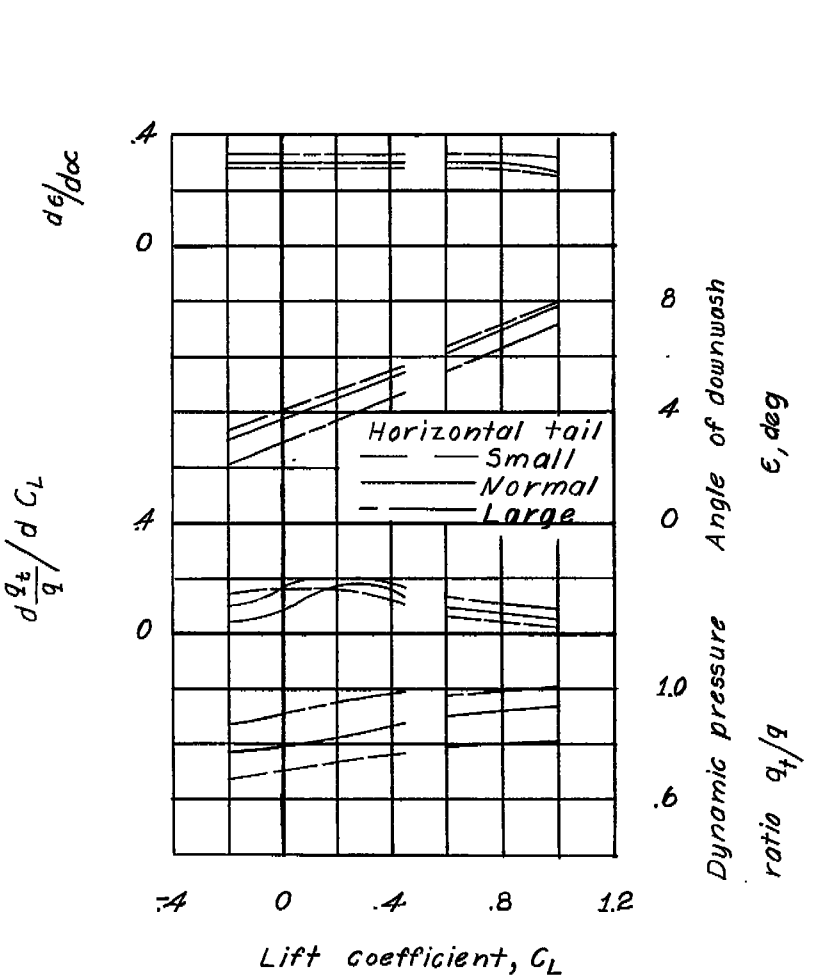

(a) Cruising configuration, windmilling propeller.

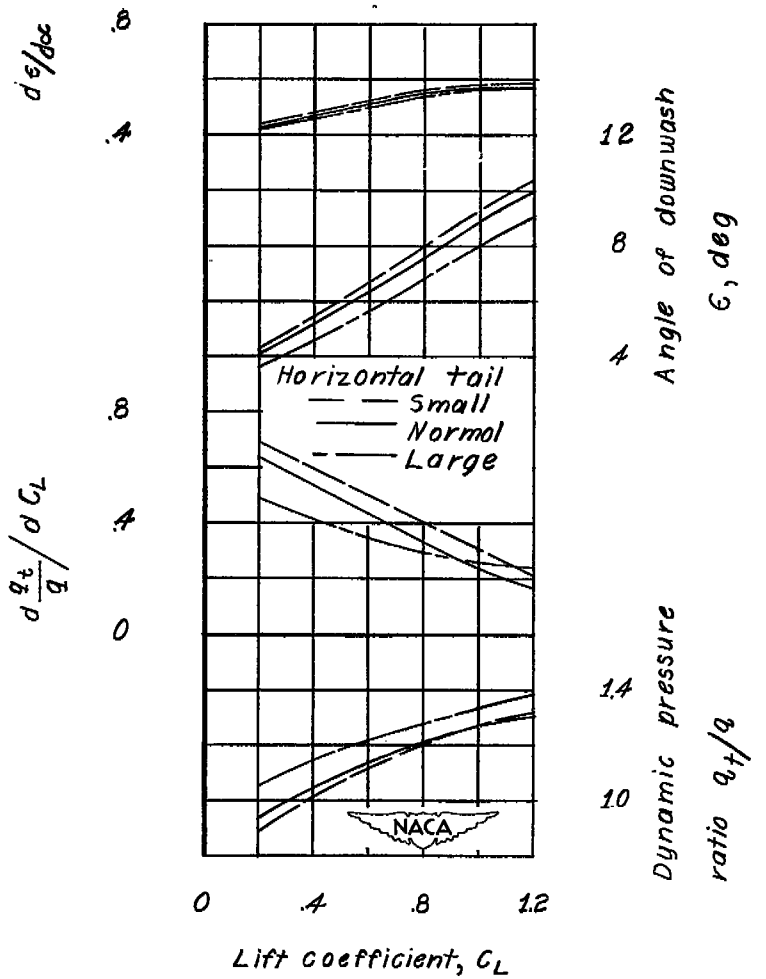

(b) Cruising configuration, power on.

Figure 38.- Effect of horizontal-tail area on the longitudinal stability parameters of the single-propeller airplane model with the short tail length.

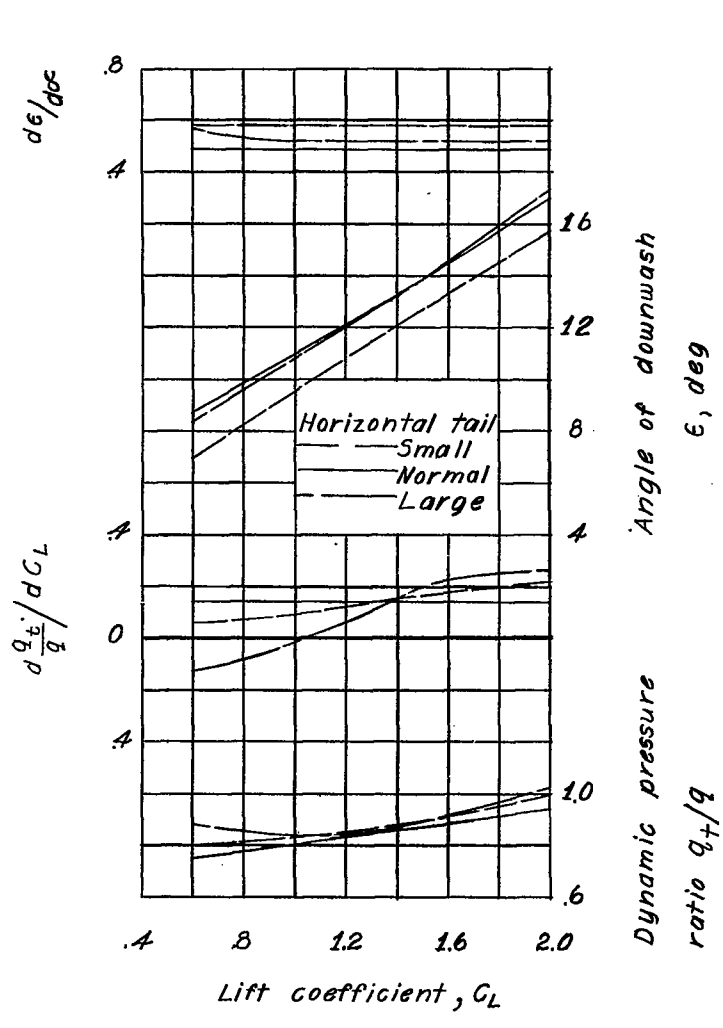

(c) Landing configuration, windmilling propeller.

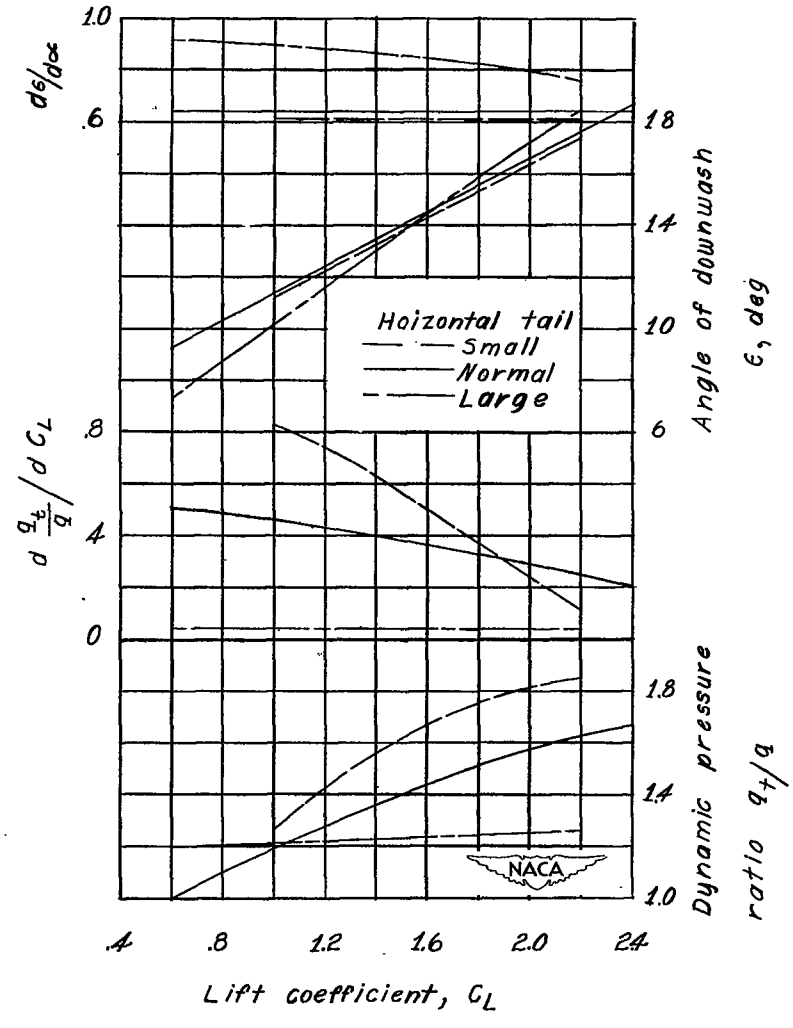

(d) Landing configuration, power on.

Figure 38.- Concluded.

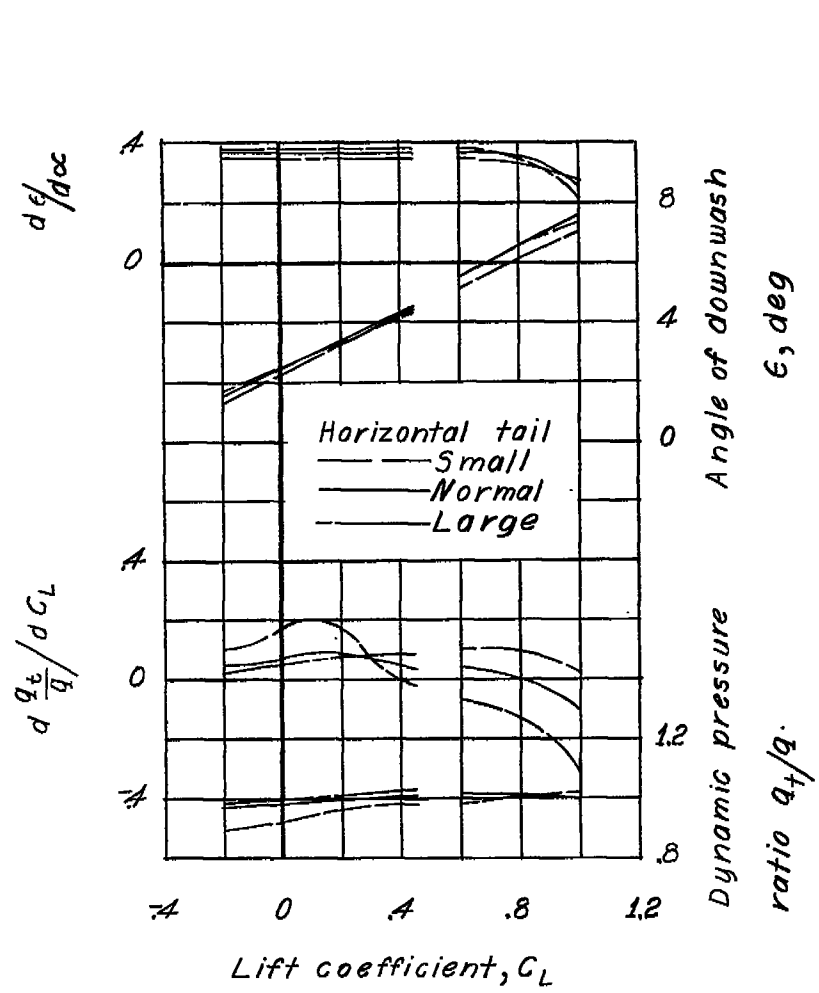

(a) Cruising configuration, windmilling propeller.

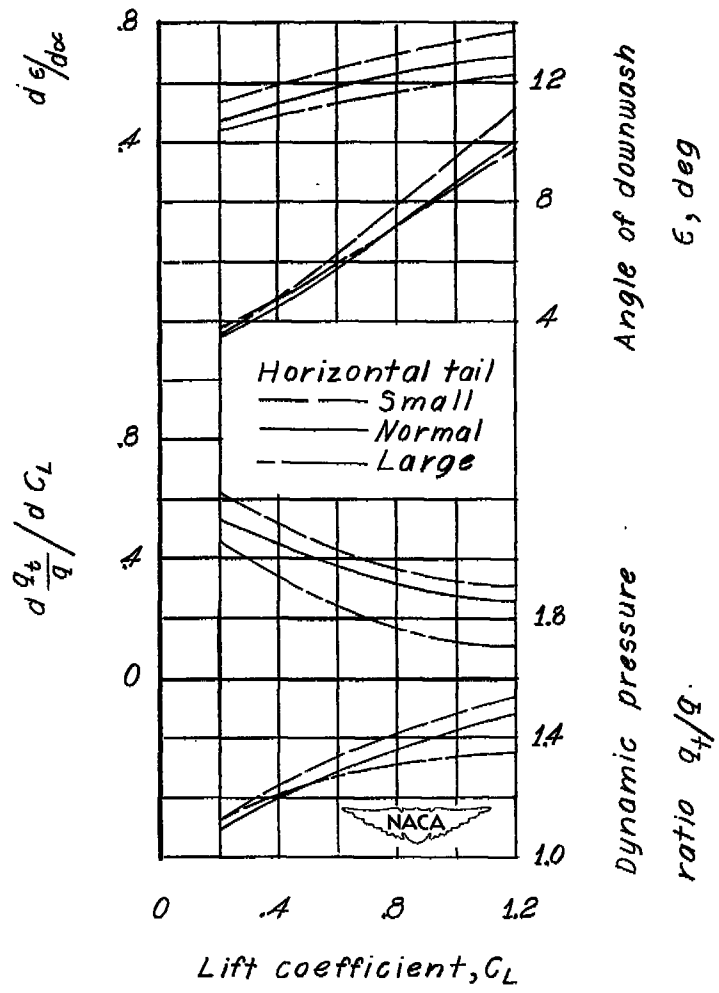

(b) Cruising configuration, power on.

Figure 39.- Effect of horizontal-tail area on the longitudinal stability parameters of the single-propeller airplane model with the normal tail length.

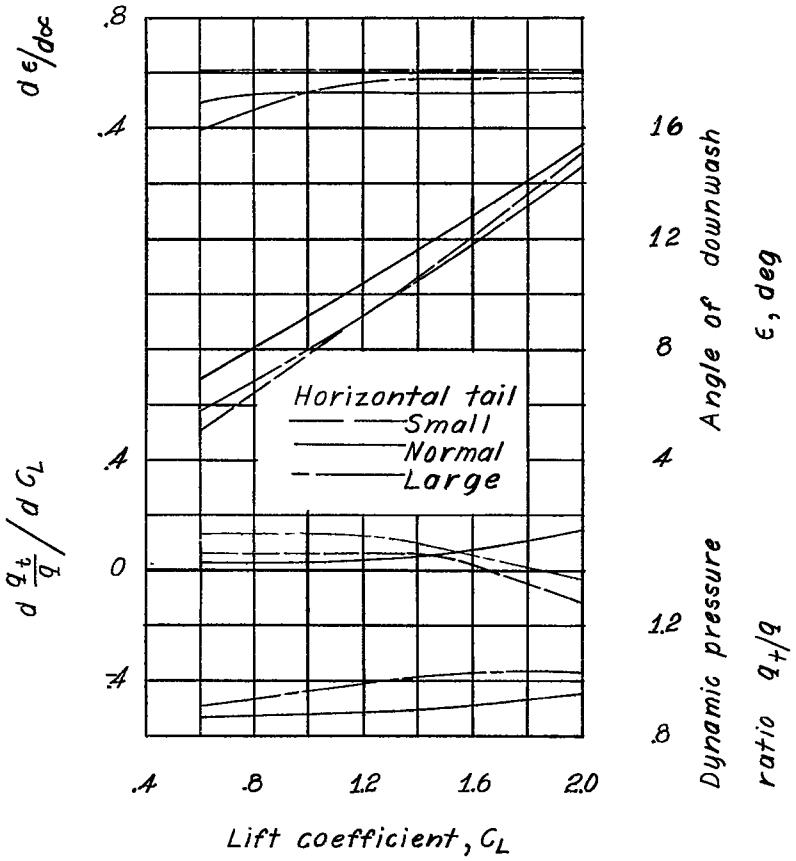

(c) Landing configuration, windmilling propeller.

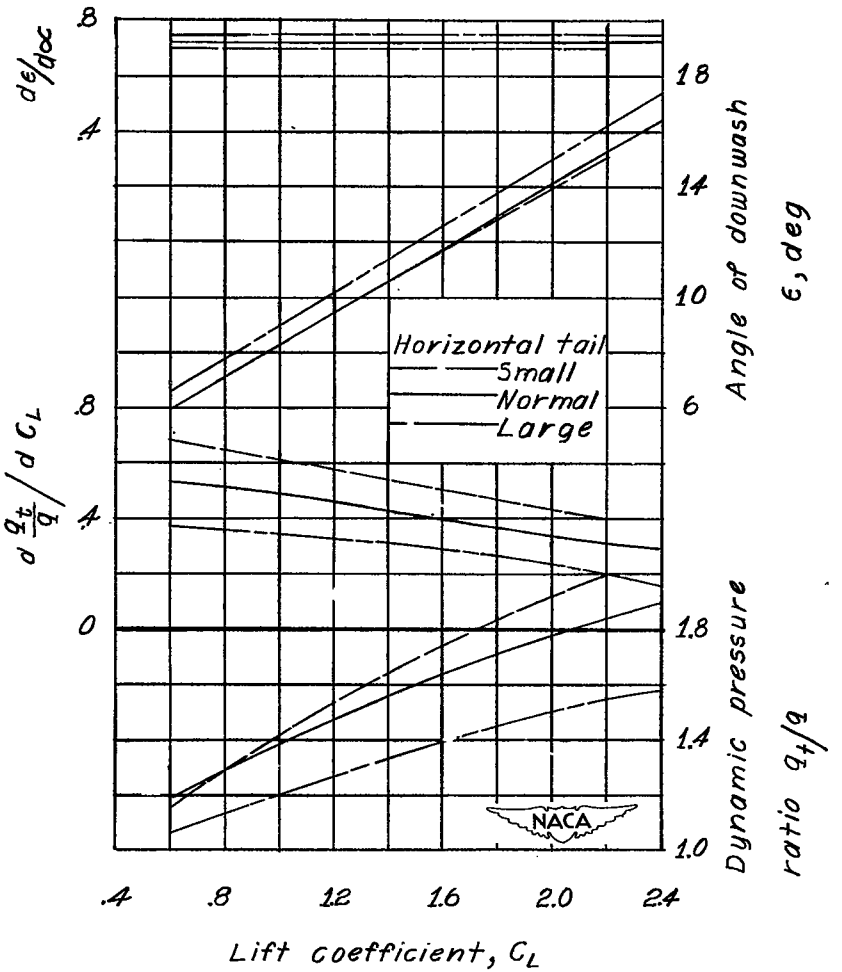

(d) Landing configuration, power on.

Figure 39.- Concluded.

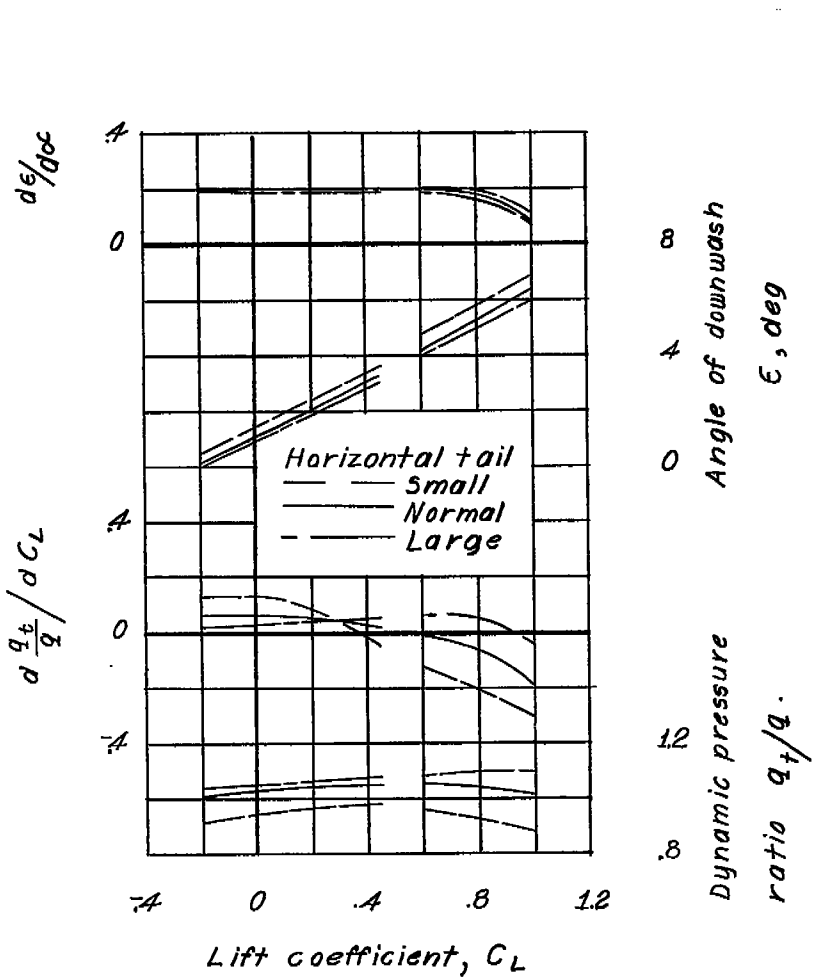

(a) Cruising configuration, windmilling propeller.

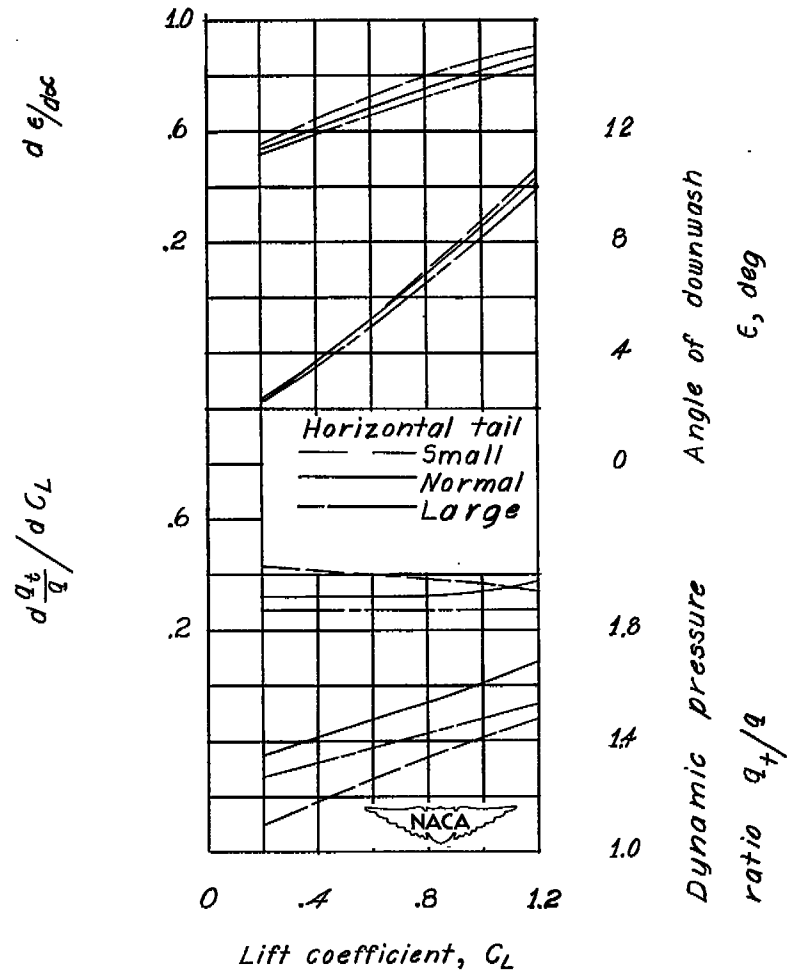

(b) Cruising configuration, power on.

Figure 40.- Effect of horizontal-tail area on the longitudinal stability parameters of the single-propeller airplane model with the long tail length.

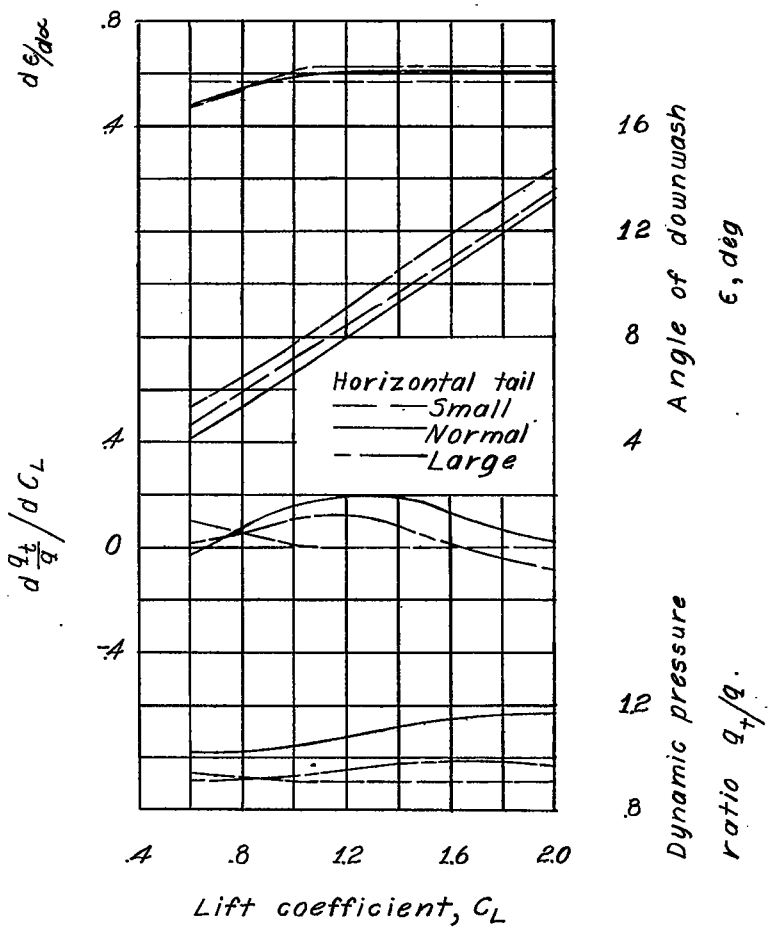

(c) Landing configuration, windmilling propeller.

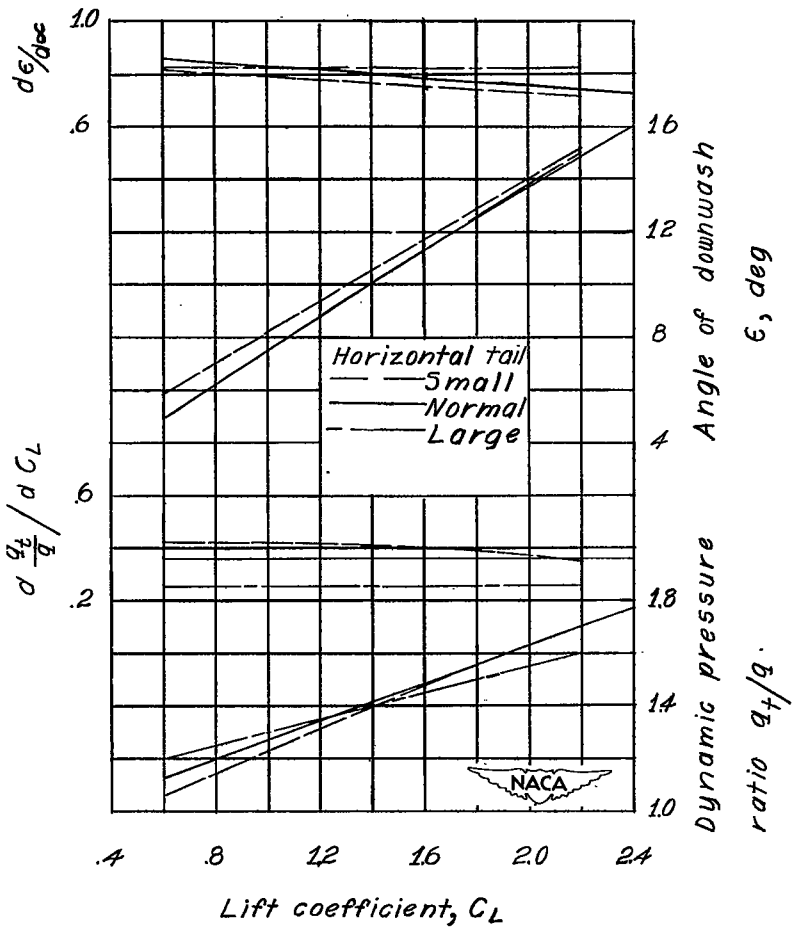

(d) Landing configuration, power on.

Figure 40.- Concluded.

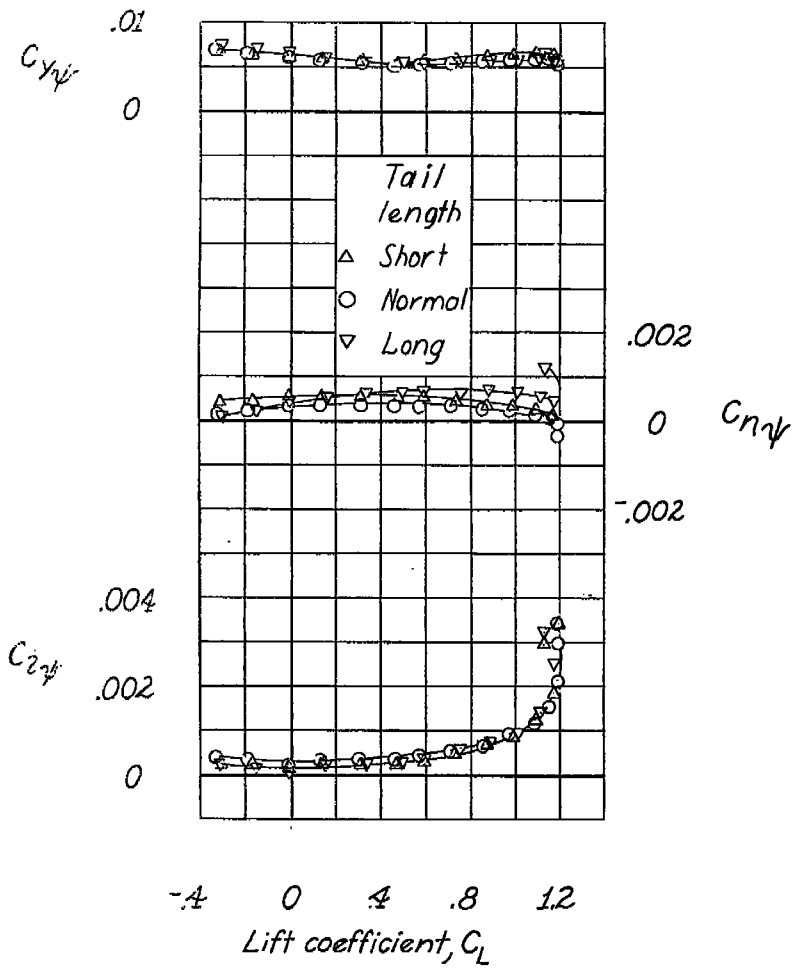

(a) Cruising configuration, windmilling propeller.

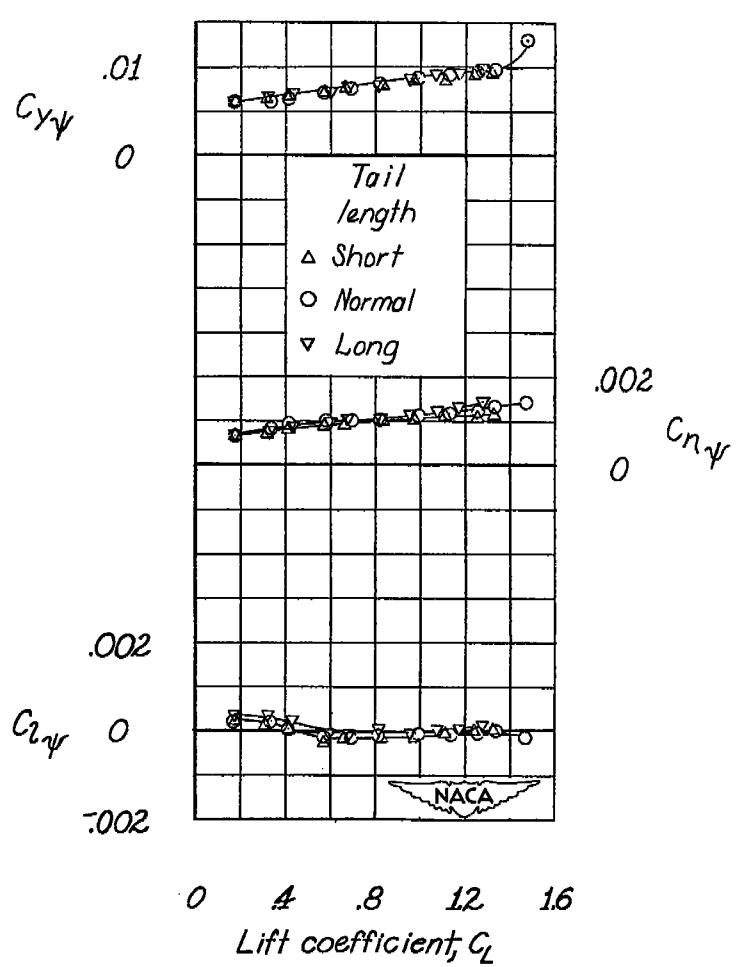

(b) Cruising configuration, power on.

Figure 41.- Effect of tail length on the lateral stability parameters of the single-propeller airplane model. Tail off.

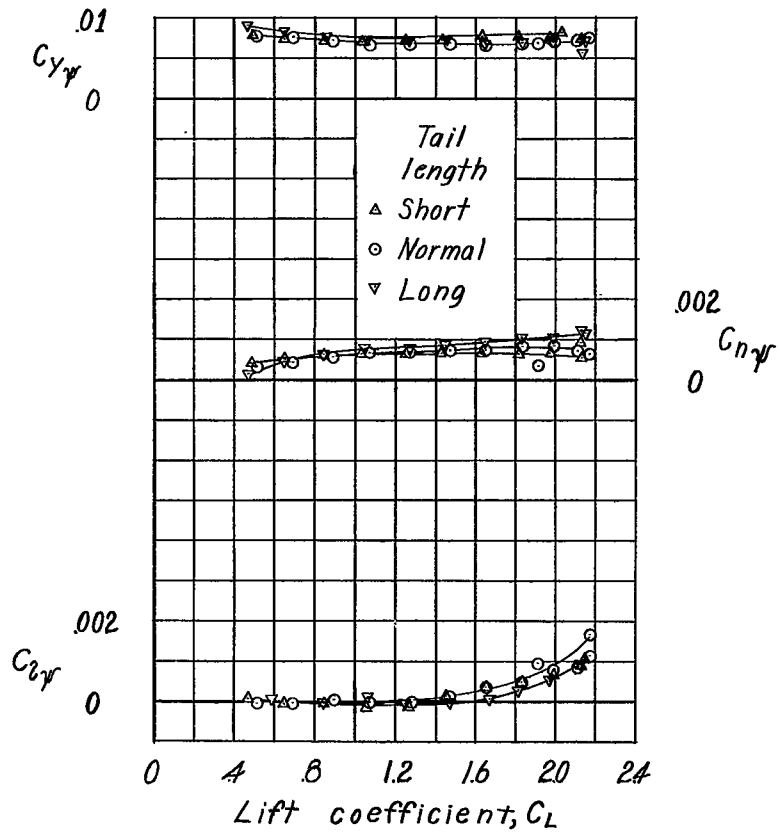

(c) Landing configuration, windmilling propeller.

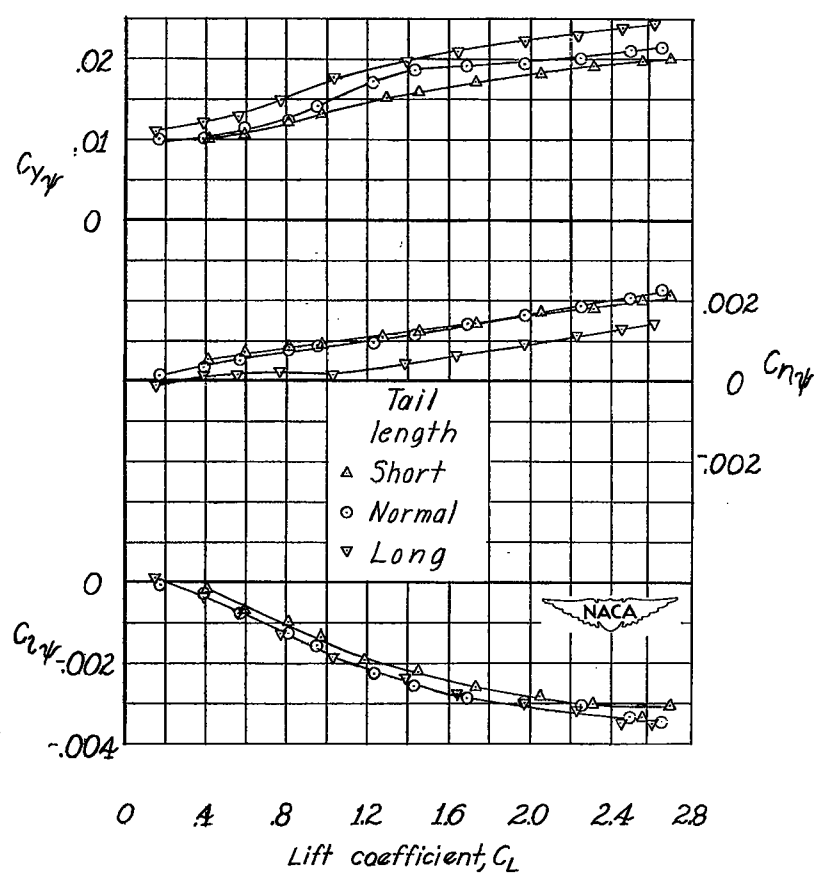

(d) Landing configuration, power on.

Figure 41.- Concluded.

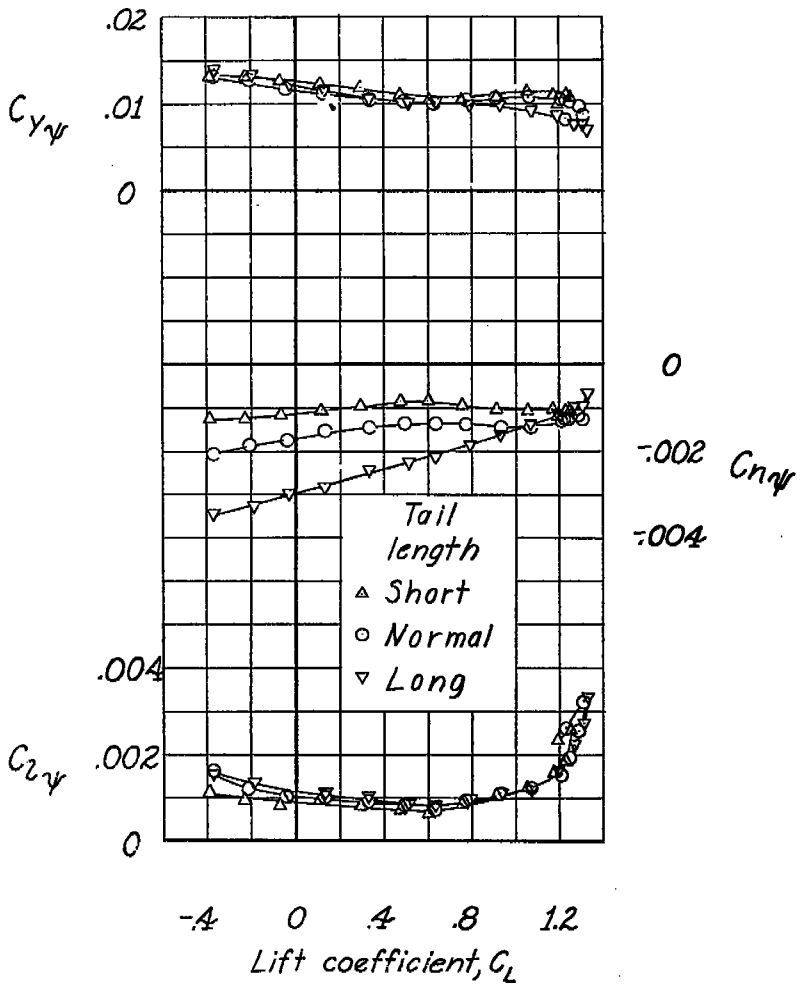

(a) Cruising configuration, windmilling propeller.

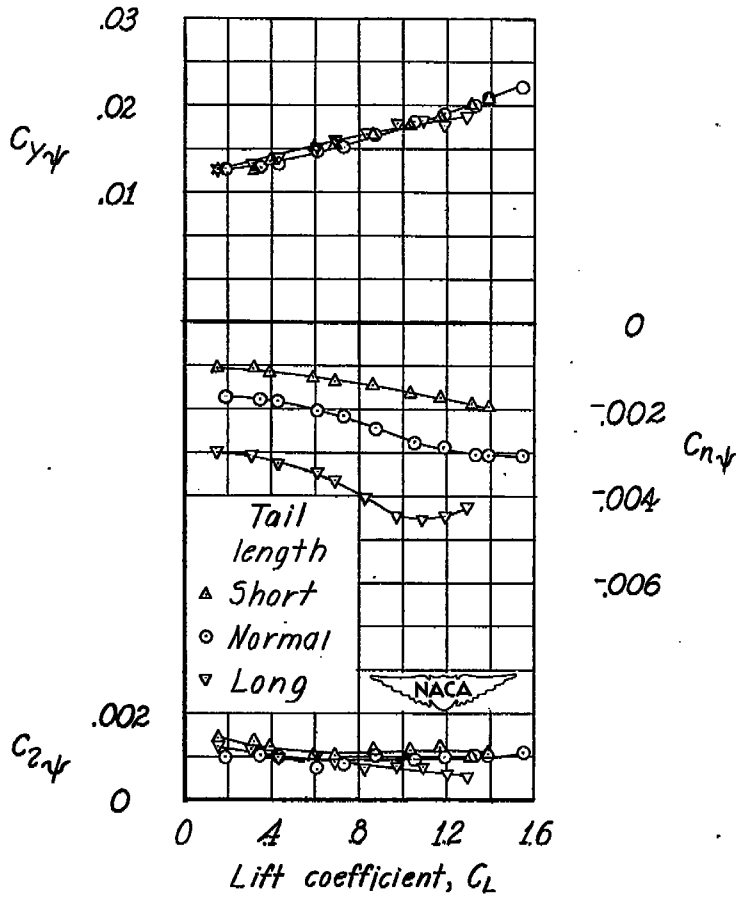

(b) Cruising configuration, power on.

Figure 42.- Effect of tail length on the lateral stability parameters of the single-propeller airplane model. Tail on.

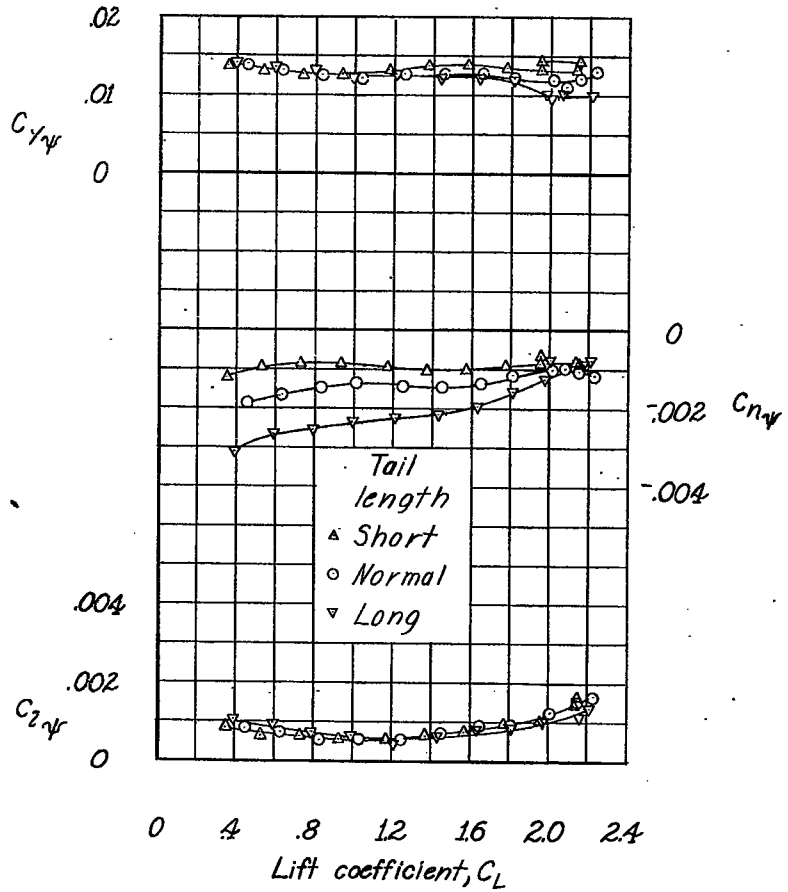

(c) Landing configuration, windmilling propeller.

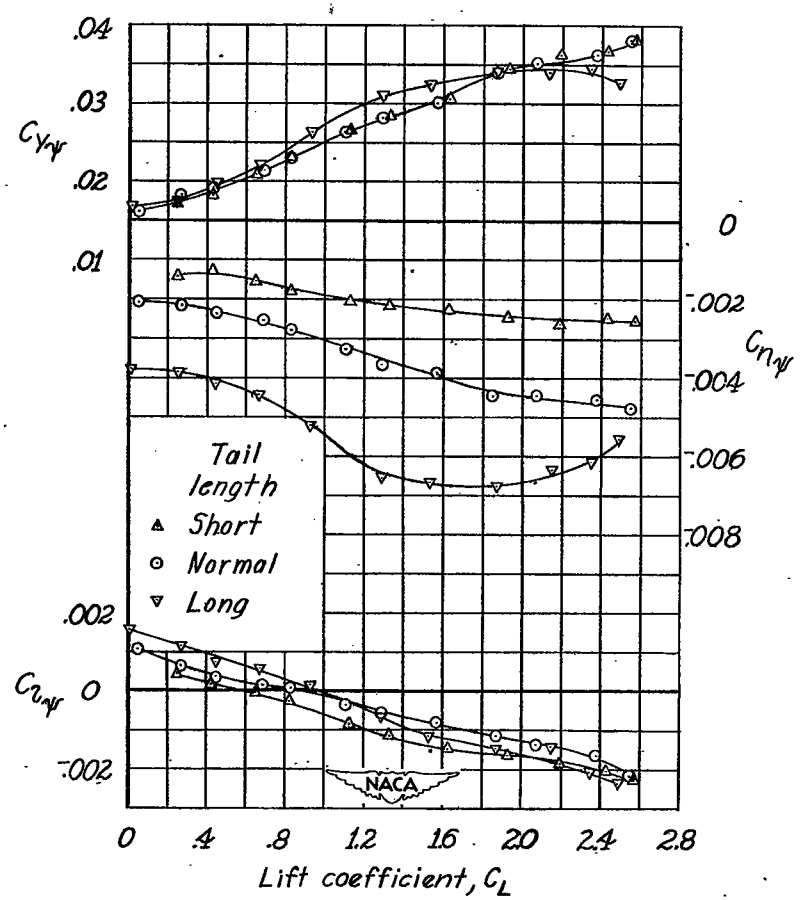

(d) Landing configuration, power on.

Figure 42.- Concluded.

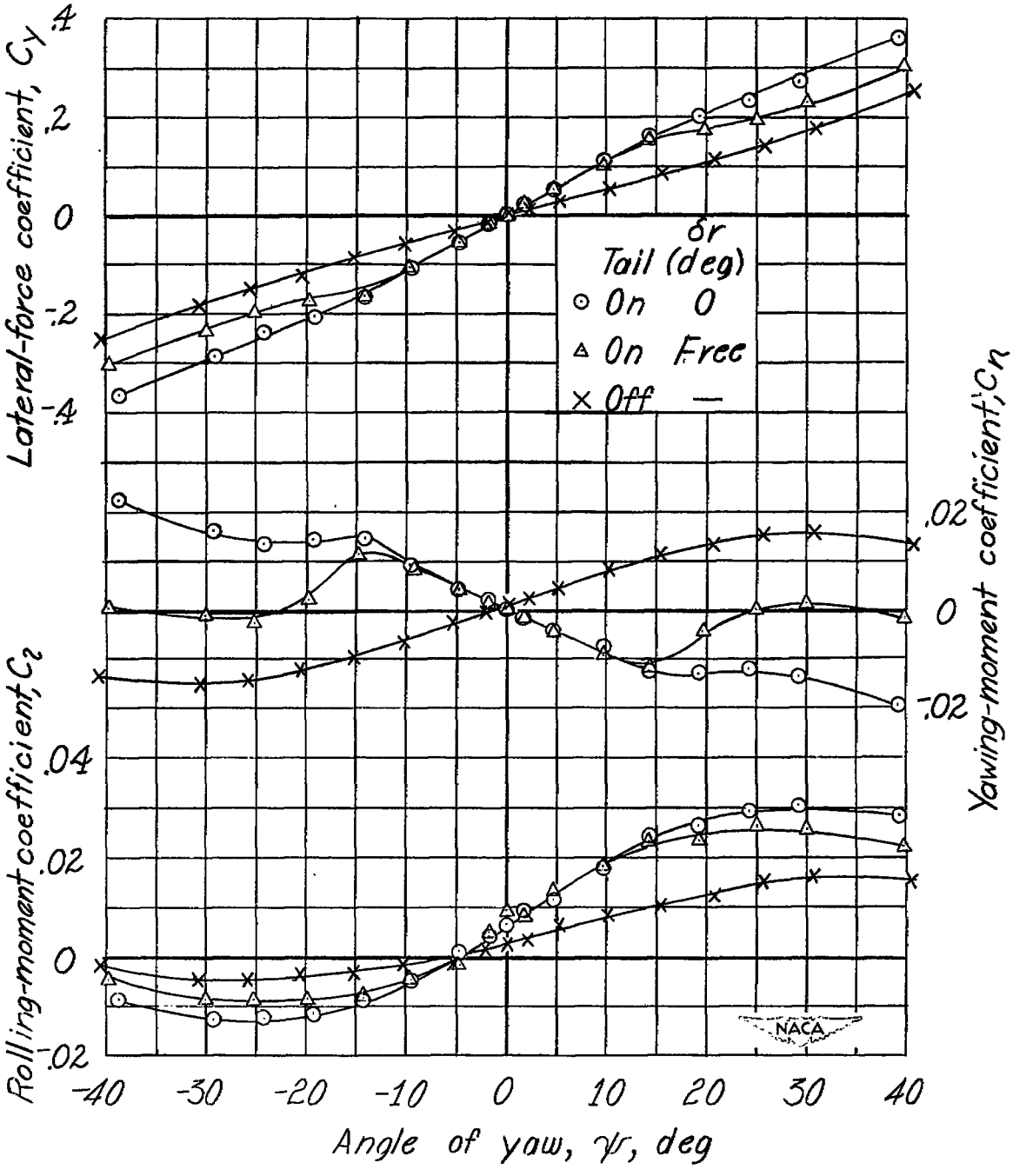

(a) Short tail length.

Figure 43.- Effect of tail surfaces and free rudder on the aerodynamic characteristics in yaw of the single-propeller airplane model. Cruising configuration, windmilling propeller. $\alpha \approx 0.2$ and $C_L \approx 0.13$ at $\psi = 0^\circ$.

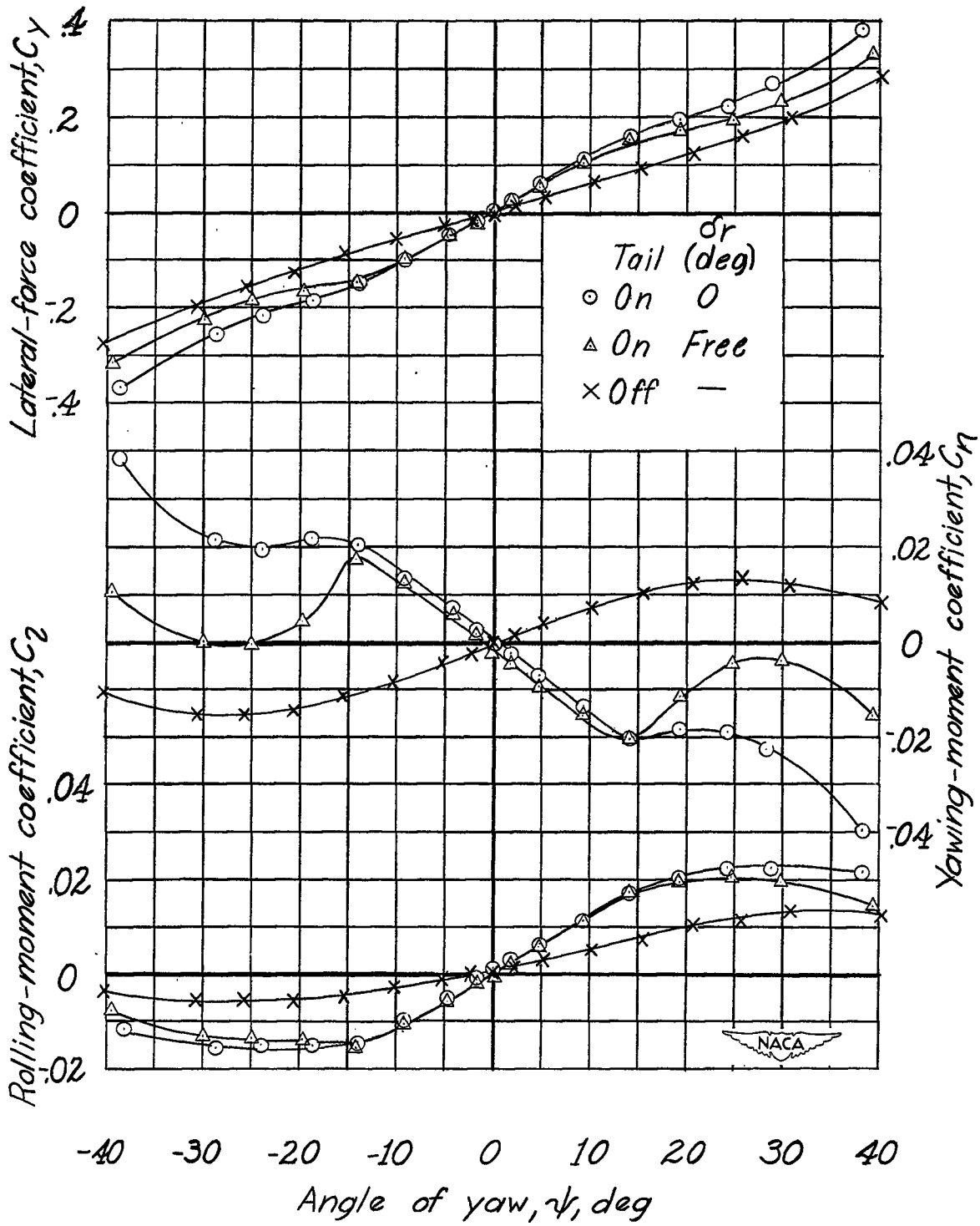

(b) Normal tail length.

Figure 43.- Continued.

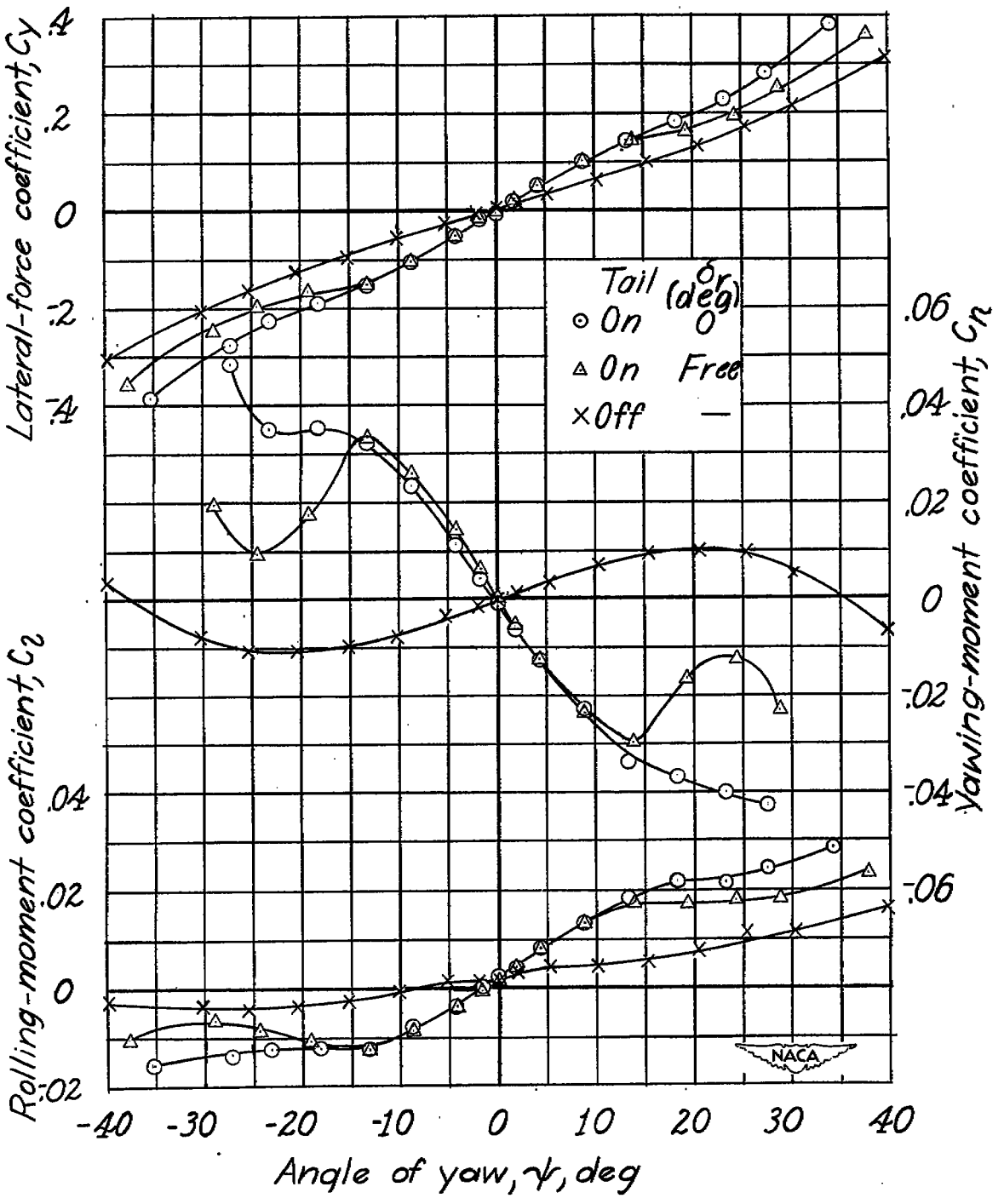

(c) Long tail length.

Figure 43.- Concluded.

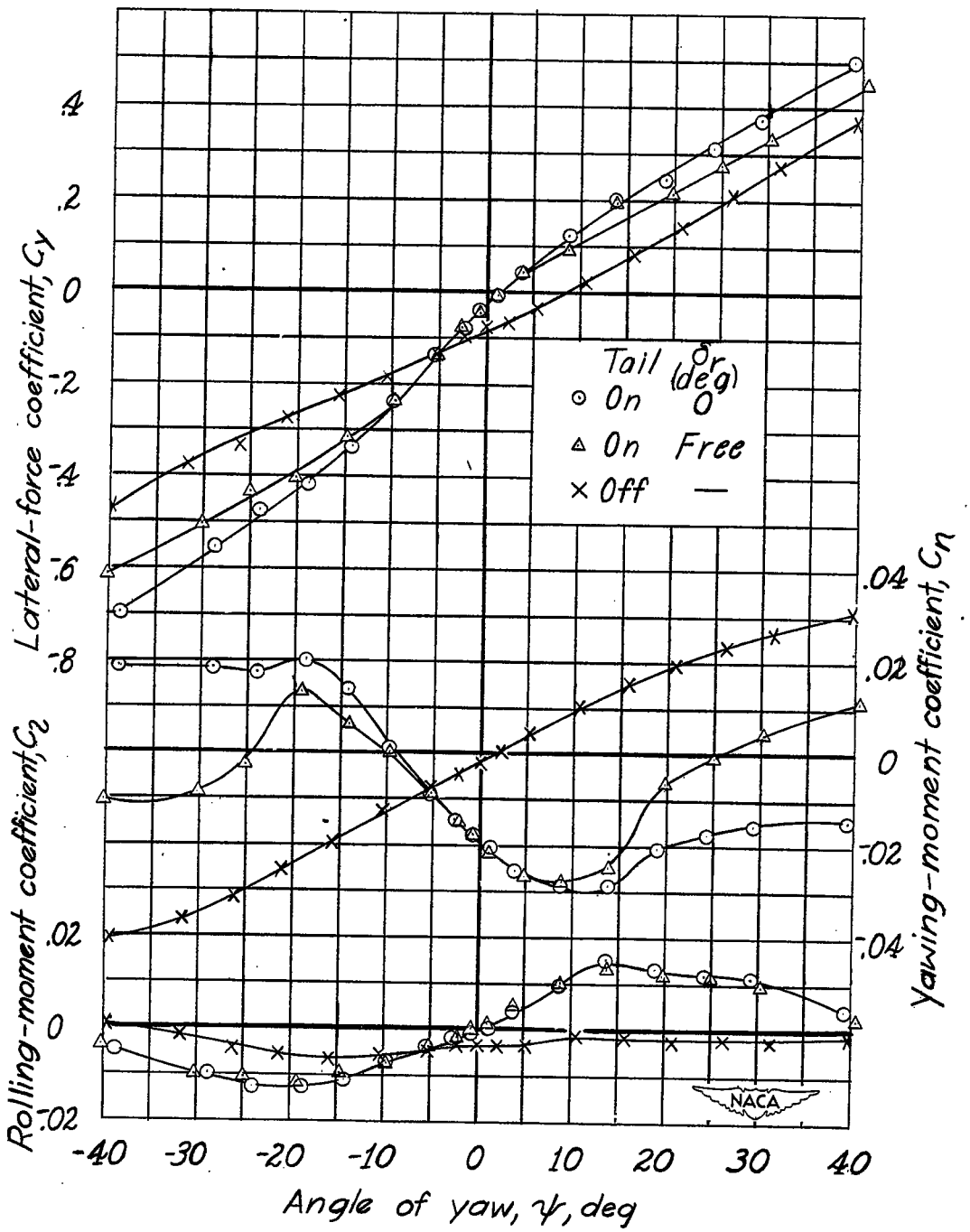

(a) Short tail length.

Figure 44.- Effect of tail surfaces and free rudder on the aerodynamic characteristics in yaw of the single-propeller airplane model. Cruising configuration, power on $\alpha \approx 11.6$ and $C_L \approx 1.11$ at $\psi = 0°$.

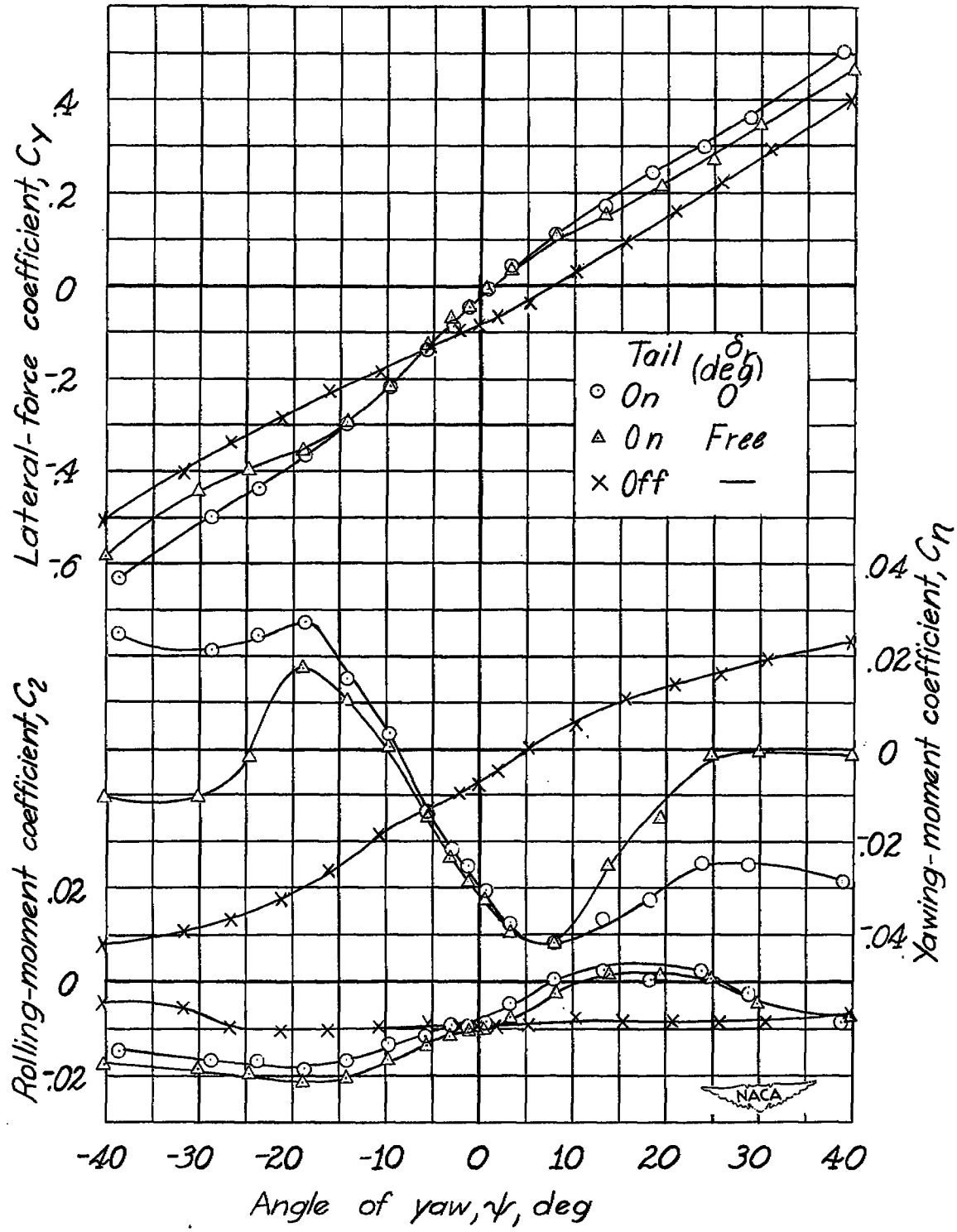

(b) Normal tail length.

Figure 44.- Continued.

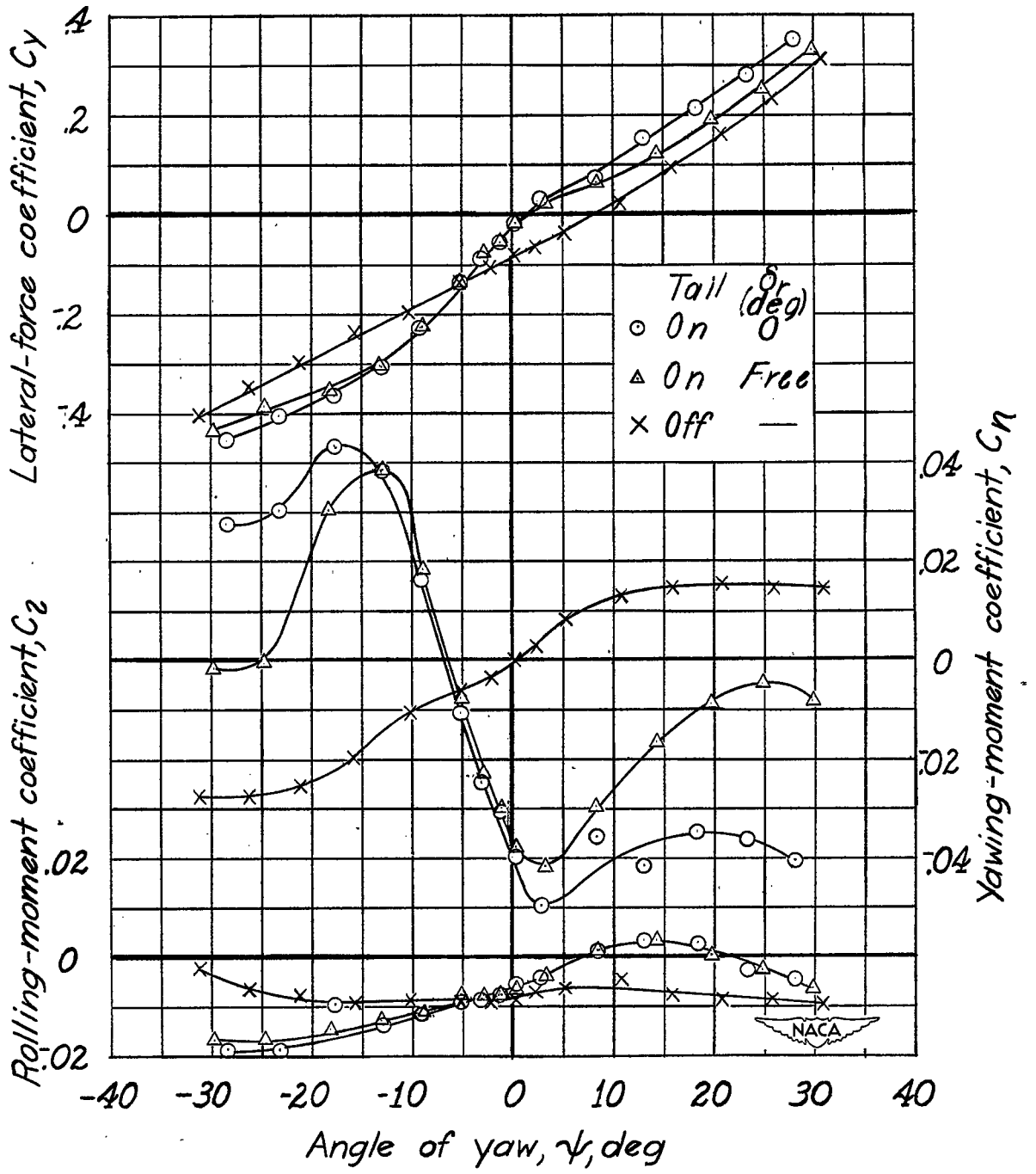

(c) Long tail length.

Figure 44.- Concluded.

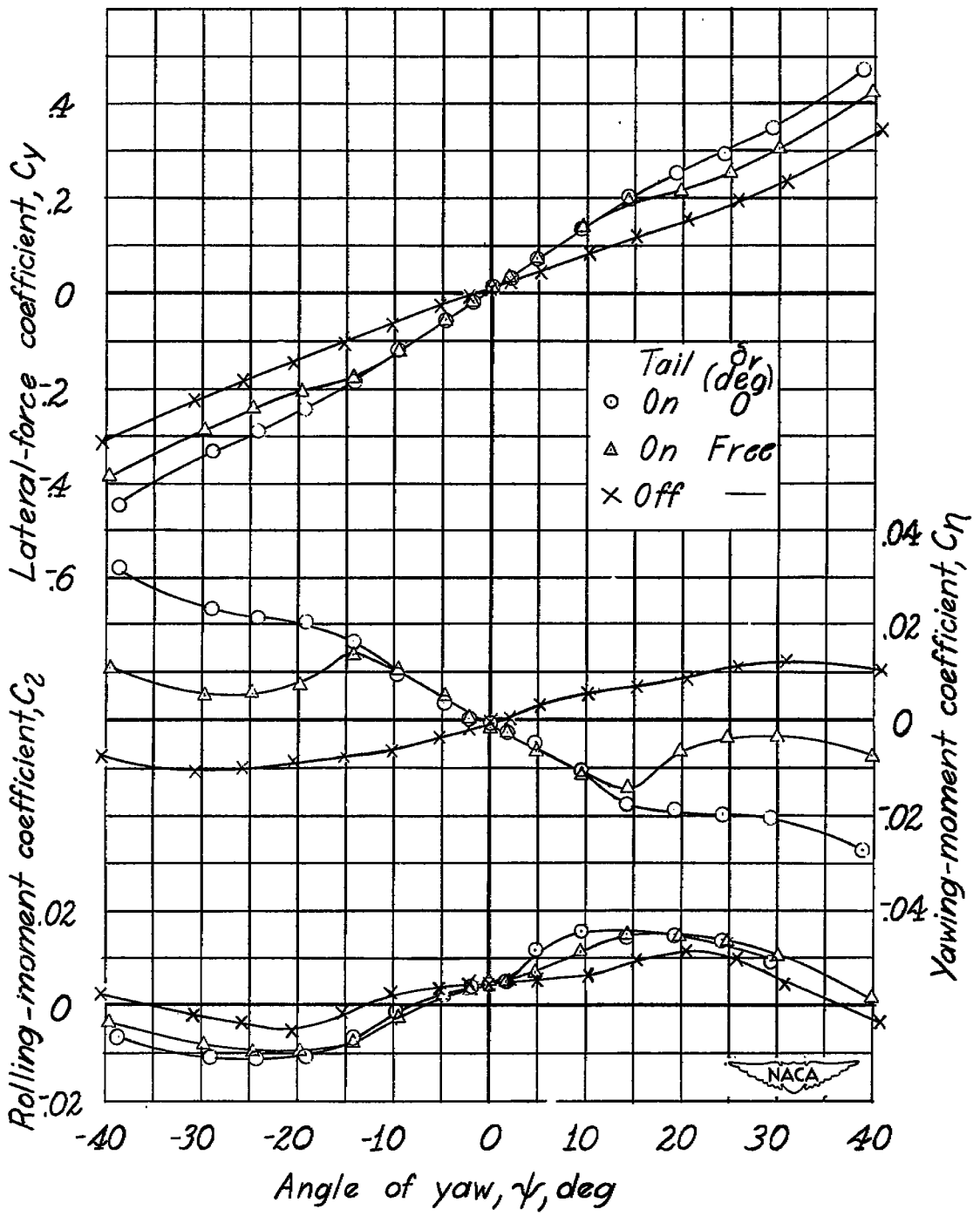

(a) Short tail length.

Figure 45.- Effect of tail surfaces and free rudder on the aerodynamic characteristics in yaw of the single-propeller airplane model. Landing configuration, windmilling propeller. $\alpha \approx 1.0$ and $C_L \approx 1.02$ at $\psi = 0^\circ$.

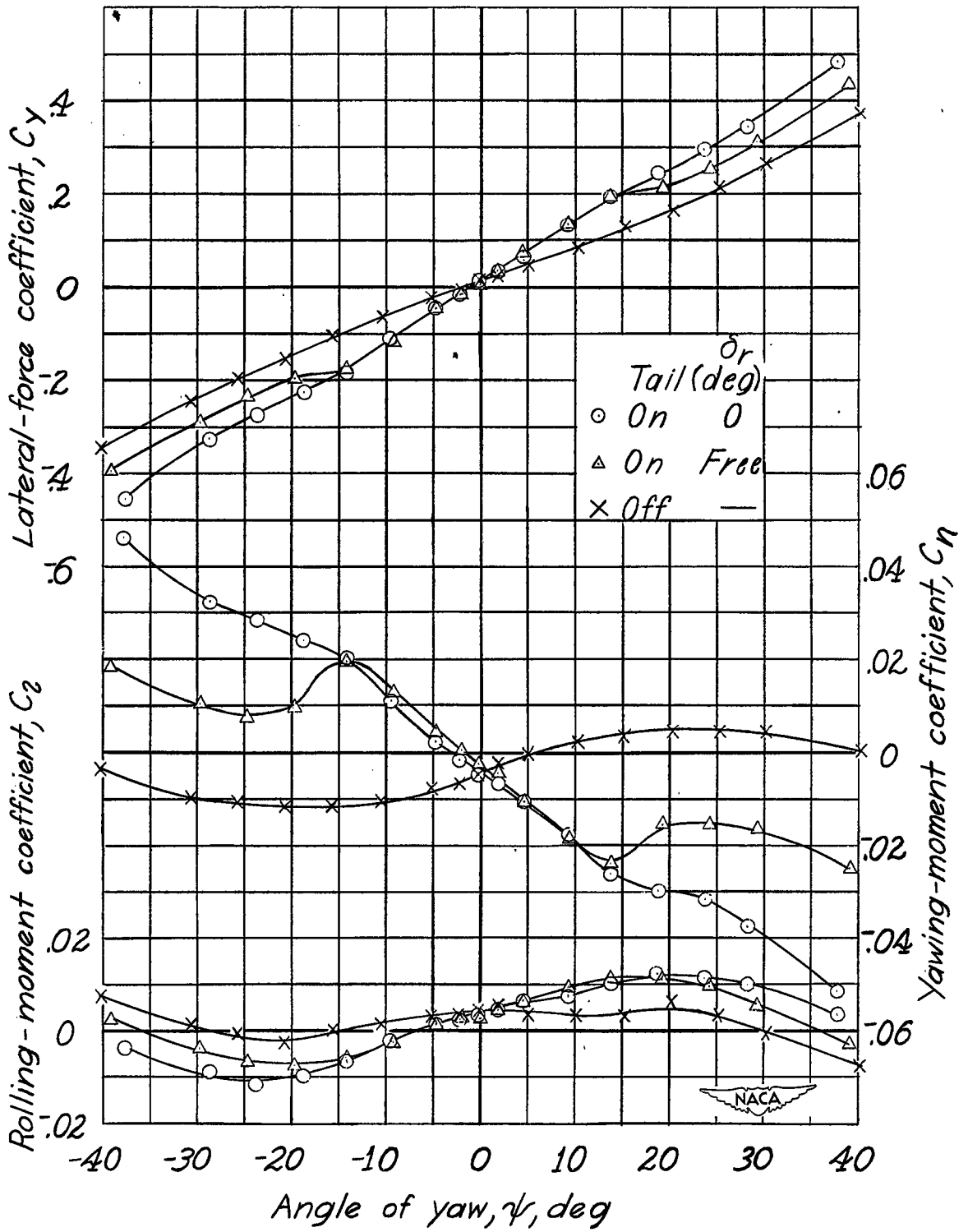

(b) Normal tail length.

Figure 45.- Continued.

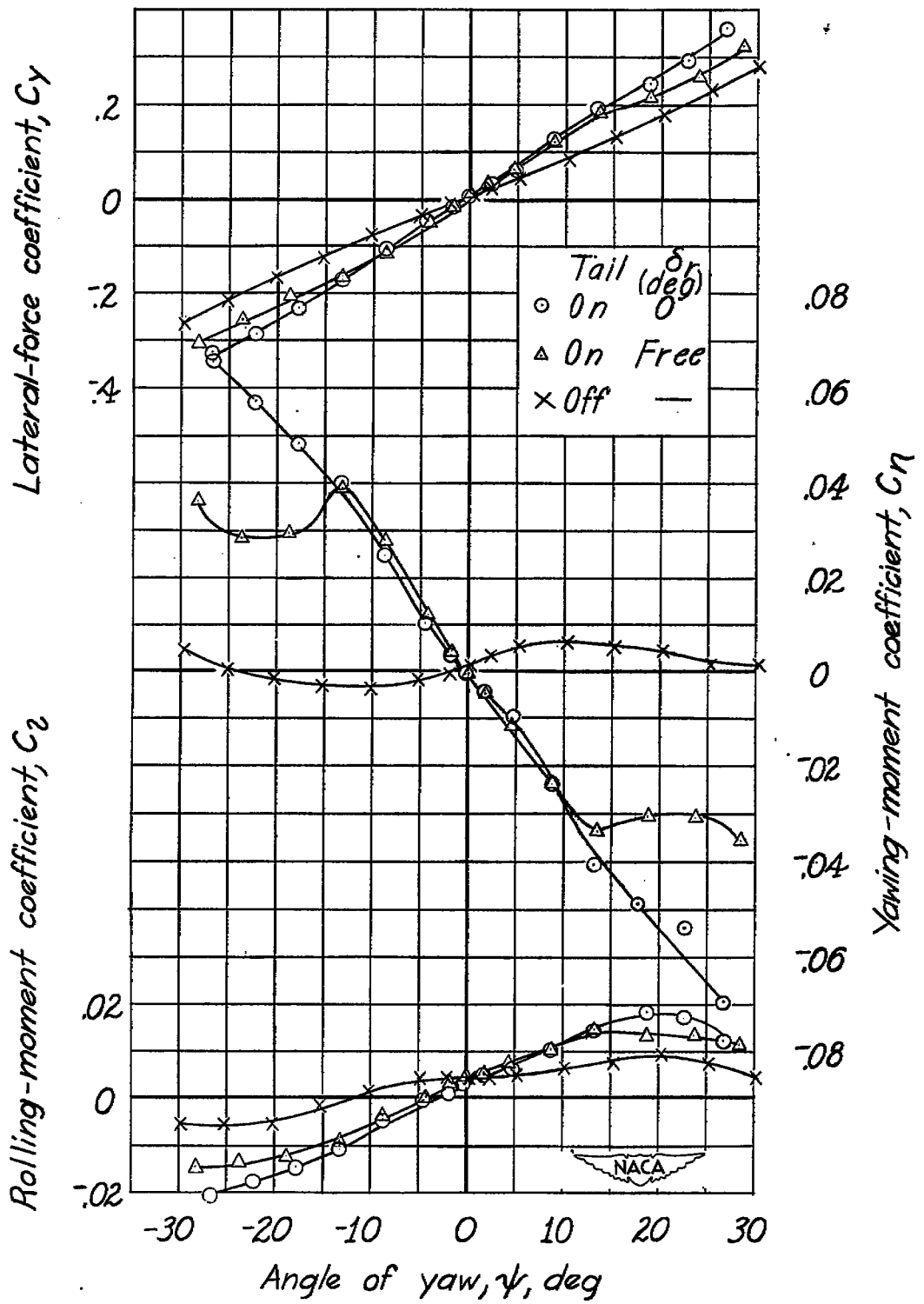

(c) Long tail length.

Figure 45.- Concluded.

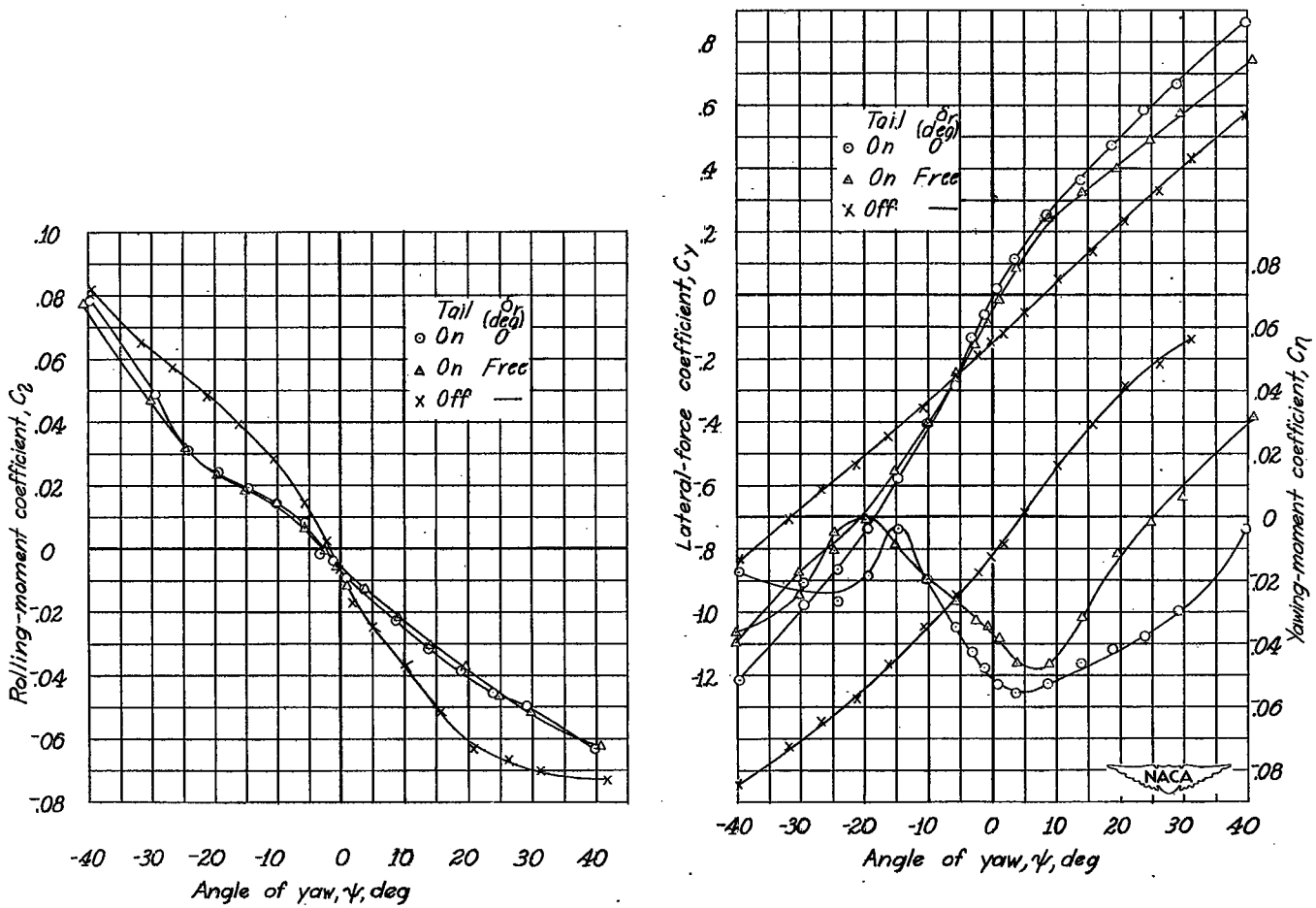

(a) Short tail length.

Figure 46.- Effect of tail surfaces and free rudder on the aerodynamic characteristics in yaw of the single-propeller airplane model. Landing configuration, power on. $\alpha \approx 9.7$ and $C_L \approx 2.36$ at $\psi = 0^\circ$.

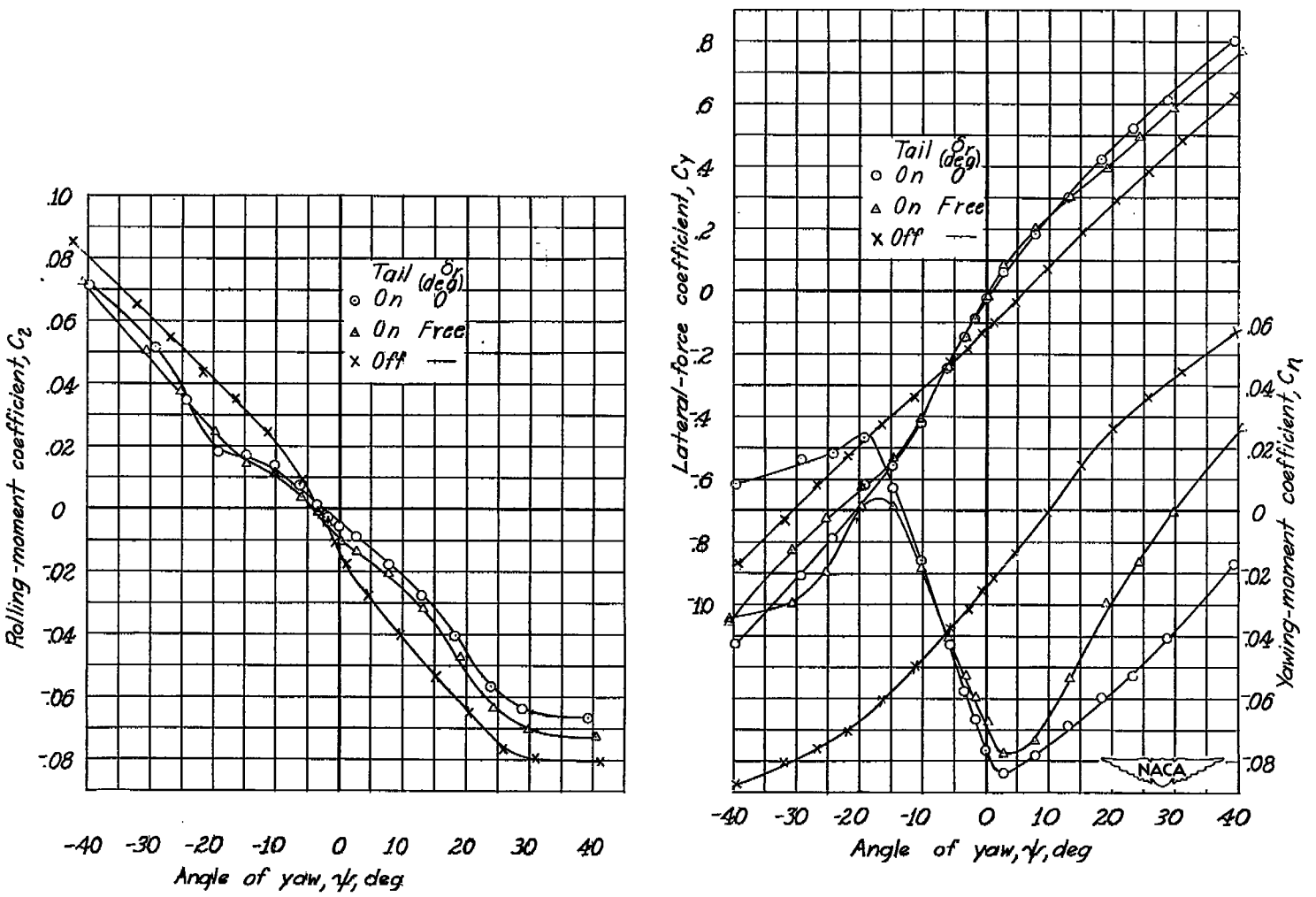

(b) Normal tail length.

Figure 46.- Continued.

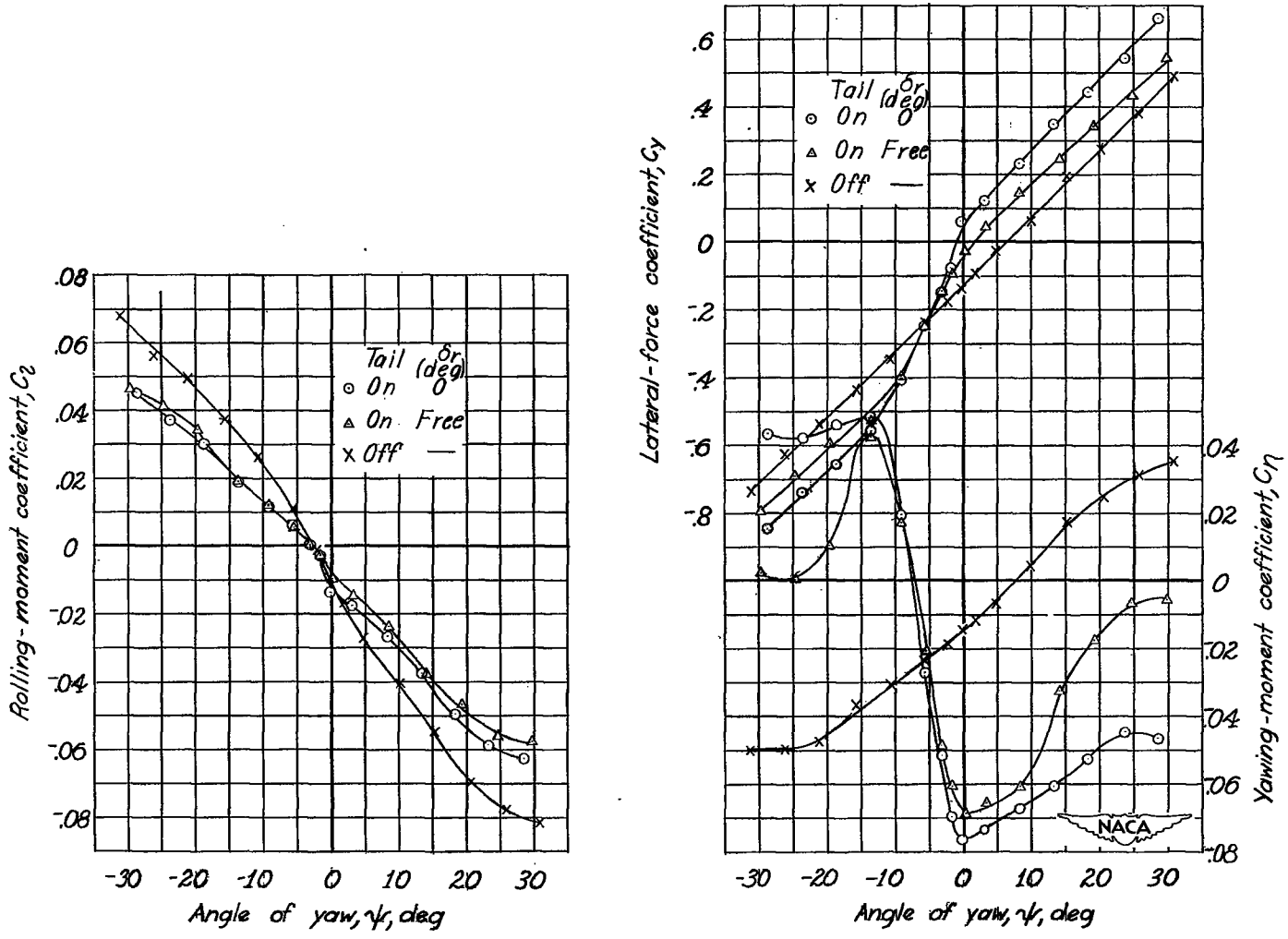

(c) Long tail length.

Figure 46.- Concluded.